2016

A role for sensory areas in coordinating active sensing motions

BOSTON UNIVERSITY

COLLEGE OF ENGINEERING

Dissertation

A ROLE FOR SENSORY AREAS IN COORDINATING ACTIVE SENSING MOTIONS

by

JOSEPH BRADLEY SCHROEDER

B.S., Case Western Reserve University, 2010
M.S., Boston University, 2013

Submitted in partial fulfillment of the

requirements for the degree of

Doctor of Philosophy

2016

Approved by

First Reader _____

Jason Ritt, Ph.D.
Assistant Professor of Biomedical Engineering

Second Reader _____

Kamal Sen, Ph.D.
Associate Professor of Biomedical Engineering

Third Reader _____

Ian Davison, Ph.D.
Assistant Professor of Biology

Fourth Reader _____

H. Steven Colburn, Ph.D.
Professor of Biomedical Engineering

Fifth Reader _____

Howard Eichenbaum, Ph.D.
William Fairfield Warren Distinguished Professor
University Professor
Professor of Psychological and Brain Sciences

DEDICATION

I would like to dedicate this work to my loving wife, Anna Christine, for her patient encouragement and unwavering support, and to my parents for fostering my early interests in science and engineering.

ACKNOWLEDGMENTS

Committee Members

Jason Ritt, PhD

Kamal Sen, PhD

H. Steven Colburn, PhD

Ian Davison, PhD

Howard Eichenbaum, PhD

Assistance with animal training: Vincent Mariano, Gregory Telian, Michael Palmiere, Allicia Imada, Smrithi Sunil, Alex Baradino, Zhengyang Zhang.

Assistance with video tracking: Vincent Mariano, Gregory Telian, Michael Palmiere, Alex Baradino, Emily Hack, Molly Heit, Zhengyang Zhang, and Bradley Sauln.

Assistance with implant construction: Vincent Mariano, Gregory Telian, Smrithi Sunil, Zhengyang Zhang

Assistance with implementation of behavioral arena: Gregory Telian, David Freedman, Ben Perone.

Chapter specific acknowledgements

Chapter 2- Previously published in the journal of Neurophysiology, Co-Authored with Jason Ritt.

Chapter 3.1- Portions previously published as an IEEE conference proceeding for the Engineering in Medicine and Biology conference, 2013. Co-Authored with Jason Ritt.

Chapter 3.2- Similar to a manuscript recently submitted to the Journal of Neural Engineering, Co-Authored with David Freedman, Gregory Telian, Zhengyang Zhang, and Jason Ritt.

Chapter 3.3- Portions were previously published as an IEEE conference proceeding for the Neural Engineering conference, 2013. Co-Authored with Vincent Mariano, Gregory Telian, and Jason Ritt.

Chapter 4- Experiments using inhibitory stimulation in SI conducted with Smirthi Sunil.

Financial Support

NIH Quantitative Biology and Physiology Training Program (5-T32-GM-8764-10)

Career Award at the Scientific Interface, Burroughs Wellcome Fund (Jason Ritt)

A ROLE FOR SENSORY AREAS IN COORDINATING

ACTIVE SENSING MOTIONS

JOSEPH BRADLEY SCHROEDER

Boston University College of Engineering, 2016

Major Professor: Jason Ritt, Ph.D., Assistant Professor of Biomedical Engineering

ABSTRACT

Active sensing, which incorporates closed-loop behavioral selection of information during sensory acquisition, is an important feature of many sensory modalities. We used the rodent whisker tactile system as a platform for studying the role cortical sensory areas play in coordinating active sensing motions. We examined head and whisker motions of freely moving mice performing a tactile search for a randomly located reward, and found that mice select from a diverse range of available active sensing strategies. In particular, mice selectively employed a strategy we term contact maintenance, where whisking is modulated to counteract head motion and sustain repeated contacts, but only when doing so is likely to be useful for obtaining reward. The context dependent selection of sensing strategies, along with the observation of whisker repositioning prior to head motion, suggests the possibility of higher level control, beyond simple reflexive mechanisms. In order to further investigate a possible role for primary somatosensory cortex (SI) in coordinating whisk-by-whisk motion, we delivered closed-loop optogenetic feedback to SI, time locked to whisker motions estimated through facial electromyography. We found that stimulation regularized whisking (increasing overall periodicity), and shifted whisking frequency, changes that emulate behaviors of rodents actively contacting

objects. Importantly, we observed changes to whisk timing only for stimulation locked to whisker protractions, possibly encoding that natural contacts are more likely during forward motion of the whiskers. Simultaneous neural recordings from SI show cyclic changes in excitability, specifically that responses to excitatory stimulation locked to whisker retractions appeared suppressed in contrast to stimulation during protractions that resulted in changes to whisk timing. Both effects are evident within single whisks. These findings support a role for sensory cortex in guiding whisk-by-whisk motor outputs, but suggest a coupling that depends on behavioral context, occurring on multiple timescales. Elucidating a role for sensory cortex in motor outputs is important to understanding active sensing, and may further provide novel insights to guide the design of sensory neuroprostheses that exploit active sensing context.

TABLE OF CONTENTS

LIST OF FIGURES

LIST OF ABBREVIATIONS

BMI ..... Brain Machine Interface

ChR2 ..... Channelrhodopsin-2

CM ..... Contact Maintenance

DR ..... Dead Reckoning

DSP ..... Digital Signal Processor

EIB ..... Electrode Interface Board

EMG ..... Electromyography

FC ..... First Contact

FES ..... Functional Electrical Stimulation

FINE ..... Flat Interface Nerve Electrode

FPS ..... Frames Per Second

FSU ..... Fast Spiking Unit

GUI ..... Graphic User Interface

HSV ..... High Speed Video

HTA ..... Head Turning Asymmetry

ICMS ..... Intracortical Microstimulation

IQR ..... Interquartile Range

IR ..... Infrared

IWI ..... Interwhisk Interval

LED ..... Light Emitting Diode

MI ..... Primary Motor Cortex

MIMC ..... Minimal Impingement / Maximal Contact

MSP.....Mean Set-Point

OC.....Opposite Contact

PCB..... Printed Circuit Board

PSTH..... Peristimulus Time Histogram

RMS.....Root-Mean-Squared

RSU..... Regular Spiking Unit

SI..... Primary Somatosensory Cortex

SLS..... Selective Laser Sintering

TDT..... Tucker Davis Technologies

VCR ..... Vestibulo-Collic Reflex

CHAPTER ONE- Background

1.1 Importance of closed-loop feedback to improved neuroprosthetic design

The rapidly progressing fields of Brain Machine Interfaces (BMI) and neuroprosthetics have made exciting advances in restoring motor function to injured patients through electrical interfacing with the nervous system at various levels (reviewed in [1]). Two distinct but potentially complementary areas of focus have been interfaces targeting either the central or the peripheral nervous system.

A remarkable amount of progress has been made at decoding motor information from cortical recordings and using the signal to drive a computer cursor or prosthetic [2–10]. A wide variety of recording targets and outputs are possible, for example recording from areas implicated in speech production and decoding intended phonemes for use in a speech prosthesis [11]. Motor cortex BMI systems have become sophisticated enough to facilitate robust control of a robotic arm with many degrees of freedom, which may ultimately allow increased independence in daily tasks [12]. Despite progressing to human clinical trials on a motor cortex controlled BMI implant [13], significant hurdles such as long-term recording stability remain [14,15]. To date, the available systems rely heavily on visual feedback, while efforts to incorporate proprioceptive and tactile feedback have lagged behind the decoding of motor intent [16,17].

In parallel, significant strides have also been made in interfacing directly with peripheral motor efferents to bypass damaged regions and restore motor function to an upper or lower extremity. This process of Functional Electrical Stimulation (FES), involves activating muscle groups in a coordinated manner through implanted or cutaneous peripheral nerve stimulation [18]. FES based approaches have had success in restoring upper extremity movement to tetraplegia patients, and have also been applied for indications such as urinary incontinence [19]. Upper extremity systems typically depend on a retained ability for small muscle movement (such as the shoulder or face muscles) in order to serve as a control signal. Stimulation specificity is achieved either by electrode design [20] or stimulus waveform selection [21]. While promising in some respects, these systems have encountered difficulties in commercialization due to high costs and difficulty in implementing outside a research setting, similar to challenges faced in commercializing BMIs. These two targets for restoring motor function may not be mutually exclusive — for example one might envision a system that records from a patient's motor cortex to estimate intended motor movements, then implements that motion in the patient's own muscles through an FES type system, rather than by actuating a robotic limb.

Both approaches share a common challenge in that they typically suffer from a functional limitation stemming from a lack of closed-loop feedback. Visual feedback (i.e evaluating cursor position relative to a target or visually observing the position of a prosthetic) has typically been employed as the sole or primary method of feedback. The importance of

closed-loop brain machine interfaces is increasingly realized, and much recent work has focused on methods for providing sensory feedback [16,17]. Stimulation targets for sensory feedback have included peripheral nerves (such as visual [22] and auditory [23]), brainstem [24], thalamus [25], and cortex [17,26–28]. An early, and somewhat indirect technique for incorporating somatosensory feedback into a motor BMI involved placing a vibrotactile actuator on an area of skin that retains afferent innervation [29], although the results have been less than optimal. Perhaps a more elegant strategy would be to provide stimulation in cortical sensory areas, while simultaneously decoding motor intent from motor areas. Such a strategy has been used in non-human primates to create artificial "textures" by delivering intracortical microstimulation (ICMS) at different frequencies when a monkey brings a cursor to various targets using a closed-loop BMI [26,30]. While demonstrating that a monkey can distinguish different frequencies of ICMS and incorporate that information into a task strategy, the perceptual quality of the stimulation is far from certain, and the description of different stimulation frequencies as textures appears premature. Other groups have sought to clarify the perceptual quality of ICMS and fine tune stimulation parameters in an effort to produce naturalistic percepts [31]. Using this information, there has been some success in delivering ICMS in a way that enables a money to perform a tactile discrimination task with comparable accuracy to natural touch [32]. The results from this discrimination task also suggest the importance of the timing of stimulation relative to behavior in determining how the stimulus is incorporated into the animal's ongoing sensing strategy. In contrast to the "biomimetic" approaches described above that seek to deliver feedback that is natural and intuitive, so

called “learning based” methods deliver a feedback signal that is initially unfamiliar and allow the subject to learn how to incorporate the new information into their task strategy. For example, animals can learn to use information from cortical microstimulation that codes for information about hand position relative to a target (artificial proprioception) and are especially successful when this feedback can be combined with visual information [33].

Relatively more progress has been made in peripheral applications of sensory feedback, where electrical stimulation using Flat Interface Nerve Electrodes (FINE) has been shown to produce a variety of perceptions in different areas of the hand that are stable over long periods and are described by human test subjects as feeling similar to natural sensations [34,35]. The problem may be more tractable in the peripheral case, where if one can activate the right fibers, it is logical to suppose that exploiting a labeled line organization of sensory pathways may lead to electrical signals arriving in cortex that are difficult to distinguish from those that arrive naturally. In the case of central stimulation and recording, the problem is complicated by many factors. The system is massively underactuated, meaning that the number of stimulation targets (neurons) greatly exceeds the number of independent stimulation sources (electrodes, optical fibers, etc.) leading to difficulties in targeting stimulation to specific neurons [36]. Furthermore, an incomplete understanding of the complex, closed-loop nature of natural sensory processing makes the determination of optimal stimulation targets and parameters difficult. Developing a

better understanding of sensorimotor loops involved in active sensing is a key motivation driving our experiments in the rodent whisker system.

1.2 Understanding sensation as an active process

Rather than passively absorbing information from the environment, many sensory modalities incorporate active behaviors to improve sensory acquisition. In active sensing, future sensing behaviors are directed by previously acquired sensory information and by the behavioral goal [37]. One of the most accessible examples of an active sensing process is in the primate visual system [38,39]. In a classic visual system study, Yarbus tracked the eye motions of human subjects while they viewed a variety of photographs [39]. His studies showed that the saccadic eye motions made by a subject viewing a photograph of a human face did not systematically scan the image line by line, but rather fixed on and quickly moved between key points of interest (i.e. eyes, mouth, nose) with comparatively fewer visual excursions to the periphery. Additionally, when a subject was shown a photograph, vastly different eye motions were observed depending on the question the subject was asked about the image. These results together demonstrate vision as an active process where motions are driven both by previously acquired sensory information and by the current goal. Similar active sensing has been observed across many sensory modalities, for example the modulation of sniffing patterns in olfaction [40]. Active sensing is perhaps most prominent, however, in somatosensation, where tactile feedback plays a central role in directing future motions. Primates rely heavily on tactile feedback when manipulating objects and actively adapt sensing behaviors based

on the type of sensory information desired (texture, shape, weight, hardness, etc.) [41–45].

Active sensing in natural, unrestrained scenarios is often accomplished by coordinated motions of both the specific sensor involved and the overall positioning of the body. For example, in human vision there is a tight coordination between the motions of the eyes and head [46]. These motions are not independent, and require the ability to maintain a stable representation of relative positioning across multiple body parts, even in cases of self-motion [47]. In primate tactile sensation, active self-motion is critical to task performance [48] and requires tight coordination of multiple joints and muscle groups as well as tactile and positional feedback [49,50]. Understanding the sensory-motor integration that enables short-latency adaptations in sensing behavior in order to improve sensory acquisition is an important area of inquiry with implications for restoring and improving sensory function.

1.3 The rodent whisker system as a model for active touch

The rodent whisker system presents a well-studied platform to address outstanding questions in active tactile sensation, and is increasingly used as an analog for active touch in humans (reviewed in [51–54]). Mice and rats interrogate their surroundings through coordinated 10–20 Hz motions of large, external tactile hairs (whiskers). These motions can be actively modulated, for example in response to object contact. The whisker system is attractive for study in part because the motion of both the whiskers and the body can be

observed in a straightforward manner (i.e. through analysis of high speed video) in order to quantify sensing behaviors. The kinematics of whisking have been well studied. Whisking in rats has been found to have a dominate frequency of around 8Hz, with a range from 1–20 Hz, and with protractions generally occurring faster than retractions [55]. Velocity profiles have been found to be variable between several stereotyped patterns [56], and whisker curvature allows the force imparted to the mechanoreceptors in the facial pad to be modulated by the animal's distance from the contacted object [57]. Although much of the work in the whisker system has focused on rats, it is believed that many of the same concepts translate directly to mice. This is reinforced by a recent comparative study which found similar whisking behaviors in mice, rats, and marsupials [58].

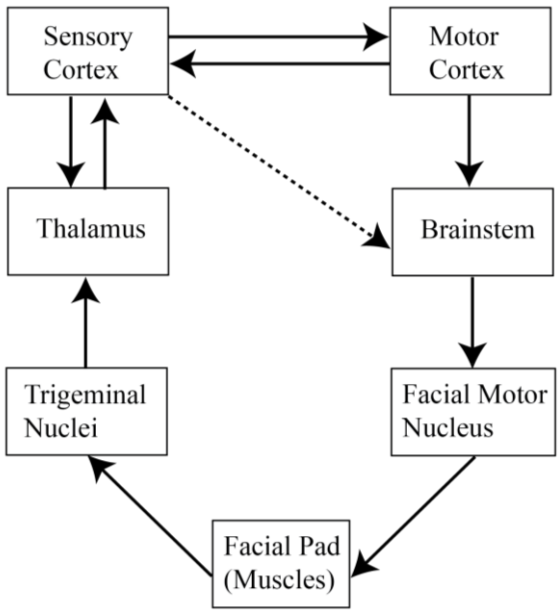

Figure 1.1 Overview of sensorimotor pathways in the rodent whisker system

Ascending and descending pathways from whiskers to cortex have been well studied and may include motor effects from sensory areas that do not depend on projections to MI [52,53,59,60].

In addition, the afferent sensory pathway from the hair follicle, through the trigeminal system, brainstem, thalamus, and primary somatosensory cortex has been well characterized [52] (Figure 1.1). A particularly advantageous aspect of the system is that each whisker follicle maps to a specific "barrel" structure in SI and these barrels are somatotopically arranged in a layout that closely mirrors the arrangement of whiskers on the face [52]. The layout of the whisker grid on the facial pad and the arrangement of "barrels" in SI are conserved from animal to animal and are the same in rats and mice. The term "barrels" specifically refers to the layer-4 cortical structures that receives the majority of lemniscal inputs containing information from whisker motions [61]. The 1:1 mapping between whiskers and barrels enables recordings from SI to be associated with the motions and contacts of a single whisker under appropriately controlled experimental conditions.

The properties of SI neurons have been studied in slice, anesthetized, and awake preparations to give a strong base of knowledge regarding SI in the rodent whisker system [62–75]. Broadly speaking, two cell classes of interest are fast spiking putatively inhibitory interneuron units (FSUs) and regular spiking units (RSUs) [65]. FSUs are thought to play a role in the coordination of local spike timing, while RSUs are primarily excitatory and include projections out of the local circuit. The tuning of SI neural activity has been shown to relate to whisker motions. Although some debate exists concerning the precise relationship, an increasingly convincing collection of evidence shows that SI activity is weakly tuned to the phase (rather than angle) of whisker motions, with a

population preference for spiking when the whiskers are near their maximal protraction (retraction onset) [62–64,76]. Additionally, whole cell SI recordings in awake mice revealed rapid, low-amplitude changes in membrane potential that correlated well with whisker motions [68]. Rodents have been shown to integrate bilateral SI information, and this ability is necessary for success in bilateral discrimination tasks [69,70]. It has also been reported that whiskers adjacent to a barrel's principal whisker can provide an inhibitory effect in SI, similar to the idea of center surround inhibition in the visual system providing increased sensitivity to the target input [77].

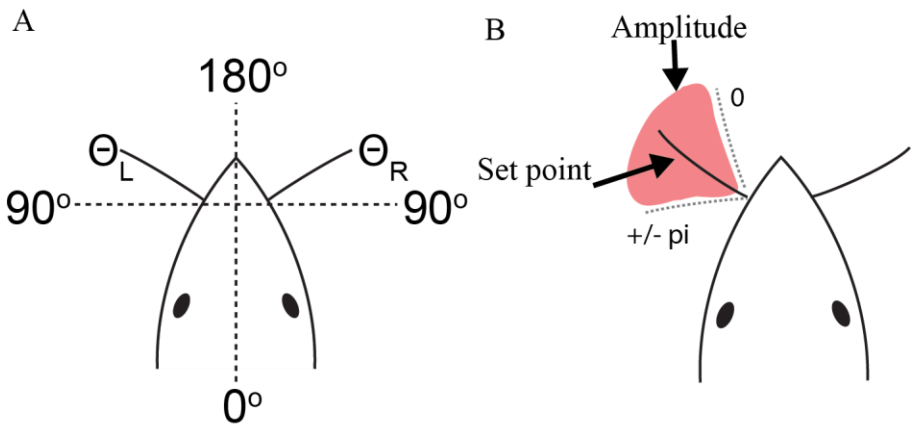

Figure 1.2 Whisking parameter definitions and angle conventions

A, Whisker positions are typically defined as angles relative to centerline of the animal's head, with 180° corresponding to full protraction. **B,** Common parameters to quantify whisking include amplitude (angular distance from maximal retraction to maximal protraction), set-point (average whisker position, smoothed to remove contribution from individual whisks), and phase (- π/π (full retraction), 0 (full protraction), describes relative timing within the whisk cycle regardless of amplitude and set-point changes).

Rodent whiskers are manipulated primarily though the action of intrinsic muscles ("slings" around each whisker follicle) which are responsible for protraction, and

extrinsic muscles implicated in retraction [78–80]. The gold standard for evaluating whisker motions has been post-hoc reconstruction of whisker angles from high speed videography [81], and significant effort in the field has focused on efforts to automate the tracking of whisker positions [82–85]. A variety of parameters can be quantified from videography to describe whisking behaviors. Whisker angles are traditionally defined relative to the animal's head, with 180° corresponding to protraction (fully forward) and 0° corresponding to retraction (fully backward) (Figure 1.2A). Phase provides a measure to evaluate the relative timing within the whisk cycle without considering the absolute angle relative to the face. A whisk proceeds from full retraction ($-\pi$) to full protraction (0) and back (Figure 1.2B). Other important whisking parameters include amplitude (angular difference from maximal retraction to maximal protraction) and set-point, which is a smoothed version of the average whisker position and reflects longer timescale changes in the average whisker angle without considering the rapid fluctuations from individual whisks. Set-point can be thought of as indicating how far forward or backward the whisker field is positioned, and is the central point that whisker angles fluctuate around (Figure 1.2B).

An alternative method for estimating whisk timing is to use facial electromyography (EMG) with electrodes placed in the whisker pad. This approach has been demonstrated in rats [86–88], and a significant methodological contribution of our lab has been adapting the approach to be used in the much smaller facial pads of mice (see chapter 3.1) [89].

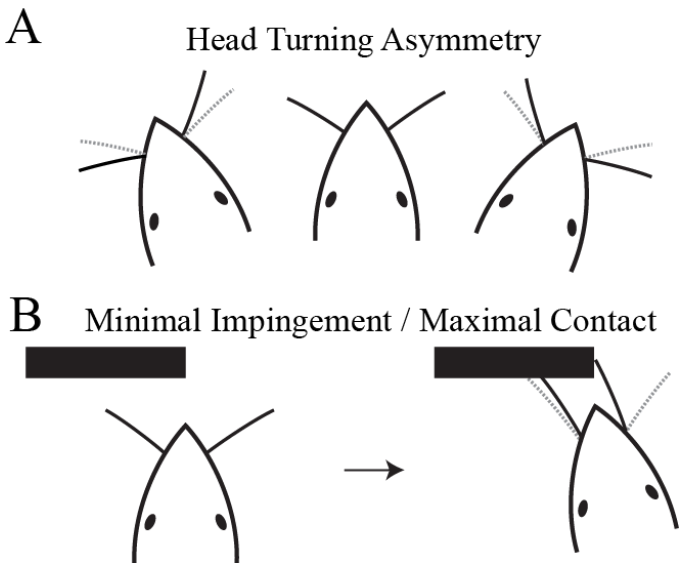

Figure 1.3 Head and whisker repositioning strategies in active sensing

A, Head Turning Asymmetry (HTA) drives whisker retractions on the side the head is turning towards and protractions on the contralateral side. This repositioning allows the whiskers to "look ahead" into the region the head is moving towards [58,90]. **B,** Minimal Impingement / Maximal Contact (MIMC) facilitates the contacting side whiskers making "light touches" on subsequent whisks and positions the contralateral whiskers to allow as many whiskers as possible to contact the surface [91].

Active tactile sensation plays a critical role in many natural rodent behaviors including navigation and food localization, as these animals spend a significant portion of their lives in underground tunnels and burrows, rendering vision unreliable [51,54]. Rodent active sensing has been studied in a variety of contexts including texture discrimination [92–95], object localization [96–103], aperture width discrimination [69,70], and free exploration [58,91,104]. It is increasingly apparent that the motions of the animal's head, along with whisker motions, play a central role in active sensing behaviors [45,71,90,96,103,105–108]. Recent evidence suggests the existence in rodents of neural structures similar to the frontal orienting field in primates [109,110], which may assist in orienting processes during active sensing. Several previously reported sensing strategies

involve the coordination of head and whisker motions. Head Turning Asymmetry (HTA) predicts that the whiskers will be repositioned during head turns in order to allow the animal to "look ahead" into the region the head will soon enter [58,90] (Figure 1.3A). Additionally, the strategy of Minimal Impingement / Maximal Contact (MIMC) suggests that, following unilateral whisker contact with an object, whisker and head motions will be modulated to ensure that subsequent sensing motions result in light contacts of as many whiskers as possible against the target [91,104] (Figure 1.3B). These strategies were initially studied in isolated preparations, and they may at times suggest contradictory responses to a given situation. A key contribution of our behavioral analysis lies in distinguishing how animals select from a repertoire of available sensing strategies (see chapter 2).

An additional advantage of studying active tactile sensation in the whisker system, particularly in mice, is the ability to leverage a large and growing optogenetic toolkit for selective activation of specific cell populations using genetically targeted opsins [111–116]. Generally, these techniques involve targeted genetic expression of genes coding for light sensitive ion channels originally isolated from various algal species. A specific channel of interest is Channelrhodopsin-2 (ChR2) which opens in response to blue light to permit inward sodium currents resulting in cellular depolarization [117]. It has been shown that mice can learn simple tasks using information delivered by optogenetic stimulation of SI [118], and subsequent work has leveraged a variety of new optical tools for selective excitation and inhibition in a range of brain areas.

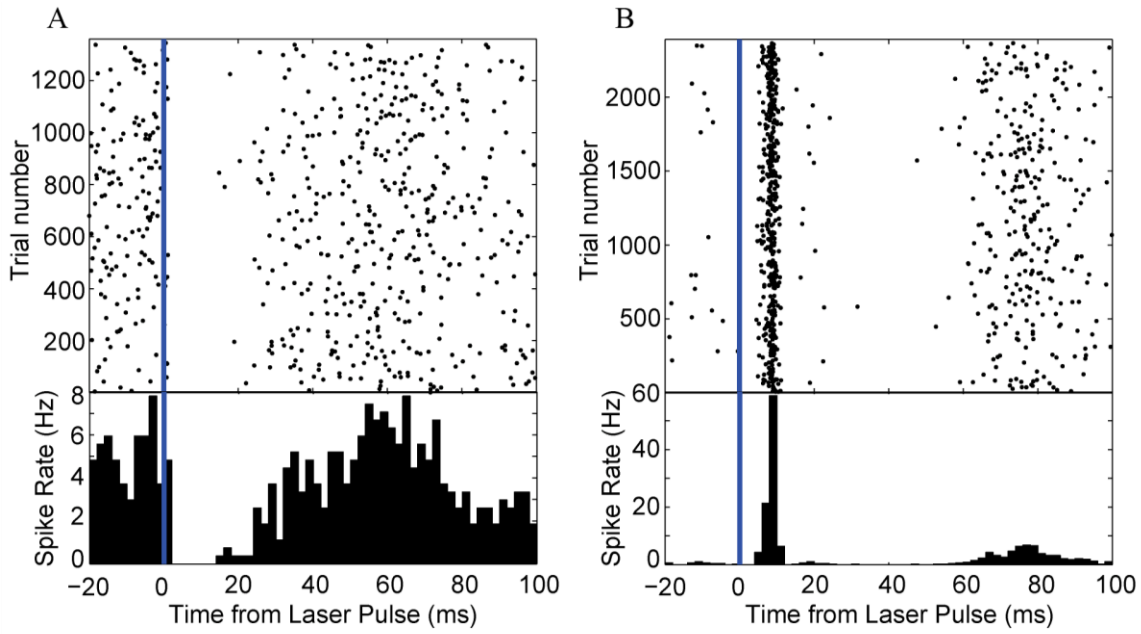

Figure 1.4 Optogenetic techniques for recruiting inhibition and excitation

A, Spike rasters (*top*) and PSTH (*bottom*) show response of an SI isolated single unit to 1 ms pulses of 473 nm light in PV-ChR2 mice, which demonstrates recruitment of post-stimulus inhibition. **B**, Same analysis as A for Thy1-Chr2 mice shows strong post-stimulus excitation.

We utilized two transgenic mouse lines to target stimulation to different cell populations resulting in either excitation or inhibition. We expressed ChR2 in PV-Cre mice (B6;129P2-Pvalbtm1(cre)Arbr/J, Jackson laboratories) [119] through cortical microinjection of a adenoassociated virus (DIO-ChR2-H134; U. North Carolina Viral Core) to achieve localized expression of Chr2 in PV+ inhibitory interneurons. Delivering 1 ms pulses of blue (473 nm) light results in decreased post stimulus firing as a result of recruited inhibition (Figure 1.4A). For excitatory stimulation, we used Thy1-Chr2 line 18 mice (B6.Cg-Th$^{(Thy1\text{-}COP4/EYFP)18Gfng)/J}$, Jackson Laboratories) [114]. These mice express ChR2 strongly in layer 5 cortical neurons without requiring viral injection or cross

breeding. Stimulation results in robust recruitment of single unit firing 5–10 ms following stimulation with single pulses (Figure 1.4B).

1.4 Research Overview

We seek to explore sensorimotor processing in the rodent whisker system during active tactile sensation. Information from this system may enhance our understanding of the role sensory areas play, not only in perception but also in coordinating active sensing motions and may ultimately prove informative to the design of improved tactile feedback systems for neuroprostheses and brain machine interfaces. For the purpose of this study, exploration of active sensing in mice has been decomposed into three major areas of focus, which are the subjects of the following chapters. Chapter 2 describes a behavioral study of mice performing an active search task, and utilizes detailed reconstructions of head and whisker motions from high-speed video to analyze active sensing strategy selection. Chapter 3 describes solutions to three engineering challenges that were met to facilitate real-time feedback experiments in the whisker system: 1) the development of facial electromyography techniques for mice, and the signal processing to extract information on whisk timing, 2) the design of the OptoZIF Drive, an improved optoelectric implant for neural recording and stimulation in freely moving mice, and 3) the development and preliminary testing of a system to deliver real-time feedback stimulation timed to whisker motions. Chapter 4 describes experiments using closed-loop optogenetic feedback, timed to whisker motions, and analyzes the behavioral and neural effects. Taken together, this body of work provides important insight into sensing

strategy selection, the coordination of sensing motions across multiple motor degrees of freedom, and the involvement of primary sensory cortex in coordinating the timing of sensing motions.

Rodent experimental procedures described in the following chapters were conducted in compliance with protocols approved by the Boston University Institutional Animal Care and Use Committee.

CHAPTER TWO- Selection of head and whisker coordination strategies during goal oriented active touch

2.1 Executive Summary

In the rodent whisker system, a key model for neural processing and behavioral choices during active sensing, whisker motion is increasingly recognized as only part of a broader motor repertoire employed by rodents during active touch. In particular, recent studies suggest whisker and head motions are tightly coordinated. However, conditions governing the selection and temporal organization of such coordinated sensing strategies remain poorly understood. We videographically reconstructed head and whisker motions of freely moving mice searching for a randomly located rewarded aperture, focusing on trials in which animals appeared to rapidly "correct" their trajectory under tactile guidance. Mice orienting after unilateral contact repositioned their whiskers similarly to previously reported head turning asymmetry. However, whisker repositioning preceded head turn onsets and was not bilaterally symmetric. Moreover, mice selectively employed a strategy we term contact maintenance, with whisking modulated to counteract head motion and facilitate repeated contacts on subsequent whisks. Significantly, contact maintenance was not observed following initial contact with an aperture boundary, when the mouse needed to make a large corrective head motion to the front of the aperture, but only following contact by the same whisker field with the opposite aperture boundary, when the mouse needed to precisely align its head with the reward spout. Together these results suggest that mice can select from a diverse range of sensing strategies incorporating both knowledge of the task and whisk-by-whisk sensory information, and,

moreover, suggest the existence of high level control (not solely reflexive) of sensing motions coordinated between multiple body parts.

2.2 Introduction

Active motion is a prominent element of many sensory systems, often involving coordination of multiple body parts, for example, coordinated eye and head motions in vision, or finger, hand, and arm motions during touch. The rodent whisker tactile system is one of the key models for active sensing (reviewed in [51–53,99,120,121] and has been especially prominent in studies of closed-loops through sensory and motor areas back to peripheral sensors [59]. However, research on sensing motions is often focused on whisker motion alone [122,123,55,124,125], while growing evidence suggests such motions are strongly coupled to head motions [45,71,90,96,103,105–108]. It remains unclear if whisker motion control is predominately reflexive, perhaps mediated by brainstem or other subcortical areas [90,91,104], or involves cortical areas also implicated in perceptual processing [60,126]. In particular, if the behavioral repertoire of rodent active touch involves tight coordination between whiskers, head and body, then a focus on neural pathways constrained within whisker areas may be incomplete.

There have been many behavioral studies of whisker sensing, but most have been designed in ways that we believe suppress understanding of "naturalistic" full body sensing strategies. To investigate specifically the animal's *selection* of coordinated sensing motions, a behavioral paradigm should have the properties that the animal (1) is

freely moving (*e.g*. as opposed to head-fixed [60,68,82,97,98,122,125,127–129]), (2) is not trained to exhibit prescribed head and whisker motions (*e.g*. as opposed to requiring placement of the nose at a particular location [28,70,71,96,108,130,131] or requiring craning over a ledge [76,90,94,103]), and (3) is goal oriented (*e.g*. as opposed to spontaneous exploration [91,104,132]). Moreover, if contacted objects are not goal related but instead irrelevant or surprising obstacles [105,107,133], it may be possible to determine important properties like reaction times, but be difficult to interpret motions in terms of choice of sensing strategies. For example animals may be ignoring whatever happens to their whiskers, or even trying to avoid contacts. In addition to these task properties, high resolution quantitative analysis should be made not only of whiskers, but also of head motions and object contacts (*e.g*. as opposed to contact-only tracking [94,134,135]). The above studies each incorporated some of these criteria, but each (appropriately) limited some aspects of behavior in order to isolate particular phenomena of interest. Our interest here is integrative, in the sense of asking what choices rodents make when all of the above criteria are met in a single task.

We quantitatively examined head-whisker coordination in freely moving mice searching for randomly located reward ports. We examine an apparent tension between "anticipatory" and "maximal contact" sensing strategies [58,90,91,103,104], and find mice can switch between these strategies in a situation-dependent manner. Moreover, we find whisker repositioning can begin prior to corrective head turns during reward search. The observed timing and situation dependence suggest a volitional contribution to

behavior not explained by simple reflexive models. In natural exploratory settings, motion for sensory acquisition may be accompanied by motions with overlapping use in navigation, threat assessment, or reward seeking. We suggest whisker repositioning may at times serve to counteract orienting head motions, in order to maintain useful sensory input despite underlying large scale motion.

2.3 Materials and Methods

Task Structure:

Six male, water-restricted mice were trained to repeatedly traverse a polycarbonate track (31 cm by 9 cm) in alternating directions to receive a water reward (Figure 2.1A,B). Rewards were dispensed from two spouts located at the center of apertures with a 1.4 cm opening. The arena was enclosed by vertical walls (5 cm high), and a polycarbonate cover wrapped in black tape that prevented rearing and provided a dark background for videography. During initial training, apertures on each side of the track were fixed in a central location. The initial training consisted of two 20-minute sessions per day for each mouse. The task was rapidly learned, and typically within 7–10 days the mice exceeded 80 trials per day, at which point one aperture became moveable.

On each trial, the aperture was moved to one of four possible locations, determined from a random ordering of positions that ensured equal sampling of each reward location within each block of 16 trials. The aperture was positioned by means of a vertical pole suspended from two stepper motor driven translation stages (Newmark System, Inc.),

located 20 cm above the arena top (the pole entered through a small sliding cover). Aperture repositioning occurred when the mouse was moving in the opposite direction (towards the fixed reward end of the track) as determined by IR photodiodes placed along the track.

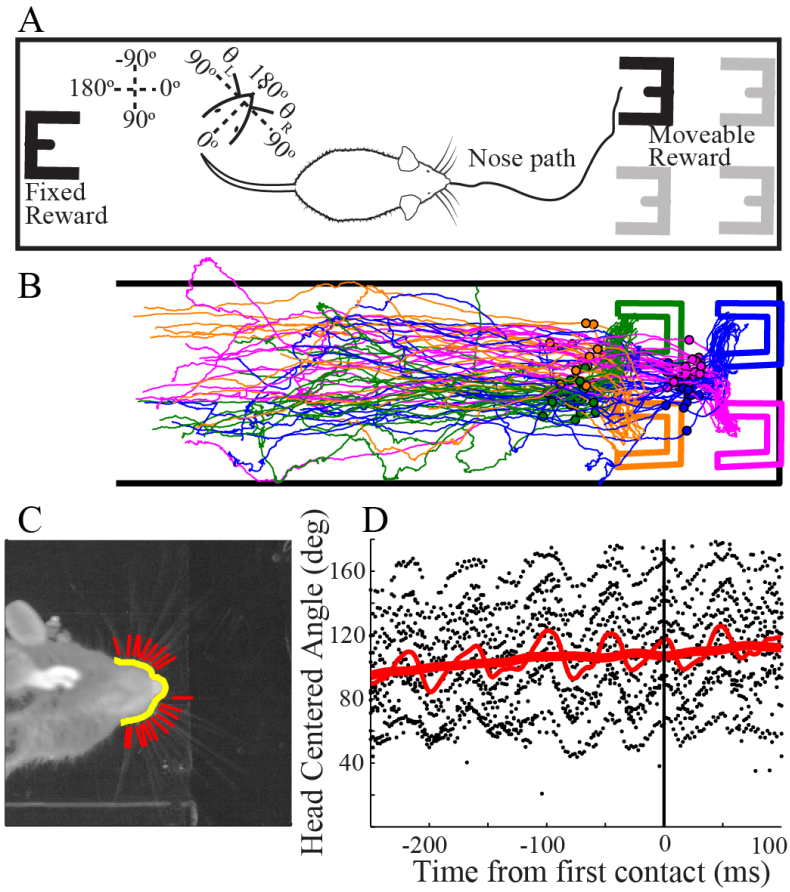

Figure 2.1: Freely exploring mice with intact whisker fields performing a tactile search task.

A, Mice were trained to repeatedly shuttle across a linear track under infrared illumination in search of a water reward dispensed within an aperture located in 1 of 4 possible locations. Insets show whisker position defined relative to the arena (counterclockwise), or relative to the head (180 degrees corresponding to full protraction). Head angles were always arena centered, with 0 degrees corresponding to rightward in the frame. **B**, Thin lines show nose paths on a subset of trials (n=85) for which the mouse made large head turns around the time of initial whisker contact with the aperture; paths are color coded to match the trial's aperture position (*thick outlines*). Dots show nose tip location in the frame identified as first aperture-whisker contact. **C**, Sample high-speed video frame showing the locations of automatically tracked snout and whiskers. **D,** Sample

whisker tracking for a single trial is shown aligned to first contact time. Black dots indicate the head centered angle of all tracked whiskers in each frame, the thin solid line indicates the robust mean whisker angle, and the thick line indicates the set-point (see Methods for definitions).

Data collection began once mice progressed to the moveable aperture task. Mice regularly performed upwards of 100 trials per 30-minute session, and the median trial duration was 1.1 seconds.

All behavioral sessions were conducted in the dark in a sound and light attenuating cabinet. The arena was illuminated by custom infrared LED panels along both long sides of the track. In order to confound possible auditory cues of aperture location, the aperture moved through a central 'home' position on its way to its new position for each trial, and stepper motors were activated for the same duration for each movement of the aperture. Trials where the mouse began an approach prior to the aperture reaching its new location were rejected. Water rewards were only dispensed once the snout triggered an IR-beambreak placed inside the aperture in order to prevent a possible olfactory cue if the reward were available early. All aspects of the behavioral session were fully automated to reduce the influence of a human operator on behavior.

High Speed Videography Tracking and Analysis:

A subset of trials each day were recorded at 500 frames per second (HSV; pco.1200hs camera, Cooke Corporation) through a mirror underneath the transparent track. The field of view of the camera encompassed approximately ¾ of the track length, focusing on the moveable aperture side of the track. Data storage was initiated by an infrared beambreak

located in the aperture, which triggered the download of the preceding frames from the camera's buffer using a custom Matlab acquisition GUI. The camera acquired the next trial after the previous clip had finished downloading, with no experimenter involvement, to minimize selection bias. We recorded approximately 20–30 high-speed clips per session. The entire session was recorded using a standard camcorder (30 frames per second) to provide an overall record of behavior.

High-speed videography was background normalized using the average of fifty frames prior to the mouse starting to traverse the track. Additionally, we identified the location of corner features on the track itself and used these locations for image registration. Preprocessed video was analyzed using the BIOTACT Whisker Tracking Tool [83], after importing video using a custom programmed loader for our file types. We first tracked snout position using the functions ppImageTransform, sdGeneric and SStShapeSpaceKalman. After ensuring accurate snout tracking, and retracking any regions with errors, we tracked whisker positions using ppImageTransform and WdIgorMeanAngle. Parameters were selected for each clip iteratively with manual reviewing of tracking results, and retracking as necessary to ensure visually accurate whisker identification. The algorithm identified each whisker in each frame, but did not attempt to track an individual whisker from one frame to another. We used raw information on the angle of each tracked whisker relative to the snout midline for further analysis. We did not make use of the mean angle calculation included in the software, but instead found it necessary to develop a robust estimate of the mean that was more reliable

in our task condition.

Using the arena-centered angles of a large subset of whiskers (~20 on each side of the face in each frame) found by automated videographic tracking (Figure 2.1C) [83], we combined the individual angles in each frame, separately on each side of the face, with iteratively reweighted least squares that reduced the impact of errors in tracking for the most posterior or most anterior whiskers, which functioned as outliers on the mean angles (Figure 2.1D). Applying the least squares fit with a window of 15 ms temporally smoothed the two mean angles to produce "instantaneous" left and right pad angles (Figure 2.1D, *thin red*). We defined the *set-point* on each side as the angle after application of additional smoothing with a 100 ms window, which removed the contribution from individual whisks and reflects the position of the whisker field on a longer timescale (Figure 2.1D, *thick red*). Smoothing operations were computed using non-causal robust weighted liner least squares [136].

We then defined the (acute angle) mean of arena centered left and right set-points as M_{SP}, the "net direction" of bilateral whisker positioning. Note that this way of estimating net whisker angle is independent of head direction. We defined the whisker positioning asymmetry, θ_{ASY}, as the difference between M_{SP} and the arena-centered head angle defined by the midline through the automated tracker's outline of the snout. In other words, if the set-points of the left and right whisker fields are equal, θ_{ASY} will be zero. This condition would correspond to whisking symmetrically on each side of the face. If

the left whiskers are more protracted than the right, θ_{ASY} will be positive, and if the left whiskers are relatively more retracted, θ_{ASY} will be negative. These asymmetric whisking conditions often arise during orienting behaviors. This approach is robust to asynchronous whisking while still providing a measure of asymmetry on a frame-by-frame basis. Given that the anterior whiskers nearly always come into contact with the target first in our task, we also modified the analysis to provide estimates for anterior and posterior whiskers separately, by first sorting tracked angles in each frame into top and bottom quartiles, respectively, and then repeating the above analyses.

Identifying whisker contact and head turn onset frames

We manually identified the frames of first whisker contact with the aperture (FC), and of first whisker contact with the opposite side of the aperture (OC) during orienting. To control for the inherent difficulties in identifying whisker tip locations and contacts, two observers independently assigned numerical scores (range: 1–3) for the likelihood of a contact in all potential first contact frames (possibly across multiple whisks), and separately chose which frame was most likely to be the first contact. The observers produced consistent results (median absolute difference 2 frames, or 4 ms, with interquartile range 16.25 frames). In addition, many of the subsequent analyses are robust to misidentification of first contact frames. For example, Figure 2.2C does not depend on accurate knowledge of first contact time, and Figure 2.5 depends only on identifying the correct contacting whisk, not the specific video frame where contact first occurs.

The noise in head angle as determined by the automated video tracker made it difficult to precisely determine head turn onsets. However, as the long axis of the arena over which animals travel is oriented horizontally in our images, the change in vertical position of the snout during turns provided another measure of onsets with smaller noise floor. We calculated the slope of a linear fit within a sliding 100 ms window (t:t+100 ms) of the frame-by-frame absolute difference between nose and reward port vertical position. We chose the window size based on typical turn durations. We identified turns as the frame with minimum slope within ±400 ms of identified first contacts. This time range allows detection of turn onsets during the majority of the trial, but prevents spurious detection of motions when the mouse is near either reward port. Identified turn onsets were visually consistent with video frames where observable head motion began.

2.4 Results

Tactile search behaviors during the task

We observed six mice performing a tactile search for a water reward located at the center of an aperture automatically positioned in one of four randomly selected locations prior to the start of each trial (Figure 2.1A). Automated tracking of head and whisker positions in high-speed video was used to facilitate the analysis of coordinated sensing motions during this search task. We observed a variety of approach trajectories. In some cases, mice happen to approach the aperture straight on, while in others they tended to traverse the track along one wall, then pull away from the wall when nearing the reward area. We focused on a subset of trials where mice made large corrective head motions during the

final stages of approach to the aperture (Figure 2.1B). We selected trials where the distance (along the short axis of the arena) from the tip of the snout to the center of the aperture was greater than the width of the aperture opening at the time of first whisker contact. These trials each contain two situations of whisker contact: first contact with the near edge of the aperture, then, after repositioning, first contact by the same whisker field with the opposite aperture edge. Also, by construction, initial contact was made by whiskers on only one side of the face. This subset of trials exemplifies whisker mediated sensory orienting, and provides a rich environment to evaluate the selection of active sensing strategies that require coordinated head and whisker motions. We analyzed 85 such trials for a total of 105.3 seconds (52664 frames) of tracked high-speed video data.

Asymmetric whisker positioning begins before head turns

The first quantification of head-whisker coordination found that, during head turns in the absence of contact, rats can adjust the difference between left and right set-points proportionally to head angular velocity [90]. For example, when turning to the left, the left set-point retracts and the right set-point protracts. A similar behavior was later reported for spontaneously exploring mice [58]. This head turning asymmetry (HTA) serves to position the whiskers in the area towards which the head is moving, possibly as a reflexive response to head turns similar to the vestibulo-collic reflex (VCR), thus allowing the whiskers to "look ahead" in space [90]. HTA was defined in the above studies by measuring the correlation of instantaneous differences in whisker position (left minus right head-centered angles) with instantaneous head angular velocity relative to the

arena. This definition has several limitations, notably the necessity of observing over large durations to obtain these distributions before HTA can be assessed. Additionally, the method encounters difficulties during periods of asynchronous whisking, which are especially prominent following contacts [90,137]. This is an especially important concern in mice, which exhibit irregular whisking compared to the nearly periodic whisking of rats [58,76,89]. During asynchronous whisking, the instantaneous difference in whisker positions may not accurately reflect both fast whisking motions and slow set-point adjustments. For these reasons, we developed a complementary analysis of HTA and similar relationships between head and whisker angles adapted for single trials and single whisks (see Methods).

A key question is whether the onset of whisker repositioning precedes head turning, suggesting a volitional or predictive sensing mechanism, in contrast to proposed analogy to vestibular reflexes [58,90]. Figure 2.2A,B shows an example single trial in which the mean set-point (M_{SP}) begins to change within the first 20 ms following first contact, while the head angle does not begin to change until around 75 ms following contact. In this example, the mouse is turning to the left and exhibits a retraction of the left whisker field, which drives M_{SP} downward prior to the onset of head turning (note in Figure 2.1 that arena centered angles follow a clockwise convention to be consistent with the direction of head centered angles on the animal's left). Visual inspection of the same trial highlights the whiskers adjustment prior to head motion (Figure 2.2A).

We investigated the relative timing over many trials by assessing the timing of changes in asymmetry (θ_{ASY}). Figure 2.2C shows summary data for 85 trials with θ_{ASY} aligned to the time of head turn onset. In order to combine data over all trials, we vertically reflected videos with rightward turns so that all turns appear to be leftward. We find that asymmetric repositioning precedes turn onsets by approximately 125 ms, and that by the time an identifiable change in head angle occurs, the asymmetric repositioning of set-points has already reached its maximum value. Whether the repositioning is a response to contact or an anticipatory preparation for a turn based on past experience, the timing argues against a reflex response to the turn itself.

The timing of initial contact is widely distributed with respect to turn onset, but predominately occurs before the start of a turn (81%, 69/85 trials; Figure 2.2D). In cases where head motion onset preceded whisker contact, 62.5% of trials (10 of 16) had the aperture located in one of the two rear positions, and for turns that preceded whisker contact by more than 50 ms, 90% of trials (9 of 10) had the aperture in a rear position. Thus mice may adjust their search trajectory once they know the aperture is not located in either of the 2 forward locations, which may account for the subset of trials in which head motions were observed prior to whisker contact. This possibility is further supported by the convergence of nose trajectories in rear aperture trials (Figure 2.1B, *blue and magenta traces*) between the forward and rear aperture positions. It is also possible some first contact times were misidentified due to limitations in videography; however, we

attempted to mitigate these issues though multi-observer identification of contact frames (see section 2.3).

Asymmetric repositioning is nearly unilateral

In the simplest model of head turning asymmetry, the whisker field on the turning side retracts and the field on the contralateral side protracts, inducing a bilateral shift towards the area the head is about to enter. Previous reports of HTA did not specifically evaluate the bilateralism of repositioning [58,90], although different adjustments of each whisker field, including pronounced contralateral side protractions, have been reported for rats responding to unilateral object contact [91]. In that study, the observed behavior appears consistent with the notion of positioning each whisker field to maximize the number of whiskers impinging lightly on the surface. Such a strategy may not be broadly applicable to all unilateral objects contacts, and so we asked whether repositioning in this task involved both whisker fields equally, and if not which side was responsible for the majority of the observed repositioning. Figure 2.2E shows the trial averaged whisker set-points for the contacting (green) and non-contacting (black) sides of the face, aligned around first contact (n=85 trials). To combine trials, we reflected trials with rightward turns, so that all turns appear to be leftward, before proceeding with analysis. Between the 100 ms before and 100 ms after contact, the whisker field on the side the mouse is turning towards adjusts by a mean 16.2 deg, compared to 1.1 deg on the contralateral side. Note that since mice are likely to be protracting at first contact (t=0), they are likely to have the whiskers relatively more retracted just prior to contact.

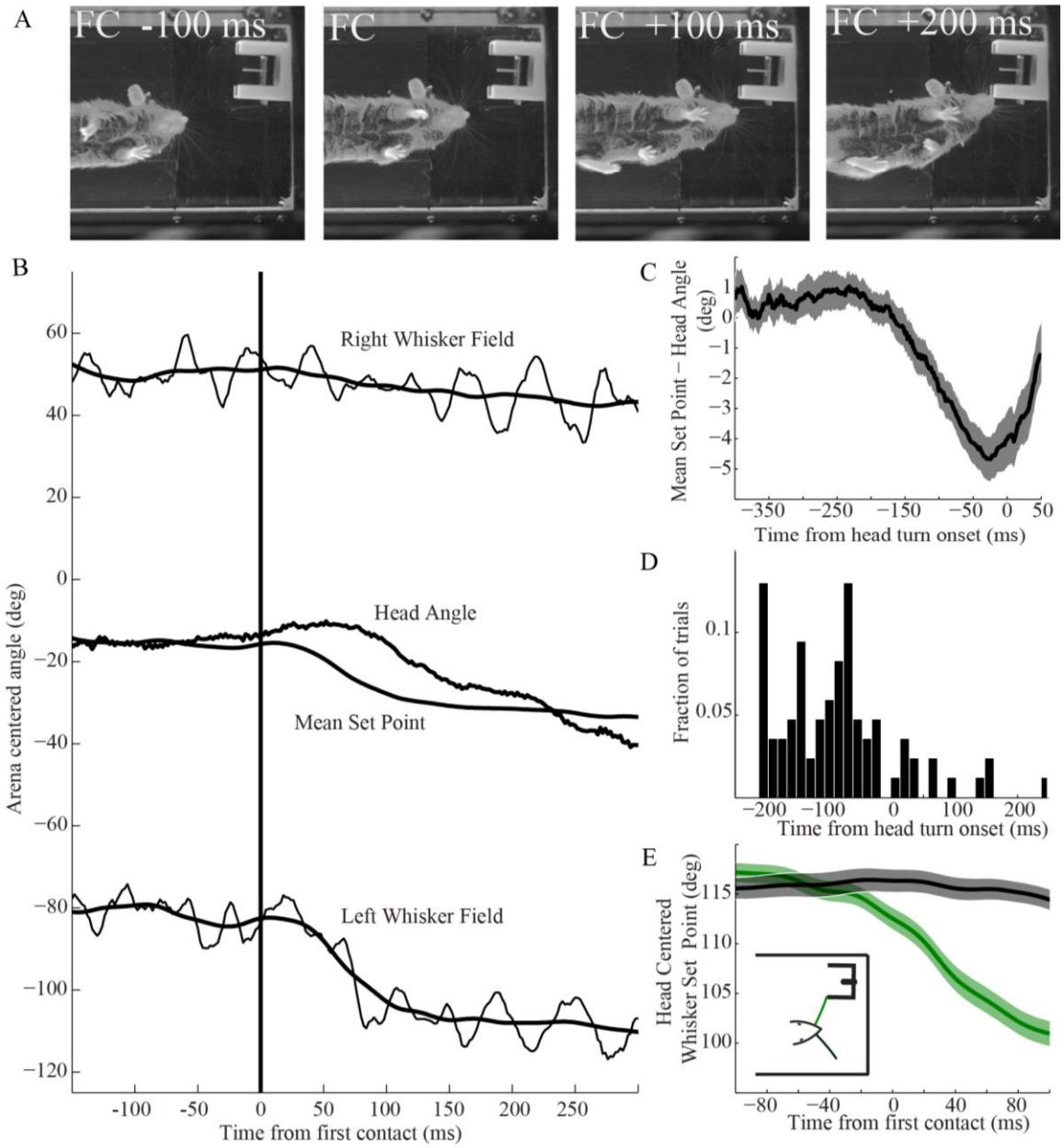

Figure 2.2: Whisker repositioning following first contact precedes head motion, is in the direction of the turn, and is mostly unilateral.

A, High-speed video frames from an example trial illustrate large retraction of the left (contacting side) whisker field within 100 ms post-contact. **B,** Arena centered whisker and head angles are shown for the example trial in ***A***, aligned to the time of the first whisker-aperture contact (unilaterally on the left side). The mean set-point shows repositioning of whisker angle prior to the onset of a head turn, which begins about 75 ms after first contact. Repositioning is dominated by retraction of the set-point on the side the mouse is turning towards, with at most a small change of the contralateral set-point. **C,** Whisker asymmetry (difference between mean set-

point and head angle) develops ~125 ms prior to the onset of a head turn, suggesting that repositioning cannot be fully explained by a reflex response to the turn itself (n=85, mean ± SE). To combine data across trials, trials with rightward turns were reflected vertically so that all turns appear leftward. **D,** Histogram of manually identified first contact times relative to turn onsets for the trials in ***C*** shows that the majority of turns follow contact, while in a small fraction of trials the mouse may initiate a turn spontaneously, possibly due to expected location of rewards (see Results for further discussion). **E,** Trial averaging of set-points (n=85, mean±SE) shows that the asymmetry following first contact is dominated by set-point retraction on the initially contacting side (mean change from 0–100 ms, 16.2 deg, *green curve*), with only small changes on the non-contacting side (mean change from 0 to 100 ms 1.1 deg, *black curve*). The mean differences between contacting and non-contacting side pre-contact (-100 to 0 ms) were not significant (p=0.28), while the differences post-contact (0 to 100 ms) were ($p= 2.0 \times 10^{-13}$). Rightward turns were reflected as in **C**. Inset shows a schematic of mouse at first contact with whisker color convention.

Averaged set-points then appear to "predict" contact (drop slightly before contact time) when this selection bias in pre-contact angle is smoothed with the decrease in set-point after contact (contrast with the individual whisks visible in Figure 2.4A). The difference between the distributions on each side 100 ms following contact are significant (t-test, $p=2.0 \times 10^{-13}$), while 100 ms before contact there is no significant difference between the two sides (p=0.28). Additionally, the differences between the pre- and post-contact contralateral whisker angles were not significant (p= 0.45). This summary agrees with our informal observation in single trials that the majority of set-point adjustment occurs on the turning side (as in the example in Figure 2.2B). The precise nature of asymmetric repositioning following contact, and how much adjustment is provided by each whisker field, is likely to be situation-dependent.

Asymmetric repositioning allows whiskers to "look ahead"

Asymmetric repositioning of whisker set-points may serve to place the whisker field in a useful location for the imminent head motions [58,90]. We estimated the amplitude by

which M_{SP} leads changes in the head angle by comparing linear regressions of the two quantities for 150 ms before and after initial whisker contact (Figure 2.3). Both before and after contact, the regression slope is near one (0.86 / 0.90) with a strong correlation ($r^2 = 0.71$ / 0.73), reflecting a strong relationship between head angle and (arena centered) whisker positioning. Prior to contact, the y-intercept is near zero (-0.03 deg), consistent with whisking at a fixed set-point relative to the head (or a whisker held at a fixed angle relative to the head). Following contact, the vertical-intercept of the distribution shifts upwards to 6.3 degrees ahead of the angle expected without repositioning, consistent with the idea that whisker repositioning serves to place the whiskers into the region that the head will soon enter.

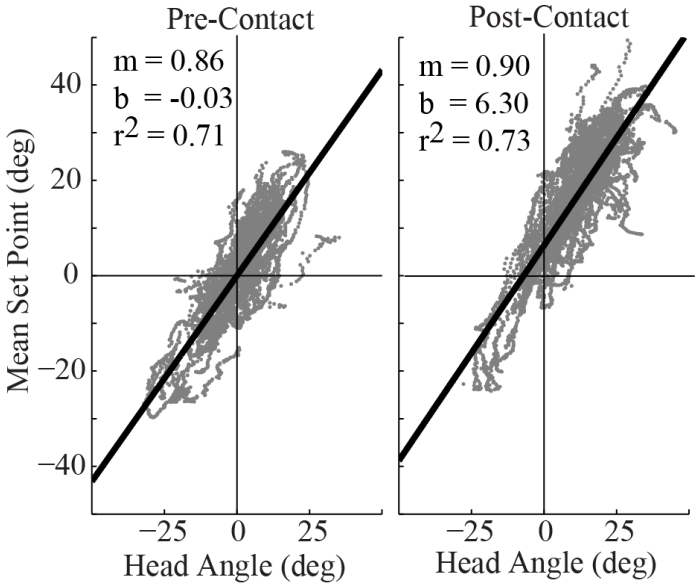

Figure 2.3: Active sensing strategy shifts following unilateral contact.

The arena centered mean set-point on the contacting side is linearly correlated with head angle, shown by grey dots for each frame within 150 ms before (*left*) or after (*right*) first contact (n=85 trials), and the best fit line (fit parameters in inset). In order to combine trials, videos were vertically reflected as needed to put all head turns in the same direction, as if to the animal's left (upward in the video frame). Following contact, the distribution shifts upward by approximately 6 degrees, indicating that the whiskers are repositioned in advance of head turns.

The observation of this shift only following contact, and not for changes in head angle prior to contact, suggests the animal is selecting an active sensing strategy for each situation and transitions from one state to another based on the information derived from aperture contact and knowledge of the arena. Note that our analysis compares whisker asymmetry against head position, in contrast to earlier analyses against head angular velocity [58,90].

Responses to contact are situation-dependent

We next asked if there are differences in repositioning of the same whisker field in two different behavioral situations within a trial. The first situation occurs when the mouse makes initial unilateral whisker contact with one of the aperture boundaries (Figure 2.4A, top left panel). The second occurs when, after changes in head position, that same whisker field makes contact with the far side of the aperture (Figure 2.4B, top left panel). If responses to whisker contact are driven primarily by simple reflexes, we would expect to see similar whisker repositioning in each of these contact conditions, and based on previous reports would predict contact induced retractions or suppression of protractions of the contacting side whisker field [60,91,104,138]. However, during the head turn the animal is likely trying to find the far side of the aperture, and would instead need to counteract head rotation, a behavior we term *contact maintenance*.

Figure 2.4A shows the averaged head-centered field angles, similar to Figure 2.2E for set-points but here without additional smoothing, and separated into anterior and

posterior whiskers, demonstrating again a retraction of the contacting side whisker field (*green*), with a comparatively modest adjustment on the contralateral side (*black*).

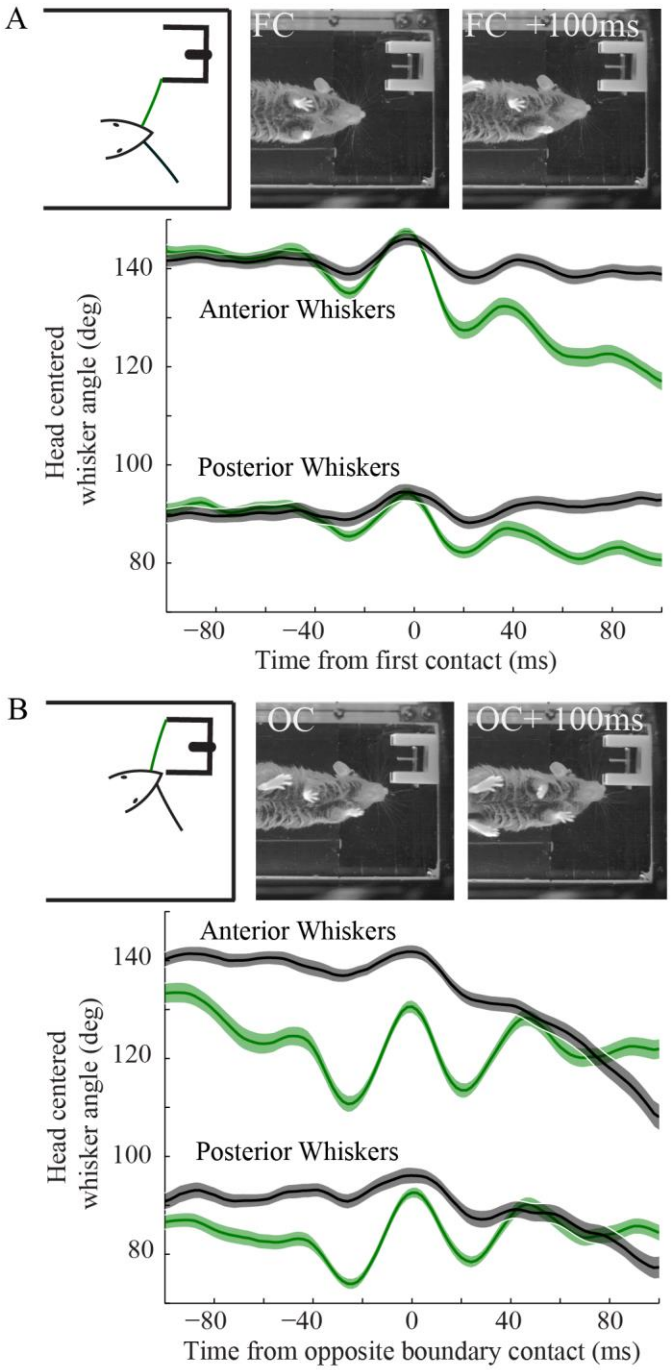

Figure 2.4: Asymmetric repositioning depends on the behavioral situation in which a whisker contact occurs.

A, Following initial, unilateral contact with the aperture (FC; whisker color convention in schematic), example video frames show pronounced contacting side retractions within 100 ms post-contact. Separate averages of anterior and posterior whisker angles (see Methods), aligned to first contact time, show rapid and pronounced contacting side retractions (*green curves*), with relatively minor contralateral adjustment (*black curves*) (n=85 trials, mean+SE). Anterior whiskers underwent greater adjustment than posterior whiskers. To combine data across trials, trials with rightward turns were vertically reflected so that all turns appear leftward. **B**, In contrast, when the same whisker field contacts the opposite aperture boundary (OC; whisker color convention in schematic), the contacting side whisker aligned average (*green curves*) reveals large amplitude whisking (temporally consistent across trials) around a nearly constant set-point (n=85 trials, mean+/-SE). The angle of the contralateral whiskers (*black curves)* decreases as they are pushed against the outer edge of the aperture. Trials with rightward turns were reflected as in A.

However, we did not observe a retraction of the contacting side whisker field later in the trial, when the same whiskers made contact with the far side of the aperture (Figure 2.4B). Instead, these whiskers maintain a relatively consistent set-point, and the appearance of periodic peaks in the contacting side aligned averages indicate that the mouse is whisking with a consistent temporal structure (across trials) around the time of initial contact with the opposite side. The different responses to putatively comparable whisker contacts suggest that repositioning could be sensitive to the specific situation of the contact within the larger task structure. The two different responses to contact are visually apparent in an example trial by comparing the retracted whisker position 100 ms after initial contact (Figure 2.4A, top right panel) with the relatively protracted position 100 ms after contact with the opposite boundary (Figure 2.4B, top right panel). While the entire whisker field is adjusted after contact, we observed a difference in magnitude across the pad, roughly similar to that reported by Grant, et al., (2009), with larger adjustments of anterior than posterior whiskers (Figure 2.4).

Contact maintenance as a parallel strategy to head turning asymmetry

We defined contact maintenance as an adjustment of set-point that counteracts head turning to sustain object contacts. In particular, during a turn towards an object of interest, contact maintenance would result in repositioning of whiskers that is in the opposite direction to the predictions based on head turning asymmetry. To quantify the possible presence of this sensing strategy, we calculated the deviation between the arena centered whisker angle and a "dead reckoning angle". The dead reckoning angle is defined as the angle in arena centered coordinates from the center of the head to the putative contact point on the aperture boundary. If the whisker angle matches the dead reckoning angle (that is, the deviation is zero up to small whisker pad/ base point displacements), the whisker field is pointing directly at the contact point, whether or not it is actually touching. The use of dead reckoning accounts for both translation and rotation of the head when comparing whisker positioning relative to the object. We evaluated the differences between the whisker angle and the dead reckoning angle to the contact points on each side of the aperture (Figure 2.5A).

Figure 2.5B shows an example trial. First contact occurs at t=0 ms, at which point the actual whisker field angle (*thin black trace*) is very close to the dead reckoning angle to the right side (*red trace*). By the next whisk after initial contact, however, the left whisker angle deviates from the dead reckoning angle to the initial aperture boundary. The left whisker field contacts the opposite aperture boundary at around t=175 ms (*vertical black indicator*). In the whisks following contact with the opposite boundary, whisking

parameters are adjusted to compensate for head motions such that the protractions on subsequent whisks track changes in the dead reckoning angle to the opposite aperture boundary (*thick black*); note head angle continues to change. In other words, the compensatory changes in whisker motion that define contact maintenance are observed only in response to contact with the opposite boundary, when the mouse is attempting to align its snout with the aperture interior to reach the reward spout. Figure 2.5C shows representative video frames corresponding to the example trial (Figure 2.5B) for first contact (FC; top), opposite contact (OC; middle), and 200 ms after opposite contact (OC + 200ms; bottom).

In order to examine this effect across all trials, we identified individual whisks between angular local maxima and minima, and evaluated the angles at protraction and retraction for the four whisks before and after initial contact. This whisk-by-whisk analysis facilitates comparisons across a range of trial durations, where simple averaging of continuous time series is ill defined. We examined four whisks preceding and following contact because the mice typically make 2–3 contacts with the far aperture boundary before the snout enters the aperture. Past this point the whiskers tend to be mechanically forced backwards. We evaluated the difference between the anterior field angle and the dead reckoning angle at both peak protractions (*green*) and retractions (*blue*) for the four whisks before and after the initially contacting whisk (Figure 2.5D). Using this metric, contact maintenance would be evident if the difference from dead reckoning at protractions (*green*) moves closer to zero following contact. Initial contact does not lead

to contact maintenance; by the next whisk after first contact, anterior whiskers pull away from the dead reckoning angle (Figure 2.5D, top panel, *green curve*). Within the next four whisks, however, whisker repositioning reduces the difference between the anterior angle and the dead reckoning angle to the opposite aperture boundary (Figure 2.5D, bottom panel, *green curve*).

If it were the case that the mouse ceased whisking and the changing field angle was due to passive mechanics of the whiskers held against the object as the head moved, the difference from dead reckoning angles at observed protraction and retraction would be the same. Instead, we see the difference between protractions and retractions increase following contact, indicating that the mouse is on average increasing the amplitude of whisking on the ipsilateral side. Rather than protractions being cut off by contact with the aperture and being unable to advance further, the set-point is being adjusted such that large amplitude whisking continues, but with the protraction amplitude modified based on object location. This analysis highlights that the mouse is not simply leaving the whiskers pressed against the contact point once locating the aperture, but continuing to whisk throughout the approach.

To further explore the question of active repositioning, we simulated a fixed whisker model (Figure 2.5D, *brown curve*) where the angle is fixed relative to the head (at the average angle within the 500 ms preceding contact). Angle changes in the fixed whisker model are wholly due to head motions and are insufficient to account for the observed repositioning with either the first or the second aperture boundary, as seen by the

differences between the green and brown curves in Figure 2.5D.

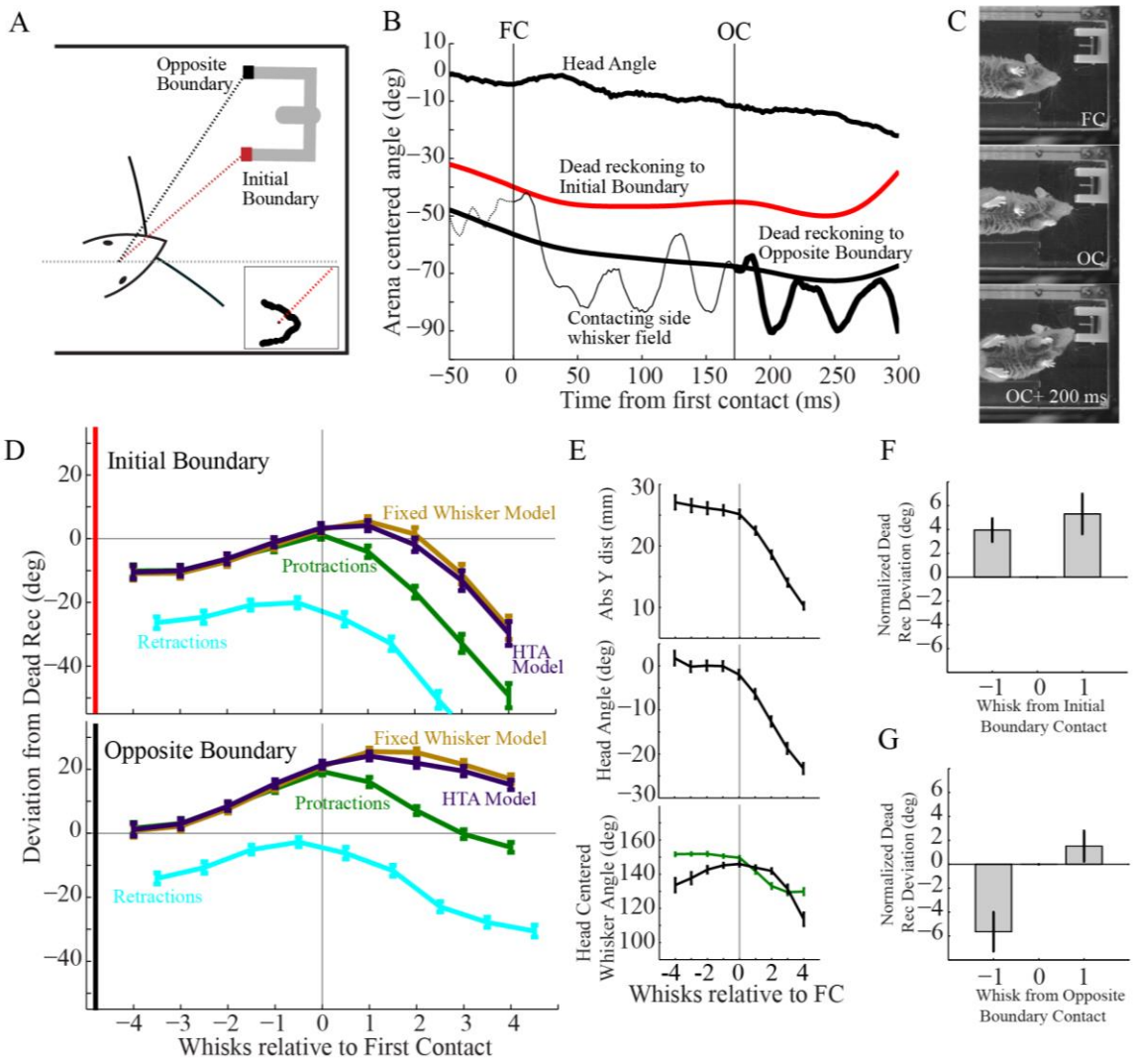

Figure 2.5: Contact maintenance is an actively selected sensing strategy.

A, Dead reckoning angles are defined by the line from the center of the head to a point of possible object contact, shown schematically by black and red dashed lines for the initial and opposite boundaries. The dead reckoning angle is the arena-centered angle at which whiskers would point directly at the object, whether contacting or not, and accounts for contributions from both head translation and rotation. Note that since whisker angles are estimated near the whisker base, ignoring curvature (and in this figure are averaged across anterior whiskers), it is possible for whisker tips to make object contact at small deviations from the dead reckoning angle. Inset shows an example frame of snout tracking with the calculated dead reckoning line from the head to the initial contact point for that trial. **B**, An example trial shows that at first contact (FC; 0 ms; *thin vertical line*) the whisker angle (*thin black curve*) is close to the dead reckoning angle to the initial boundary (*thick red curve*), but by the next whisk shifts closer to the opposite boundary

(*thick black curve*). After contacting the opposite boundary (OC; ~175 ms; *thin vertical line*, and *thickened whisker angle curve*), the protraction amplitude tracks the opposite boundary dead reckoning angle. **C,** Video frames corresponding to the example trial shown in **B** for times of FC, OC, and OC+200 ms. Following opposite side contact, the snout trajectory passes very close to the near aperture boundary, resulting in the contralateral whiskers being mechanically forced backwards. **D,** Trial averaged deviations from dead reckoning are shown for peak protraction (*green*) and retraction (*cyan*) angles, in whisks around the first contact with the initial aperture boundary (n=85, mean ± SE). Videos were vertically reflected as needed to make turns appear leftward. Contact maintenance with the first aperture boundary is not observed, as protraction angles move away from zero in the four whisks following contact (top panel). Contact maintenance is observed when the second aperture boundary is contacted (bottom panel; note alignment is still to first contact with the initial aperture boundary), as the green trace moves towards zero in the four whisks following contact. For comparison, a model whisker fixed relative to the head (*brown*) and a model whisker whose position is simulated to match published head turning asymmetry (*purple*; see Results) show that neither of these mechanisms is sufficient to account for the observed repositioning. **E,** Head translation (top), arena centered head rotation (middle), and whisker rotations (bottom; initially contacting whiskers in *green*, contralateral whiskers in *black*) are shown relative to time of first contact. Dead reckoning incorporates both head translation and rotation, to place the object in head centered coordinates for direct comparison to whisker angle. Rightward turns were reflected as in **D**. **F,** Summary of normalized deviations from dead reckoning for the whisk before and after initial boundary contact (the deviation during the contacting whisk is subtracted) show significant differences from dead reckoning on both the pre- and post-contact whisks, and an absence of contact maintenance (n= 85, mean±SE). **G,** Same analysis as ***F*** for the whisks before and after contact with the opposite boundary shows small deviations post-contact and maintenance of contact angles (n= 85, mean ± SE).

Furthermore, we evaluated whether a model of head turning asymmetry was sufficient to explain the repositioning (Figure 2.5D, *purple curve*), without requiring any further retraction. We found the average whisker angle during the pre-contact period by subtracting the anticipated contribution from HTA in each pre-contact frame (head angular velocity x HTA coefficient) from the mean pre-contact whisker angle. We then estimated an expected amount of asymmetry for each frame following contact by multiplying the instantaneous head angular velocity by the largest HTA coefficient (115 ms) reported in the literature [90]. We then adjusted the whisker angles on both sides from their pre-contact means by the equal amounts with opposite signs to achieve the

predicted value of asymmetry for each frame. We found that, at the head angular velocities experienced in this task, the degree of repositioning far exceeds what would be expected from reports of HTA

The comparison between arena centered whisker angles and the dead reckoning angle incorporates changes introduced by head translation, head rotation, and whisker rotations. Figure 2.5E shows that head translation (measured as the absolute distance in the Y direction from the snout to the aperture), head angle, and contacting side whisker angle are all modulated in the whisks immediately following first contact. In contrast, the contralateral whiskers (Figure 2.5E, bottom panel, *black trace*) do not show adjustment until approximately the third whisk post contact. The mice generally adopt a strategy where the snout remains close to the near side aperture boundary during repositioning, as opposed to pulling the entire head backwards and approaching again. As a result, once the animal begins entering the reward aperture, the contralateral side whiskers are mechanically forced backwards by the near side aperture boundary, rather than engaging in an active repositioning strategy such as contact maintenance (example shown in bottom panel of Figure 2.5C).

We further quantified dead reckoning deviations for the whisks immediately preceding and following initial contact (Figure 2.5F), and preceding and following contact with the opposite aperture boundary (Figure 2.5G). The deviation on the frame of contact is subtracted (hence the deviation at whisk ‘0’ is 0 deg) from the deviations before and

after; this normalization accounts for small errors between the true contact location in each trial and the point selected to compute dead reckoning. We find that around the initial contact, both the preceding and following whisks showed large differences from dead reckoning (3.9±0.11 deg and 5.3±0.18 deg, respectively), both significantly different from zero (t-test, $p= 7.7x10^{-5}$ and p= 0.002, respectively). Around contact with the opposite side, however, a large deviation on the preceding whisk (-5.6±0.18 deg, significantly different from zero, t-test, $p= 7.4x10^{-4}$) is followed by a smaller deviation after opposite boundary contact (1.5±0.14 deg, not significantly different than zero, t-test, p= 0.23). This reduction in deviation only to the opposite boundary contact point supports the hypothesis that contact maintenance is employed selectively and is not a fixed motor response to contact.

We also asked if the magnitude of initial angular adjustment following first contact appeared directed towards the opposite boundary. If mice are able to estimate the distance to the aperture (for example, by sensing radial distance of whisker contact [101]), they could use that information along with knowledge of the arena to predict the opposite boundary location. To address this question, we compared the magnitude of the retraction following first contact to the size of retraction that would have been needed to match the whisker angle to the opposite boundary dead reckoning angle (Figure 2.6A). Values less than zero show retractions that exceeded the size needed to match the dead reckoning angle. We observed mice typically exhibited larger retractions (-9.1±1.9 deg) than would

have been expected if they were modulating the retraction towards an expected, learned position.

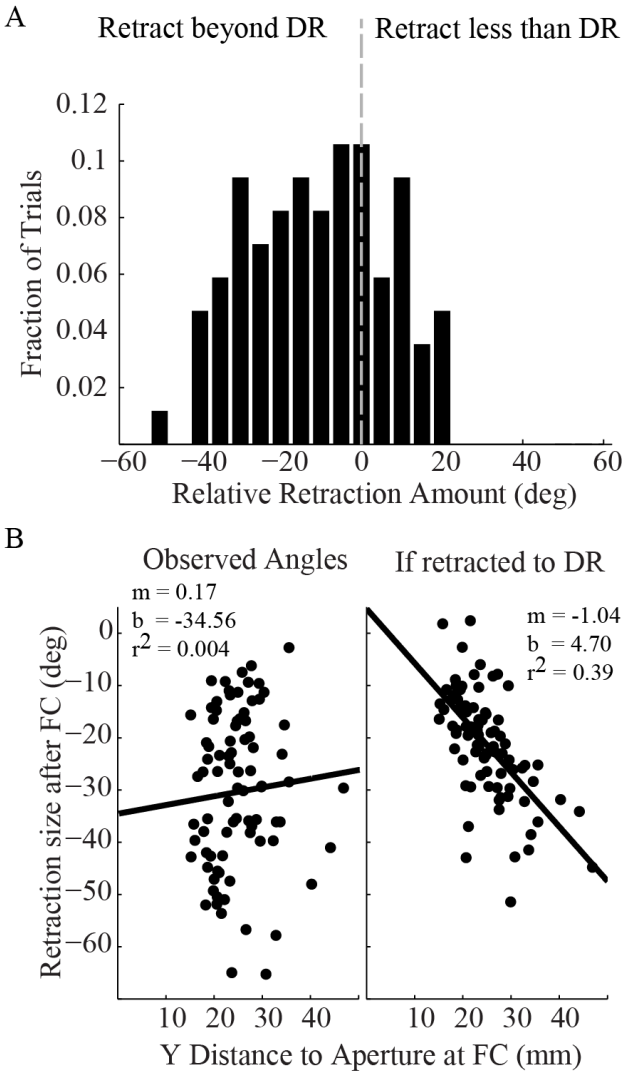

Figure 2.6: Retraction following first contact (FC) is not directed towards the opposite boundary.

A, Histogram showing the magnitude of post-FC retraction, relative to the size of retraction that would have placed the whisker field on the dead reckoning line to the opposite boundary (n=85 trials). Values less than zero indicate retraction magnitudes larger than necessary to match dead reckoning. **B,** Scatter plots of the size of post-FC retraction against the distance (along the short axis of the arena) from the snout to the aperture at FC time (n=85 trials). Real data (*left*) shows no correlation. There would be a negative correlation if the retraction magnitude equaled the dead reckoning angle (simulated in *right panel*).

To test whether mice adjusted their retraction amplitudes by their location relative to the aperture, we regressed the size of the retraction after first contact versus the (vertical) distance from the snout to the near aperture boundary (Figure 2.6B, left). We observed a wide range of retraction amplitudes (typically 15–35 degrees), but found no relationship between the distance at first contact and the size of retraction. For comparison, we examined what this relationship would look like for a simulated retraction made equal to the size needed to match dead reckoning (Figure 2.6B, right), and found a correlation between distance and retraction size ($r^2 = 0.39$). These results together suggest that the mouse is not using contact distance to adjust the size of retraction immediately towards the opposite boundary. Instead, the large post-contact retractions appear similar to head turning asymmetry during the head turn towards the aperture, followed by upregulation of whisking amplitude until opposite contact occurs.

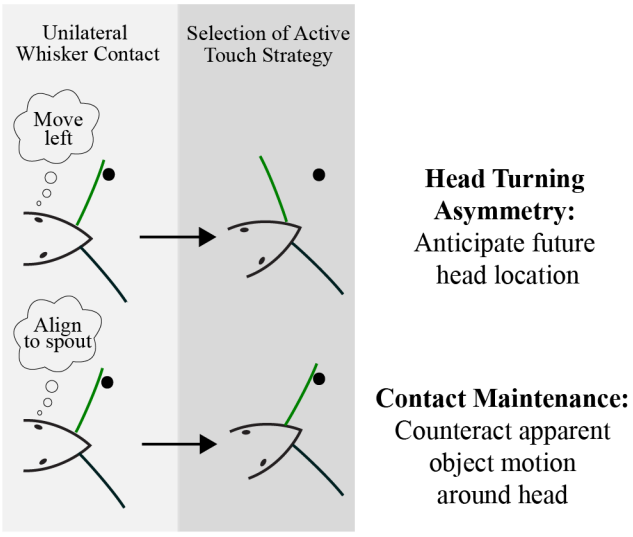

Figure 2.7: Conceptual summary of active sensing strategy selection.

Mice may exhibit a range of sensing behaviors following similar unilateral whisker contact, depending on the behavioral situation. When moving the head into a new area (*e.g.* reorienting after contact with the initial boundary), we observe contacting side set-point retractions expected

from previous reports of head turning asymmetry [58,90]. In contrast, when keeping whiskers on a surface is useful for task completion (*e.g*. contacting the far side aperture boundary), mice might employ a strategy of contact maintenance, where set-point adjustments counteract head motion in order to ensure repeated contact on subsequent protractions. The latter is consistent with a maximal contact strategy [91], now conditionally situated within a goal-oriented task, and not necessarily dependent on force feedback from contacts. The ability of mice to select from diverse sensing strategies based on the behavioral context of unilateral whisker contact suggests possible higher level whisk-by-whisk control, beyond contact induced or vestibular reflexes.

Although whisker contacts between the two sides of the aperture are unlikely to be mechanically identical, they are similar in the respect that they involve contact with an identically shaped and textured boundary by the same whisker field, and the two different situations of unilateral whisker contact are available for comparison within a given trial. The proposed selection between alternative sensing strategies in response to similar unilateral whisker contacts is summarized in Figure 2.7. The strategy of contact maintenance requires set-point adjustments that oppose those expected by head turning asymmetry, and we observe this strategy in some behavioral situations, where such contact maintenance may be most useful for the fine positioning needed to reach reward.

2.5 Discussion

The information available in neural pathways during active touch will depend on behavioral choices involving multiple body locations (*e.g*. feet, head, and whiskers), so that neural function occurs within the context of a "global" sensing strategy. We investigated how multiple degree of freedom coordination is organized in mouse whisker touch, specifically head-whisker coupling.

Previous reports showed mean whisker angles to be negatively correlated with head angular velocity [58,90], without determining the individual contributions of each whisker field or the timing of whisker repositioning relative to turn onset. We estimated the turn onset time in our task by a change in head position, which provided a more precise and conservative (early) measure than head angle change. The timing could in principle by improved by electromyography (*e.g.*, in neck muscles), however with additional challenges related to muscle response times and interpretation of noisy EMG data. We observed mice asymmetrically reposition their whiskers ~100 ms prior to the onset of head turning, suggesting head-whisker coupling would not be due solely to a vestibular reflex, and may be under more sophisticated control. This would be true whether the turns were in response to unilateral whisker contact, the expectation of contact, or a central efferent signal.

Head turning asymmetry was reported for whisking in air [90] and spontaneous head turns during exploration of a largely featureless arena [58]. While persistent floor contacts occurred in the second study, no obvious benefit would accrue from orienting based on those contacts. Unsurprisingly, rats trained to make large sweeping head turns while craning from a platform and whisking into empty space [90] exhibited a larger degree of HTA than rats making spontaneous turns while exploring an enclosed arena containing no objects and minimal features, but including floor and wall contacts [58,106]. These differences in effect size, along with our finding of different repositioning in different circumstances (Figures 2.4, 2.5), suggest that rodents make

positioning decisions influenced by informational factors. The conclusion that simple, feed-forward motor programs or reflex responses are insufficient to explain the observed repositioning seen here, combined with previously described efferent signals in SI [51,76,139], the presence of sensory information in M1 to SI projections [140,141], the reported use of contact phase as an error signal to update estimates of distance [103], and short latency changes in whisking following SI stimulation [27,60], all support a whisk-by-whisk role for SI during selection of sensing motions.

A widely considered hypothesis is that bilateral control places each whisker field where it will acquire the most useful information, for example head turning asymmetry repositioning whiskers to "look ahead" into the region the head is moving [90] or mice modulating protraction amplitudes based on expected object locations [103]. We found both whisker fields need not contribute equally to repositioning, finding adjustment primarily of the turning and contacting whisker field. A mouse searching for a single object in a known arena, such as in our experiment, may have no reason for contralateral repositioning following unilateral contact. In a prior study where rats showed contralateral protractions when orienting towards a unilateral contact [91], the absence of repositioning in trials without orienting was attributed to attentional choice, and is consistent with our finding that repositioning responses are situation-dependent. Natural sensing strategies are complex and likely include reflexive contributions as well as central control. We have identified several aspects of sensing motions that do not appear to be explained solely by low-level feedback loops.

Experiments that independently manipulate the number and relevance (*i.e.* target/distractor) of anticipated object contacts would help clarify the mechanisms underlying detailed differences in whisker sensing strategies. It is worth contrasting search tasks with sensory discrimination tasks typically designed to study limits on sensory capabilities [92,131,94,134,142,55]. While the sensing strategy may influence the quality of acquired information, and hence task success [96,123], such studies likely underplay the closed-loop iteration that drives subsequent sensing motions. In contrast, here each contact is expected to be highly salient, and only minimal demands are placed on discrimination capabilities. Since the choice of active sensing behavior is of primary interest, the emphasis is placed on the sequence of acquired pieces of information and the associated iterative decision process. We suggest such designs should become more common for whisker based tasks, as a potentially powerful complement to studies of sensory fidelity, overt and covert attention, and decision making investigated extensively in visual and other systems [53,143–147]. Comparison of humans and rats in a simple localization task demonstrated that both used an iterative, convergent process to identify object location [102], and extensions of this paradigm could benefit from explicitly considering integration of other inputs (*i.e.* head or body motions) into the establishment of object perception. A distinct literature with overlapping conceptual content is sensor planning in robotics, which has also been informative to and informed by whisker touch paradigms [148–153].

We found that a similar contact by the same whisker field on the same trial can produce different repositioning in different situations (first contact with object, versus first contact on the opposite side of the object). Mice positioned their whiskers to maintain contact on subsequent whisks, but only when doing so was likely to be useful for task completion (Figure 2.7). Significantly, we saw adjustments on the next whisk following contact [104,125], in contrast to reports of rats taking 3–6 contacts to localize an object [96,143]. These differences may depend to some degree on task difficultly. A recent study of head-fixed mice [125], showed larger amplitude motor changes after initial compared to subsequent contacts with the same object (a pole). The differences we found between contacts with the near and far aperture boundaries reveal coupling to head motion that is not accessible for study in a head-fixed experiment. An additional confound in the head-fixed study was that the animal often responded to acoustic noise as the pole had to be moved into the whisker field, and not contact alone [125]. Another recent study [108] showed that rats are able to modulate sensing motions to maintain stable perception in the face of perturbations (*i.e.*, artificial wind); however, the animals needed only to determine relative pole locations while walking towards reward ports. Since maintaining contact with a located pole would not provide additional information, the strategy they observed of short initial contacts followed by a change in head trajectory toward an appropriate port is consistent with our view that animals select from available active sensing strategies in part based on behavioral goal. We find whisker motions are actively modulated throughout the approach, in a task that relies on tighter head-whisker coupling and in which the contacted object is the goal. The divergence from fixed whisker or

simple HTA models reinforce that active repositioning is dependent on whisker contacts. Mice engage in different repositioning behaviors given the situation in which a particular whisker contact occurs, from which we infer that repositioning incorporates contact information with past experience. Future interventional studies that manipulate activity in SI through stimulation timed to whisker motions [27], and measure resulting shifts in whisker and head motion could help clarify this relationship (see chapter 4).

Similarly, head-fixed experiments necessarily remove the contributions of head motion, which is likely important to navigation and sensory orienting, as suggested by evidence from the rodent head direction system [154–156]. The ability of rats to perform a bilateral discrimination task that requires intact whiskers, but in which they did not whisk [71] further highlights the importance of considering head and body positioning in addition to whisker motions. A highly interesting emerging technique simulates body motion in head-fixed mice using a virtual reality track ball system [157]. However, mice still are unable to significantly move their head relative to their body, and likely adopt other compensatory behaviors. While head-fixed and virtual reality experiments have strong utility for intracellular recordings and *in vivo* imaging [158–160], we believe such experiments complement but cannot replace studies of unrestrained animals. As mice orient to the reward in this task, it is clear that both head and whisker motions are critical to their strategy.

We chose to train mice with the full whisker field intact rather than trimmed animals. The

mice are freely exploring, and repositioning based on contacts that are relevant to a behavioral goal. While trimming to a single row of whiskers may aid videographic tracking, we believe that trimming is also likely to induce non-natural sensing strategies as the mouse seeks to cope with newly limited sensors. Additionally, the extensive plasticity induced by modifying the whisker field [161–165] may also alter whisking strategies.

We note that evaluating contact times from videography can be challenging. We mitigated the difficulty in visualizing whisker tips by using multiple observers and analyses robust to small errors in contact frame identification (*e.g*. Figures 2C, 5). Importantly, untracked microvibrissae were often in contact with the aperture during orienting. Microvibrissae likely enhance object recognition [135] and rats may alter head position to bring them into contact with a surface [166]. Future work should clarify what role is played by the microvibrissae.

An important question addressed by the concept of contact maintenance is that previously described repositioning behaviors sometimes predict whisker motions in opposite directions. One key issue is whether the whiskers "anticipate" head placement, as in head turning asymmetry, or "counteract" head motion, as in the minimal impingement / maximal contact strategy. There are really two hypothesized mechanisms at issue. First, the animal selects the mode of head-whisker coupling (to anticipate or counteract). Second, even in the latter case, contact maintenance / minimal impingement could be

employed without direct coupling to head motion; for example, the Prescott group initially proposed negative feedback from contact force to whisking amplitude as a basis for the behavior. With the term *contact maintenance,* we are seeking to describe a broader concept of combined head and whisker behavior that volitionally brings the whiskers into repeated contact with objects of interest, possibly driven by a combination of the animal's expectations with actual object contact. For example, the anticipatory aspect of HTA could apply also to alignment of the whiskers with an object of interest, as we've addressed through our dead reckoning analysis. Prescott has recently proposed a more general framework of viewing whisker motions as a form of covert attention, using behavioral observations as motivation, but implemented in simulation and robotics [167]. We have presented data consistent with this broader view of whisker motions, with a particular emphasis on head whisker coupling, and how its changes over time align with task demands. We stress again that both head turning asymmetry and minimal impingement/maximal contact strategies were studied and described in contexts without goal relevant whisker contact, as if they are autonomous behaviors. We suggest that analyzing these behaviors in a true localization task, post-contact, is more informative of the underlying active sensing strategies of the animal, and advances our understanding of the nature and extent of sensing choices during active whisker touch.

Our results show that mice can select from a diverse range of sensing behaviors, that the selection is driven at least in part by the behavioral situation, and that the timing of changes is incompatible with a purely reflexive mechanism. Significantly, the responses

we observed in different situations often require the animal to act counter to the predictions of a previously observed sensing strategy (HTA or minimal impingement/ maximal contact), while in another situation they may obey those predictions, suggesting a level of volitional control over the selection of sensing strategy. Considering both sensor (*e.g*. whisker) and more general body motions, within a goal-defined context, is likely to be critical to understanding the organization of neural activity underlying perceptual events during active sensing.

CHAPTER THREE- Methods development for closed-loop feedback

The analysis of coordinated head and whisker motions during goal oriented tactile exploration (chapter 2) suggests the possibility of cortical control in the selection of active sensing motions. Of particular interest is whether (and to what degree) primary somatosensory cortex participates in driving motor outputs during active sensing. To investigate these questions, specific tools were needed to deliver closed-loop feedback timed to active sensing motions. Section one describes a method for using facial electromyography to estimate the timing of whisker motions, section two describes the development of a novel light-weight optoelectric recording implant, and section three describes the development and preliminary testing of a real-time feedback system to deliver optogenetic cortical feedback.

3.1 Extraction of whisker motion timing from facial electromyography

3.1.1 Executive Summary

In support of ongoing efforts to assess the role of cortical sensory areas in coordinating active sensing motors, we developed feedback strategies to deliver optogenetic stimulation to the somatosensory cortex of behaving mice, coordinated in real-time with their active sensing whisker motions. Here we describe methods for extracting the timing of whisker motions from bilateral, bipolar facial electromyograms (EMG). In particular, we show onset times extracted offline from EMG envelopes lead whisker motion onsets extracted from high speed video (HSV) by ~16 ms. While HSV provides ground truth for sensing motions, it is not a feasible source of real-time information suitable for neurofeedback experiments. As an alternative, we find the temporal derivative of the EMG envelope reliably predicts whisker motion onsets with short latency. Thus EMG, although providing noisy and partial information, can serve well as an input to control algorithms for testing neural processing of active sensing information, and providing stimulation for artificial sensory feedback experiments.

3.1.2 Introduction

While high speed videography is the gold standard method for recording whisker motions [58,81–85,90,92], current automated tracking methods are computationally intensive, lack robustness across viewing conditions, and may be difficult to apply in real-time settings such as those required in BMI experiments. A more immediately available signal

comes from facial electromyography (EMG), which has been used in rats to track the timing of whisks [80,86–88,91]. Methodology for mice has lagged that for rats, in part because of the difficulty of making devices small and light enough for animals an order of magnitude smaller [168,169]. Here we describe adaptation of EMG recording and signal processing methods to mice, and demonstrate the effectiveness of our approach for extracting times of whisks in a way readily applicable to implementation in real-time feedback systems for sensory neuroprosthetic and neurostimulation research.

3.1.3 Methods

Electrode Construction and Implantation

We developed bipolar electrodes, implant techniques, and signal processing for facial electromyography (EMG) in behaving mice, adapting methods previously reported for rats [80,86,88]. Each EMG electrode consists of a bipolar, twisted pair electrode constructed using insulated 50 μm stainless steel wire (A-M System, part #790500). The lower stiffness of stainless steel, compared to tungsten used in the above rat studies, placed less mechanical strain on the smaller mouse facial pad. We heat fused a twisted pair of wires, whose contacts were spaced approximately 1 mm apart to approximately match an effective dipole of the aggregate muscle activity across the pad. EMG electrodes were implanted in the same surgical procedure as hyperdrives for cortical recording and optical stimulation [168] (see chapter 3.2). The electrodes were placed inside a needle (23 g), and passed subdermally from the anterior edge of the scalp incision and through the facial pad. The needle was removed and the electrodes retracted

until the distal tips were just under the pad. Electrode placement targeted the larger posterior whiskers, and was confirmed by eliciting small whisker motions under current stimulation (10 Hz, biphasic, 50% duty cycle, ~100 μA). The electrodes were secured to the skull with dental acrylic. A posterior skull screw provided electrical ground.

Behavioral arena

Prior to implant, water restricted animals were trained to traverse a 31cm by 9cm polycarbonate track in alternating directions to receive water reward, similar to the task described in chapter 2, but without the repositionable reward ports. Post-implant sessions were conducted in a sound and light isolated cabinet under IR illumination to minimize external sensory cues. Once trained, mice consistently completed > 100 trials in a 45 minute session. Trials lasted approximately 2 seconds and contained 30–40 whisks.

High-speed videography

A subset of trials were recorded at 500 frames per second by high-speed video (HSV; pco.1200hs camera, Cooke Corporation), through a mirror underneath the transparent track. Five to ten clips per session could be saved to disk due to data rate limitations; in order to avoid selection bias, clips were saved as soon as the previous save completed. For comparison to EMG, whisker position was manually scored from the HSV using a custom Matlab GUI. For preliminary studies, a single user tracked the position of a single large, posterior whisker on each side of the face (typically C2), and the position of the tips of the nose and mouth. The angle of each whisker was determined relative to the

snout, with 180 degrees indicating full protraction and 0 degrees indicating full retraction. Whisker angles were smoothed with a Gaussian kernel (10 ms width) before further analysis.

Signal Acquisition

A digital signal processor based acquisition system (RZ2, Tucker David Technologies) collected all signals at 24.4 kHz sampling rate. The tether from a 32-channel headstage at the implant ran through an overhead motorized commutator, to facilitate animal movement, before connecting to a preamp and AD converter (PZ2, TDT). Recorded signals consisted of 4 EMG contacts (bilateral bipolar electrodes) and 24 cortical electrodes. The system also collected timing of camera synchronization and IR beambreak signals (used to track mouse position), and drove reward delivery.

3.1.4 Results

A primary motivation to validate EMG as a measure of whisker motion is to enable the use of EMG for real-time feedback and neurostimulation applications [170], in place of more demanding whisker tracking derived from HSV. In general EMG does not report the true angle of the whisker to the face [88], but in some neurostimulation contexts, finding the onset times of whisks may be adequate. We therefore focused on signal processing conducive to detection of whisk onsets (Figure 3.1A).

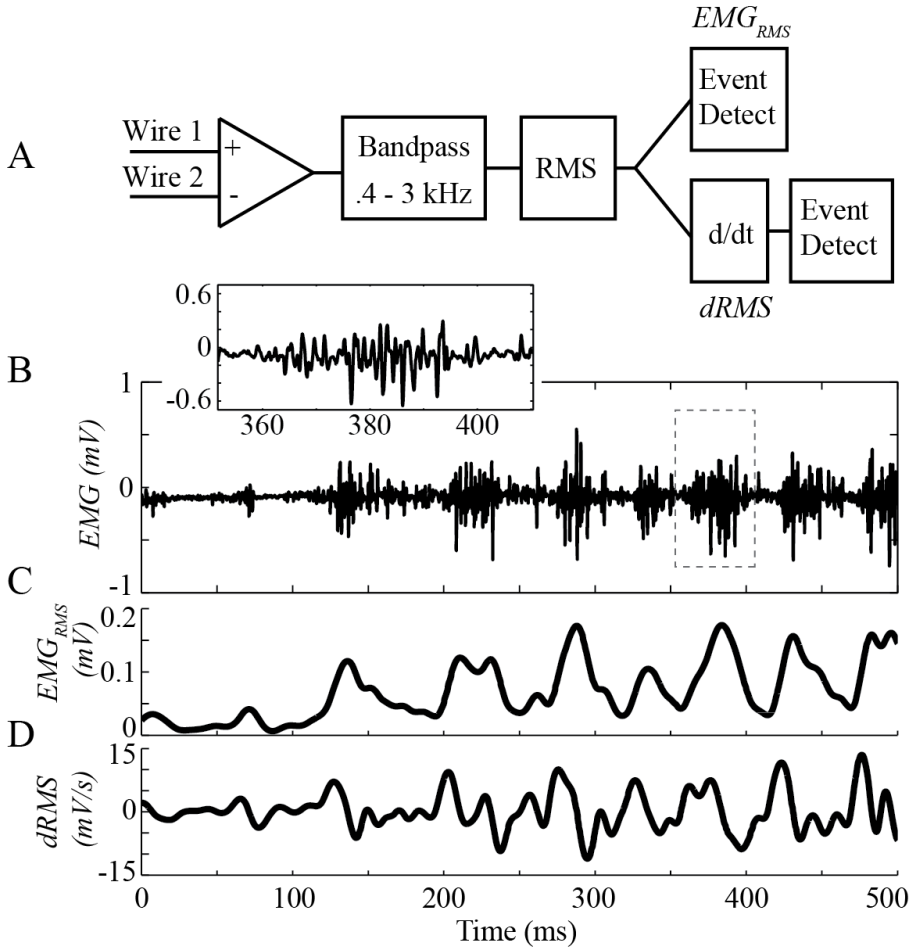

Figure 3.1 Signal processing chain for facial EMG.

A, Block diagram. The differential recording is bandpassed, and the envelope found as the RMS using a 10 ms Gaussian. The derivative of the RMS can also be computed in real-time. **B**, Example of raw EMG signal. Inset shows a zoom of the signal within the dashed box. **C,** Example of EMG_{RMS} used for offline event detection. **D**, Example of *dRMS* signal used for real-time event detection.

We estimated the envelope of EMG activity, EMG_{RMS}, as the root-mean-square (RMS, computed with a 10 ms width Gaussian kernel) of the bandpassed differential of the bipolar electrode (all steps computed digitally). Figure 3.1B shows an example half-second segment of the differential signal, during a transition from quiescence to

whisking, with EMG_{RMS} shown below (Figure 3.1C). EMG_{RMS} was used for offline (non-causal) comparison of EMG to HSV whisker motion estimates. However, to predict individual whisk onsets, we found it useful to take the derivative of the RMS signal (Figure 3.1D), which eliminated low frequency plateaus that develop over bouts of whisks and disrupt threshold detection. *dRMS* is simple to calculate and robust, and may be more useful for real-time processing than the RMS itself, although both EMG_{RMS} and *dRMS* are potentially informative signals for closed-loop feedback.

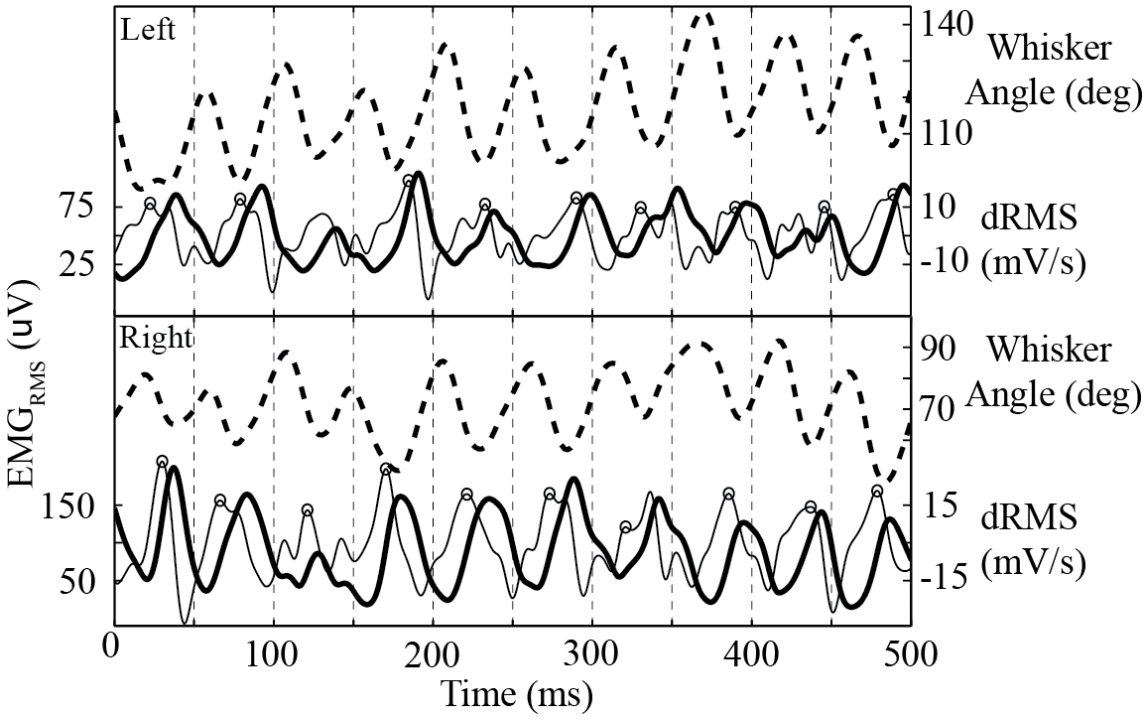

Figure 3.2 Comparison of EMG to videographically reconstructed whisker angles

Example comparison of left (top) and right (bottom) EMG_{RMS} (*thick line)* to HSV tracked whisker angles (*dashed line*). dRMS peaks (*open circles)* tend to occur near the onset of whisker angle increase (protractions).

Comparison of EMG_{RMS} to the videographically reconstructed angle shows the typical relationship between the two measures of whisker motion (Figure 3.2). Peaks in EMG_{RMS} occur near valleys in the angle (maximal retractions), indicating that EMG_{RMS} generally rises prior to each whisk, consistent with the expectation that facial EMG arises primarily from "extrinsic" muscles responsible for (forward moving) whisker protractions [80,88]. To quantify the latency from EMG_{RMS} to whisker motion, we identified local extrema in both timeseries offline (using zero-phase non-causal filters). We then computed the amplitude from each minimum to its adjacent local maximum, and eliminated small events for noise rejection (inclusion criteria computed separately: angular displacement $\geq$ 7°, EMG_{RMS} displacement $\geq$ 50% above the median event computed over all recorded events). Figure 3.3A demonstrates this peak and valley identification, with open and closed circles respectively. Visual inspection confirms that the majority of EMG peaks and angle deflections in this session were identified correctly. We calculated the EMG-angle latency as the time from the EMG_{RMS} valley preceding each angular valley. The latency distributions for both sides of the face are presented in Figure 3.3B. The median delay values were 16.5 ms (left) and 16.0 ms (right).

The preceding analysis shows the behavioral relevance of the EMG signals, and quantifies the latency from electrical events to muscle contraction inherent in the physiology of muscle activation. However, we desire a method that will enable real-time predictions of angular onsets given the EMG.

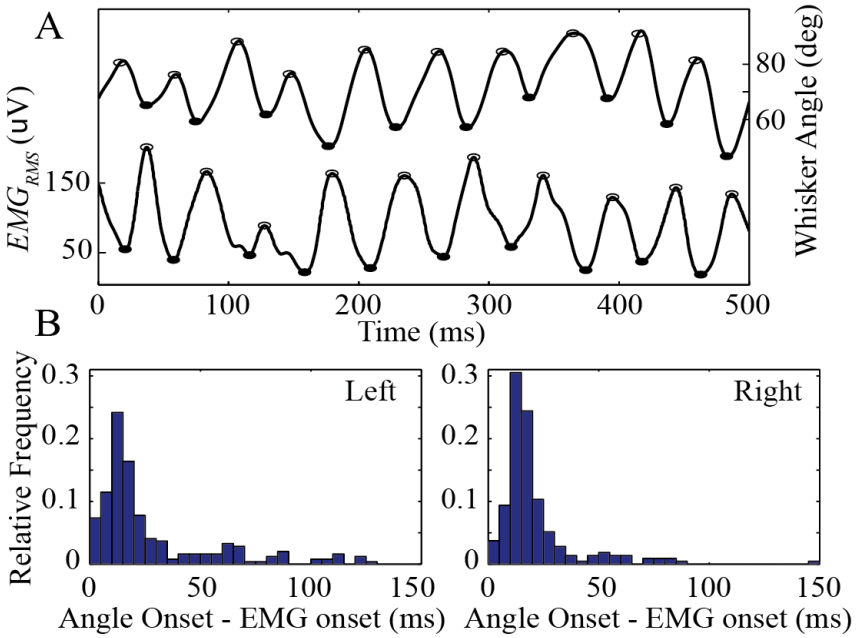

Figure 3.3 Offline analysis of EMG timing

A, Example of 0.5 sec of EMG_{RMS} and whisker angle with onsets (valleys) identified by filled circles, and peaks by open circles. **B**, This peak/valley identification was used to quantify EMG timing (1 mouse, 6 HSV trials). Histograms show the latency from EMG_{RMS} onset to whisk onset for left (n=244 events) and right (n=213 events) whiskers respectively. Median latencies for left and right are 16.5 ms and 16.0 ms.

Since whisker palpations begin with fast forward acceleration, and our recordings are preferentially sensitive to muscles driving this motion, we observed that high narrow peaks in *dRMS* appeared temporally close to whisk onsets as determined from HSV. Peaks in the *dRMS* signal were identified as local maxima between successive upward and downward crossings of *dRMS* through a positive threshold. Additionally, we imposed a refractory period of 25 ms to suppress high frequency noise contamination in the threshold crossings. In order to evaluate the effectiveness of this method at predicting angular motion onsets given *dRMS* information, we define a measure, A, of prediction accuracy as:

$$A = \frac{\#\ detected\ angle\ onsets}{\frac{1}{2}\left[(\#\ total\ angle\ onsets) + (\#\ dRMS\ peaks)\right]} \quad (3.1)$$

The numerator is the total number of HSV-determined whisk onsets that fell within $\pm$ 25 ms of a *dRMS* peak. The denominator normalizes these correct detections by the total number of whisk onsets and the total number of *dRMS* peaks. Perfect detection of whisk onsets without any superfluous *dRMS* peaks would produce A=1. Whisk onsets that are missed, have multiple *dRMS* peaks associated with them, or *dRMS* peaks in the absence of whisking would all reduce A. A central question in detection of whisks by *dRMS* peaks is choice of threshold. We determined the selection of threshold for *dRMS* peak identification by evaluating Equation 3.1 over a range of thresholds (mean(*dRMS*) + X * std(*dRMS*), where X ranged from 0 to 1.5). As shown Figure 3.4A, the predictive accuracy is largely flat for thresholds between 0.5 and 1.0. Accuracy diminished outside this range. Lower thresholds introduced too many spurious *dRMS* peaks, while larger thresholds missed peaks corresponding to true whisk onsets. Based on the curve in Figure 3.4A, a threshold of 0.75 STDs above the mean was selected. Using this threshold, the probability of having a whisk onset within $\pm$25 ms of a detected *dRMS* peak was 71.3% (left) and 70.0% (right). The time between each identified *dRMS* peak and the nearest whisk onset, which also measured predictive accuracy, is shown in Figure 3.4B. The median time from *dRMS* peak to the nearest whisk onset was 10.8 ms (left) and 10.6 ms (right).

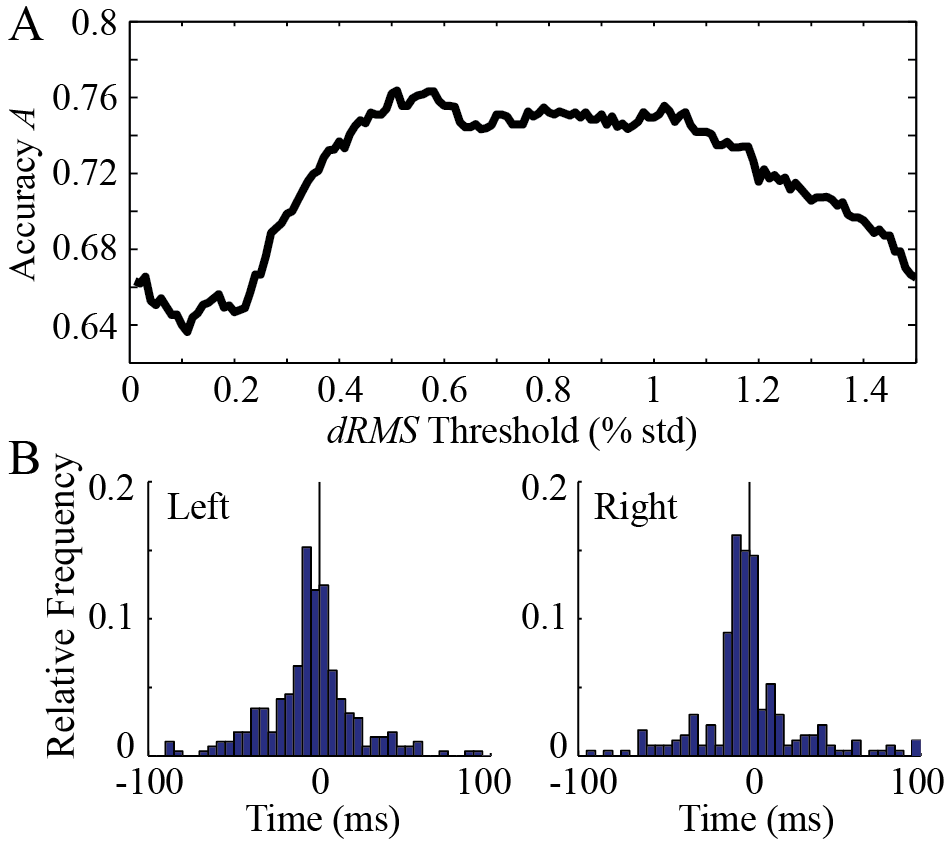

Figure 3.4 *dRMS* peaks predict whisk onsets.

A, The prediction accuracy from equation 3.1 for a range of *dRMS* threshold values, normalized to *dRMS* standard deviations above the mean (over all trials). Comparable results are obtained over a wide range of threshold values between 0.5 and 1.0. **B**, Histograms show the time from each *dRMS* event to the nearest angle onset for left (n=289) and right (n=269) whiskers. Given that a *dRMS* event occurred, the probability of an angular onset within ± 25 ms was 71.3% and 70.0% for the two sides. (1 mouse, 6 HSV trials).

3.1.5 Discussion

We have demonstrated a reliable detector of whisker motion onsets in mice using facial EMG. Peaks in EMG_{RMS} predict an onset of angular motion approximately 16 ms later, a latency from the first detectable electrical signal to the first observable motion significantly longer than computational time requirements in real-time feedback

applications for experiments in sensory prosthetics during active sensing [28]. The ability to use facial EMGs as a surrogate for whisker motions is significant because it reduces the emphasis that must be placed on whisker tracking in HSV, which even if automated is time consuming, computationally intensive, and not feasible for real-time applications. Extraction information on whisk timing from facial EMG enables real-time access to information on motion onsets and allows for analysis of all trials rather than the subset captured by HSV.

We further demonstrated that the temporal derivative *dRMS* of EMG_{RMS} provides a reliable indicator of an impending whisk onset. Since the derivative is just a scaled version of the two-sample difference, this method can be used in real-time, and is subject only to user-configurable latencies needed to define local maxima. With causal filters, there will be an additional small (~5 ms) latency due to the high pass filter placed before the rectifier. Since EMG activation precedes angular motion onset, this method enables control strategies that involve providing neural stimulation before whisking motion occurs. Future experiments will seek to leverage this capability to deliver cell type specific optogenetic stimulation [111] that is precisely timed relative to whisker motions. For example, to selectively active either excitatory or inhibitory networks in primary somatosensory cortex prior to and continuing through whisker motion onset could clarify the strength, cellular origin and timing of thalamocortical “windows of opportunity"” for integrating sensory inputs in the cortex [171].

The most significant limitation of this method is that limited information is available about absolute whisker angle. In some cases, we observed a slight positive correlation between the smoothed magnitude of *dRMS* (100 ms wide Gaussian kernel) and the magnitude of angular deflection occurring in the 25 ms following peaks detected in the original *dRMS* signal. This correlation was not sufficiently robust to predict angular information from *dRMS* signals. Although the relationship between EMG amplitudes and angle deflections remains an important direction for future work, we concentrated on determining activation times and the relative timing of EMG and whisker motion, which are robust and may be adequate in many settings. Additionally, EMG recordings can be corrupted by artifacts from motion, sniffing, or other non-whisker muscle activation. It is important to note that no subselection has been done in this study for periods in which the mouse was actively whisking. In other words, our estimates of prediction accuracy reflect a reasonable summary of how the method would perform over a range of animal behaviors not known in advance. We expect that examining only periods of large amplitude whisking would significantly increase the performance of our prediction method. A key strength of the current method is that it is relatively insensitive to the choice of *dRMS* threshold. While thresholds may be set daily in a short calibration epoch if required, we observed EMG amplitudes to be highly consistent from day to day and found small errors in threshold selection to have a minor impact.

We have demonstrated that electromyographic recording techniques can be successfully adapted for use in the much smaller facial pads of mice, and that EMG provides a robust

indication of protraction onsets. This technique provides an important tool to facilitate experiments in actively behaving mice to better understand sensorimotor loops implicated in active tactile sensation through closed-loop feedback.

3.2 OptoZIF Drive: a 3D printed implant and assembly tool package for neural recording and optical stimulation in freely moving mice

(Chapter 3.2 has been adapted from a submitted manuscript co-lead-authored with David Freedman.)

3.2.1 Executive Summary

Behavioral neuroscience studies in freely moving rodents require small, light-weight implants to facilitate neural recording and stimulation. Our goal was to develop an integrated package of 3D printed parts and assembly aids for labs to rapidly fabricate, with minimal training, an implant that combines individually positionable microelectrodes, an optical fiber, zero insertion force (ZIF-clip) headstage connection, and secondary recording electrodes, e.g. for electromyograms (EMG). Starting from previous implant designs that position recording electrodes using a control screw, we developed an implant where the main drive body, protective shell, and non-metal components of the microdrives are 3D printed in parallel. We compared alternative shapes and orientations of circuit boards for electrode connection to the headstage, in terms of their size, weight, and ease of wire insertion. We iteratively refined assembly methods, and integrated additional assembly aids into the 3D printed casing. We demonstrate the effectiveness of the OptoZIF Drive by delivering real-time optogenetic

feedback in behaving mice. A novel feature of the OptoZIF Drive is its vertical circuit board, which facilities direct ZIF-clip connection. This feature requires angled insertion of an optical fiber that still can exit the drive from the center of a ring of recording electrodes. We designed an innovative two part protective shell that can be installed during the implant surgery to facilitate making additional connections to the circuit board. We use this feature to show that facial EMG in mice can be used as a control signal to lock stimulation to the animal's motion, with stable EMG signal over several weeks. To decrease assembly time, reduce assembly errors, and improve repeatability, we fabricate assembly aids including a drive holder, a drill guide, an implant fixture for microelectode "pinning", and a gold plating fixture. The expanding capability of optogenetic tools motivates continuing development of small optoelectric devices for stimulation and recording in freely moving mice. The OptoZIF Drive is the first to natively support ZIF-clip connection to recording hardware, which further supports a decrease in implant cross-section. The integrated 3D printed package of drive components and assembly tools facilities implant construction. The easy interfacing and installation of auxiliary electrodes makes the OptoZIF Drive especially attractive for real-time feedback stimulation experiments.

3.2.1 Introduction

Behavioral neuroscience often requires the ability to record neural activity in freely moving animals by implanting light-weight devices. The increasing availability of optogenetic tools for studying specific neural circuits [113,117,172–174] makes the integration of optical fibers for open and closed-loop manipulation of neural firing an

important design criteria. The challenge of building neural interfaces is exacerbated when working at rodent scale (e.g. compared to primates with larger, fixed electrode arrays and headstages), especially in mice, that are about one tenth the size of rats. However, mice are heavily favored for genetic approaches for targeted optogenetic expression, making the continuing development of light-weight chronic recording technology an important technical problem. A well developed and ubiquitous design features a ring of electrodes (often 2-channel stereotrodes or 4-channel tetrodes) that can be independently vertically positioned by adjusting screws (microdrives) in an encasing "hyperdrive" [175,176]. 3D printed versions have been used in rats [177,178] and mice [168], with the latter also incorporating an optical fiber for simultaneous neural recording and optogenetic stimulation. More recent work has made significant strides in weight reduction while at the same time allowing for increased flexibility and higher channel counts [179–181]. There are now a wide variety of design approaches. Examples include lightweight motorized drives for improvements in positioning precision over manual screw adjustments [182–185], "optrode" technologies that seek to bring the stimulation source into close proximity with the recording electrodes [186–188], microelectrode arrays with integrated optical fibers [189,190], and silicone probes that incorporate micro scale LEDs [191]. Other approaches sacrifice size and repositionability to make high channel count arrays for mice [192], or focus on incorporating wireless technology to remove the need for a tether/commutator during behavioral tasks [193,194]. Each of these devices accepts trade-offs to optimize features important to a particular research need. Some devices are

labor intensive to assemble, may have poor reproducibility from build to build, and/or require specialized knowledge or equipment.

The OptoZIF Drive presented here facilitates assembly by 3D printing a package of not only drive parts, but also assembly guides and tools for straightforward construction. The drive is light-weight (~3 g), supports a fiberoptic channel and six adjustable drives, and can be assembled with minimal training. An unusual feature of the OptoZIF Drive is design for the ZIF-clip® system used by Tucker-Davis Technologies. Zero force insertion (ZIF) connectors snap over the hyperdrive electrical connector, without requiring tension between the headstage and drive during attachment and detachment (contrasted, for example, with the common Omnetics connectors used in NeuraLynx and Plexon systems). This process lowers the risk of drive damage and animal stress or injury, which while small on each day, can be problematic over weeks of daily recording sessions. Some existing systems use adaptors or other *ad hoc* assemblies to create a right angle between the connector and a traditionally horizontal circuit board (e.g. Tucker Davis Technologies ZCA-OMN32). We made ZIF-clip support “native” to our drive through a vertically oriented printed-circuit board (PCB) that allows direct ZIF-clip connection. An additional novel OptoZIF Drive element is a multi-part protective shell that is installed during the implant surgery to facilitate electromyography (EMG) electrode implantation; this approach is contrasted with fixed plastic cones that are usually secured to drives before implantation [168]. Together these features provide a light, low profile, flexible design for optogenetic experiments in freely moving mice.

3.2.3 Material and Methods

The OptoZIF Drive incorporates a number of novel innovations that build off of previously reported optoelectric hyperdrives [168] and are adapted to our experimental requirements [27]. Specifically, the implant required a vertical facing electrode interface board to reduce the height associated with ZIF-clip adapters, precise control of microelectrodes over time, an optical fiber for optogenetic stimulation, the ability to easily connect and validate the positioning of EMG electrodes during the implant surgery, and a simple and robust manufacturing process (Figure 3.5).

Implant Fabrication Process

The drive bodies used in previous designs [168] were manufactured using a stereolithography (SLA) process to produce large batches of drives. This process frequently results in a large number of drives that were found to be unsuitable during the assembly process due to a variety of defects. Selective Laster Sintering (SLS) was selected as a low-cost, quick, and relatively cheap 3D printing process that allowed rapid development and iterations of the designs. This process enables single drives to be manufactured quickly and cheaply. Additionally, the properties of the SLS polyamide were found to be favorable for the numerous post-processing steps (described in Appendix 1) and comparable long-term structural performance was also observed. Thus, the implant was designed to be 3D printed in single batches with the necessary supporting mechanical components 3D printed in parallel with the main implant. The main block contains the drive body, 2 part protective shell, and protective caps (Figure 3.5F). In

addition, the top of the block provides holders for the microdrives during assembly and grooves on the top of the main block provide length guides when cutting metal and polyimide tubes for subassemblies. Finally, we also 3D printed the distal cannula of the drive in high detail stainless steel in order to provide a consistent implant height and ensure a smooth bevel on the distal end (Figure 3.5B).

Recording Electrode Configurations

OptoZIF Drive is designed to support up to eight independently positionable microdrives. A variety of different recording configuration could be incorporated using this system- for example a single drive could be assigned to move 1 tetrode, 2 stereotrodes (i.e. fused together, but at different lengths), or 4 single electrodes. Each drive corresponds to a single polyimide guide tube that opens at the base of the drive. These guide tubes are arranged in a ring surrounding a larger polyimide tube that serves as a guide to place the optical fiber (Figure 3.5C, *inset*).

Drive Mechanism

For chronic neural recording, it is often desirable to be able to vertically reposition microelectrodes both to target specific brain regions and to optimize the quality of neural recordings. This is accomplished through an array of integrated micromanipulators that allow precise positioning of electrodes using a shuttle tube that is affixed to a “top piece” manipulated using a small control screw, similar to previous designs [168,177].

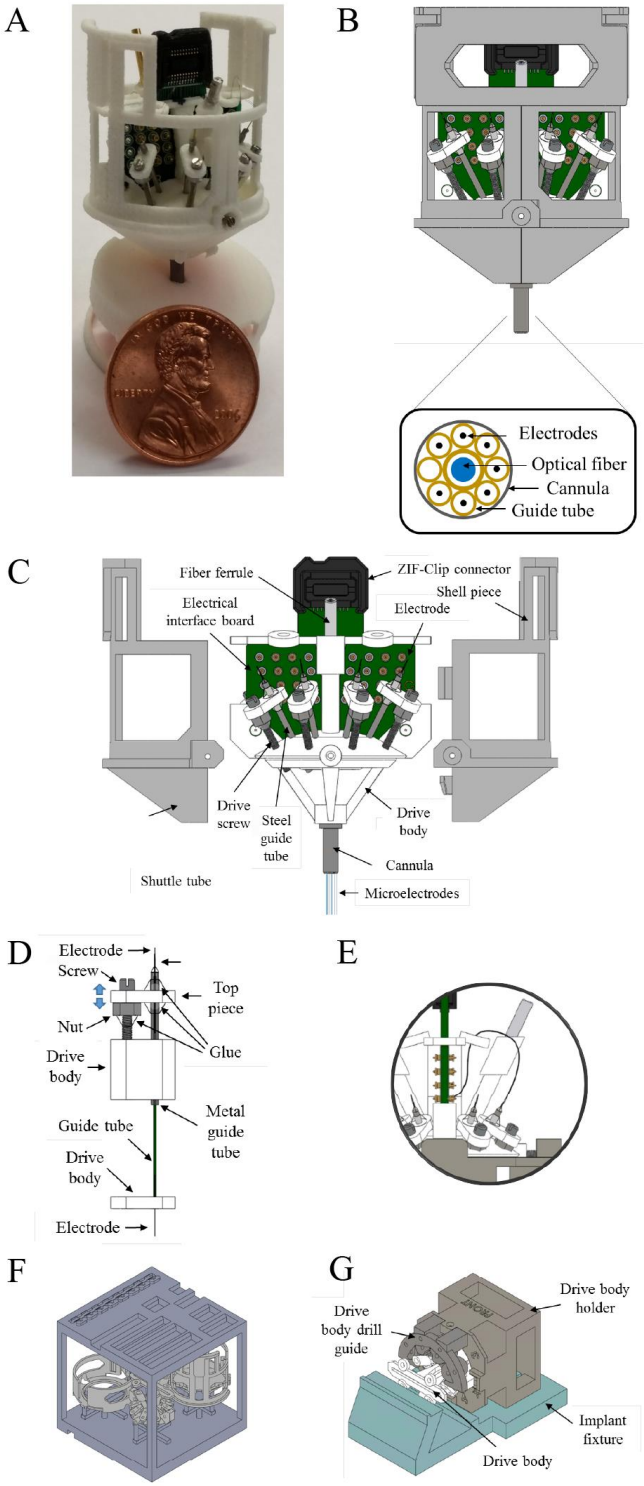

Figure 3.5: Assembled OptoZIF-Drive with component detail

A) Photo of OptoZIF Drive with scale reference. **B)** Assembled OptoZIF Drive with protective shell and cap attached. *Inset-* Arrangement of guide tubes and optical fiber in cannula. **C)**

Exploded view of drive with components labeled. **D)** Drive mechanism for positioning microelectrodes. **E)** Zoomed drive image highlights the angled optical fiber receptacle and microelectode wiring method. **F)** Main 3D printed "block" of OptoZIF drive body and parts. G**)** Assembly aids include a drive holder, a drill guide, and an implant fixture for connecting microelectrodes to EIB.

OptoZIF Drive incorporates top pieces that are 3D printed along with the main drive body. As shown in Figure 3.5D, the shuttle tube is affixed to the microelectrodes and metal guide tubes so that turning the control screw results in a precise movement of the microelectrode. The screws have a 0.8 mm diameter and 127 threads per inch. Thus, one turn advances the screw by 200 microns. Partial rotations of ¼ turn (50 microns) or even 1/8 turn (25 microns) can be used for small electrode advancements. We used screws 0.32" (8.1 mm) in length, which provided about 6.2 mm of useable threads once the drive is assembled, giving a safe travel range of 4.0 mm through the drive body.

Vertical electrode interface board facilitates direct ZIF-Clip connectivity

A recording drive's design must factor in the requirements of the recording apparatus that it will interface with. In our case, a Tucker Davis Technologies (TDT) DSP was selected for use in ongoing real-time feedback experiments in part because of the flexibility offered in developing real-time control algorithms. The TDT system utilizes ZIF-clip (zero insertion force) headstages that offer significant benefits for easily connecting awake animals to the recording equipment in a way that minimizes the forces on the drive and the stress experienced by the animal. Many previous drive designs featured an Omnetics connector on a horizontal EIB, requiring the use an Omnetics to ZIF adapter for use with TDT recording hardware. The adapter not only negated the benefits of the

zero insertion force concept (inserting and removing the adapter requires significant force) but also nearly doubled the height of the implant, which impaired the mouse's ability to perform certain experimental tasks.

OptoZIF Drive has met this connectivity challenge by incorporating a vertically positioned EIB for direct, low-profile connection to the ZIF-clip system. A custom printed circuit board (PCB), which is 1/32" thick (0.79 mm) was made to properly use the ZIF-clip and is held in place by a dedicated receptacle on the 3D printed drive body (Figure 3.5C,E).

Optical fiber placement

While past designs have placed a vertical fiber directly in the center of the drive through a small hole in the EIB and adjusted the positioning of other components (such as the recording connector) to accommodate it, this strategy is contraindicated by the design features needed to facilitate a vertical PCB. In the OptoZIF Drive, the optical fiber runs parallel to the drive cannula at the distal end, but is bent at the proximal end with the ferrule protruding from a specially designed fiber optic receptacle at a 25-degree angle (Figure 3.5E). The fiber is placed prior to loading the recording electrodes and the ferrule is fused to the polyimide receptacle using cyanoacrylate adhesive. Bending the fiber in this way may slightly reduce the efficiency of the light transmission, but since large fibers are used (200 microns), and the bending is slight over a few millimeters, the implant has relatively high optical efficiency. The physical coupling process and bending

of the fiber resulted in coupling efficiency of approximately 70% from the input fiber to the output of the implant. The optical fiber is positioned so that it just reaches the end of the implant cannula, without extending past and entering the brain. This system facilitates a fiber sitting near the surface of the brain post-implant.

Multi-part protective shell facilitates EMG implantation

The implant contains sensitive electronic, mechanical, and optical components. Thus, for chronic implant experiments, it is important that the implant is properly protected. This is typically accomplished with some form of protective shell surrounding the implant. This shell may also serve a secondary function by incorporating conductive material and providing a conductive path to ground for electromagnetic interference reduction. Previous drives have addressed this shielding/protective function using simple cone shaped shells. Such designs have a large volume compared to the drive itself. Specifically, it extends the lateral boundaries of the drive further past the animal's head, which can be unwieldy in behavioral experiments.

To keep the volume of the drive to a minimum while still protecting the internal components, a 3D printed protective shell was created. Initial designs required a protective shell to be installed prior to implantation by sliding the shell over the implant. While meeting the goal of using minimal volume while protecting the implant, it became very difficult to implant EMG electrodes, which must be connected to the EIB during the implant surgery. Thus, the shell was split into two pieces that snap together near the end

of the implant procedure and are secured to the drive base with two screws. This enables the EMG electrodes to be implanted, tested, and connected to the EIB without the shell obstructing these steps during the implant surgery. The split shell and drive are shown in Figure 3.5C.

Two versions of the cap piece to seal the top of the shell are available. The first is used for completely protecting the implant, but cannot be used during recordings. A second cap has an opening that allows the fiber optic cable to be attached as well as the ZIF-clip headstage. During recordings, the drive is covered with a plastic sleeve lined with aluminum foil, which is connected to a ground pin on the drive body to reduce electromagnetic interference during neural recording.

Fixtures and assembly aids speed construction and boosts repeatability

The implant contains a number of small components that must be delicately assembled, often in small batches by users with limited training. OptoZIF Drive was designed to be assembled quickly over 1–2 days and has a number of additional parts, tools, and guides that have been 3D printed to facilitate rapid and repeatable assembly. On the drive itself, in addition to 3D printing the drive body, the bottom cannula from which the recording electrodes exit has been printed in stainless steel to increase the repeatability of the implant to brain distance and insure a smooth bevel on the distal end.

We also developed additional 3D-printed assembly aids (Figure 3.5G; Appendix 1) that allow the implant to be assembled while protecting the most fragile components (i.e. the microwires). The first piece, the holder, keeps the drive affixed and allows the drive to stand-up on its own. This holder is used during the majority of the implant construction process and significantly reduces the probability of accidental damage. The second piece, the pinning fixture, used in combination with the holder, allows gold pins to be "pinned" to the EIB without exerting large forces on the EIB or implant (Figure 3.5G).

3D printing of the drive base pieces involves small dimensions and tight tolerances that are near the current technical capabilities of the SLS technology. This is especially a problem for small holes. To combat this problem, all holes for steel guide tubes and screws have been purposefully undersized and require clearing by manual drilling. In order to ensure consistent drilling of holes in the base piece, we designed a drill guide that can be 3D printed in stainless steel (Figure 3.5G). This drill guide, which fits into grooves on the implant holder to ensure consistent positioning, ensures that the angles of the holes are consistent across drives, and more importantly that the holes for guide tubes and screws are parallel to each other, which is a common source of drive failure.
Finally, we developed a fixture to aid in gold plating recording electrodes. Traditionally, this process had a significant risk of damaging electrodes while lowering the drive into a small well of gold solution (for example using a bench vise or micromanipulator). This fixture consists of two parts, the drive holder in which the implant is secured similar to the holder used during construction, and the base. The base has a small well in the center

that is filled with the gold solution with an electrode at the center of the well. The drive holder is then pressed into grooves at the top of the base (after final cutting electrodes to the desired length). This fixture ensures that the electrodes are held at the proper depth to be immersed in the gold solution, but prevents any lateral motion that may damage the electrodes by bringing them into contact with the sides of the well. We have paired this fixture with a breakout interface board that allows easy plating of a specific wire without needing to make electrical contact directly with the ZIF connector or the gold pins on the EIB itself.

3.2.3 Results

To demonstrate the capability of OptoZIF Drive for neural recording and optical feedback, we implanted the drive in mice performing an active sensing task. Mice had been trained to locate a randomly positioned reward port in the dark using whisker palpations [195]. We sought to deliver optical stimulation to primary somatosensory cortex (SI) that was timed to the whisker motions of the animal. In this mouse strain, Thy1-ChR2-line 18 (B6.Cg-Tg$^{\text{Thy1-COP4/EYFP)18Gfng)/J}}$, Jackson Laboratories), the optically sensitive channel is cortically expressed most strongly in an excitatory cell population in layer 5 [111,114], suggesting an increase in neural activity from simultaneous SI recordings. Multiunit spikes from the bandpassed field potentials over many laser pulses are shown as rasters in Figure 3.6A (*top*) compared to mock trials where the signal processing was identical but no output was sent to the laser *(bottom*). Putative single units were isolated by thresholding at 4 standard deviations above the mean and sorting with mclust. Figure 3.6B (*top*) shows example clusters from a typical tetrode recording.

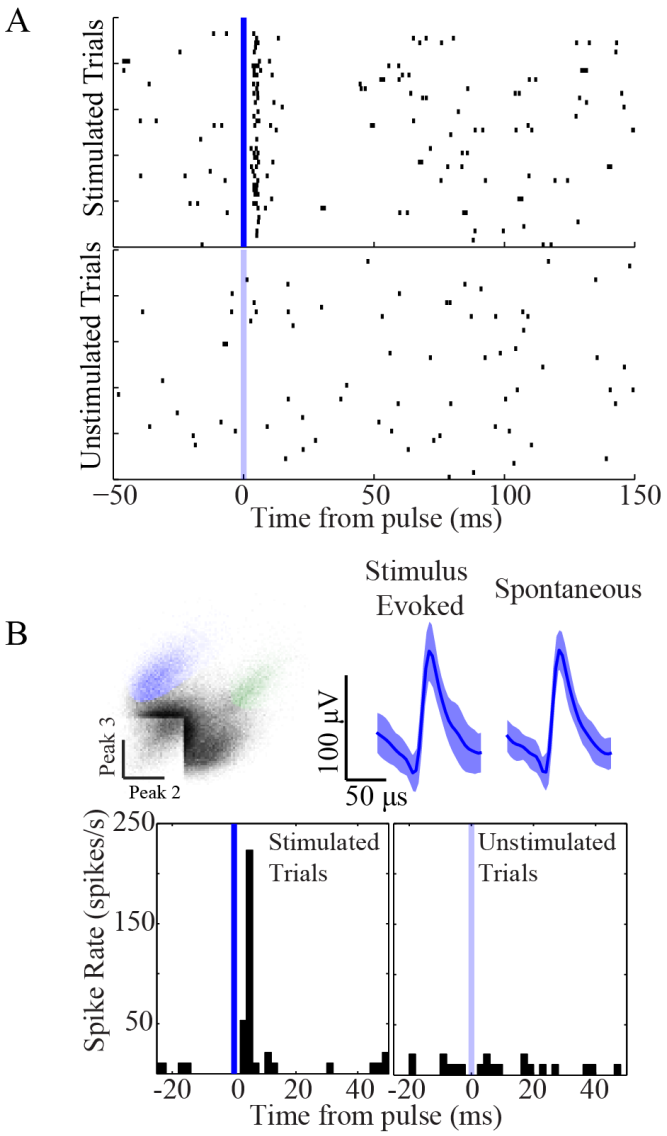

Figure 3.6: Multi Unit and Single Unit responses to optogenetic cortical stimulation

A) Rasters of multiunit spiking for SI recordings bandpassed (0.6–6 kHz) and thresholded to find spike times (5 std. above mean threshold) during real-time feedback stimulation locked to whisker motions. Stimulation pulses (*top*) show a robust recruitment of multiunit spiking ~5 ms after pulse onset compared to unstimulated trials (*bottom*) when the signal processing was identical but no output was delivered to the laser. **B)** Clusters for a sample tetrode recording from SI. Waveforms for stimulus evoked (*top-middle*) and spontaneous (*top-right*) spikes demonstrate that SI stimulation is recruiting SI activity comparable to naturally occurring. PSTHs for a single isolated unit in SI (*blue cluster above*) in response to the same stimulation conditions as A. Stimulation (*bottom-left*) produces a reliable increase in firing of this unit compared to the mock pulse condition (*bottom-right*).

Stimulation evoked waveforms in this sample unit were comparable to those that occurred spontaneously during the same session (Figure 3.6B, *top*). Isolated single unit spiking activity over the same pulses and fictive pulses as Figure 3.6A also shows a robust increase in firing following SI optical stimulation (Figure 3.6B, *bottom*). An example single trial (Figure 3.7B, *top*) also shows robust recruitment of multiunit spiking in the bandpassed neural recording.

To facilitate closed-loop optogenetic feedback, we utilized facial electromyography (EMG) to estimate whisker protraction events in real-time as described previously [89] (see chapter 3.1). An important advantage to OptoZIF Drive is its two part protective shell, which facilities EMG electrodes (or other secondary recordings) to be connected to the drive during the implant surgery prior to enclosing the drive. Figure 3.7A shows an example of bilateral EMG RMS recordings (*solid black traces)* compared to "gold-standard" whisker angles (*dashed traces)* estimated by manually tracking whisker angles in high-speed video (500 frames/ sec). We observed here and reported previously that EMG provides a reliable estimate of protraction times, as the EMG signal generally begins increasing prior to an observed increase in whisker angle.

The processed EMG was used as a control signal to estimate protraction events in real-time and trigger a laser to deliver a single 1 ms pulse of blue light (473 nm, ~35 mW/mm^2) to the optical fiber in the implant. Figure 3.7B shows an example trial where stimulation was delivered at EMG estimated protraction times determined by positive

crossings of an upper threshold. The system must be reset by a negative crossing of the lower threshold before the next stimulus will be delivered [27].

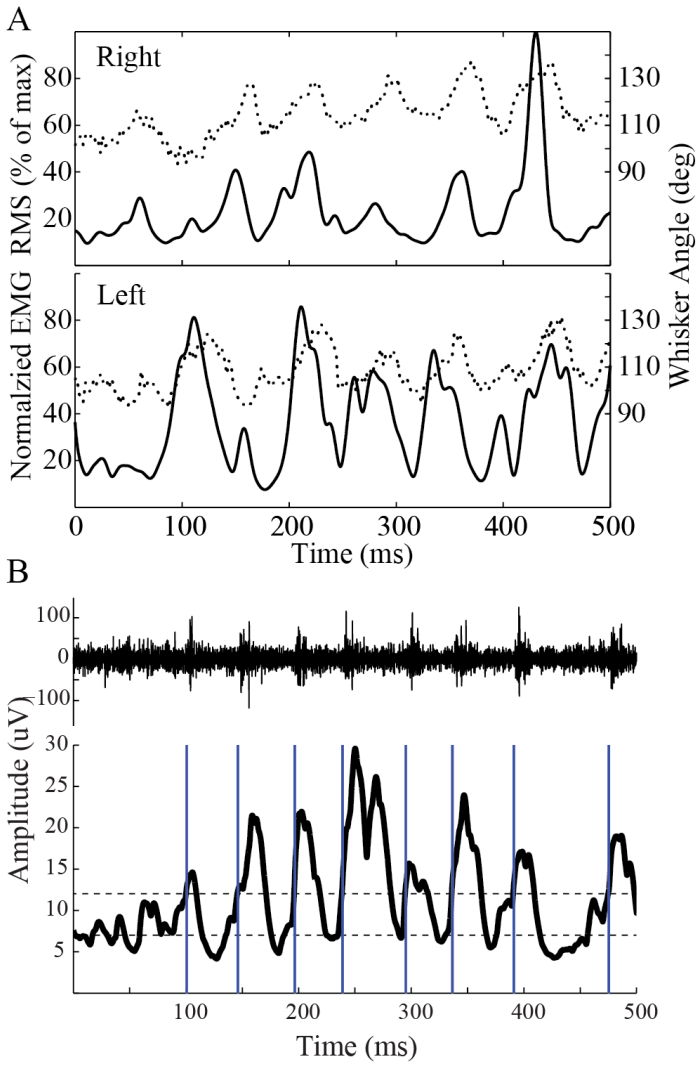

Figure 3.7: Facial Electromyography tracks whisker motions and drives real-time feedback stimulation

A) Right (top) and left (bottom) EMG signals were processed offline to compute the signal RMS (*solid traces*) and compared to videographically reconstructed whisker angles (*dashed traces*). The comparison shows that EMG provides a reliable estimate of whisk timing, particularly an indication of protraction onsets, and verifies its utility as a control signal for real-time feedback stimulation. **B)** This example trial shows that optogenetic stimulation of SI (*blue bars*) can be successfully timed to whisker motions using EMG (bottom, *black trace*). A sample recording from SI (top) (bandpassed 0.6–6 kHz) shows robust multiunit activation timed to stimulation.

Stimulation times are indicated by vertical blue bars and show reliable locking to whisker protractions. Importantly, the timing of the stimulus is driven by the motions of the animal, rather than a previously configured choice of stimulation times. Shown along with the EMG is a sample neural recording from SI (bandpassed 0.6–6 kHz).

In order to serve as a robust control signal for real-time feedback experiments, EMG recordings must remain stable over a period of many weeks. While much has been done to characterize the stability of tetrode recordings, the stability of EMGs has received less attention. Since EMG electrodes may experience more direct perturbations than intracortical electrodes (e.g. facial grooming), it is important to establish that reliable placement and stable recordings can be achieved.

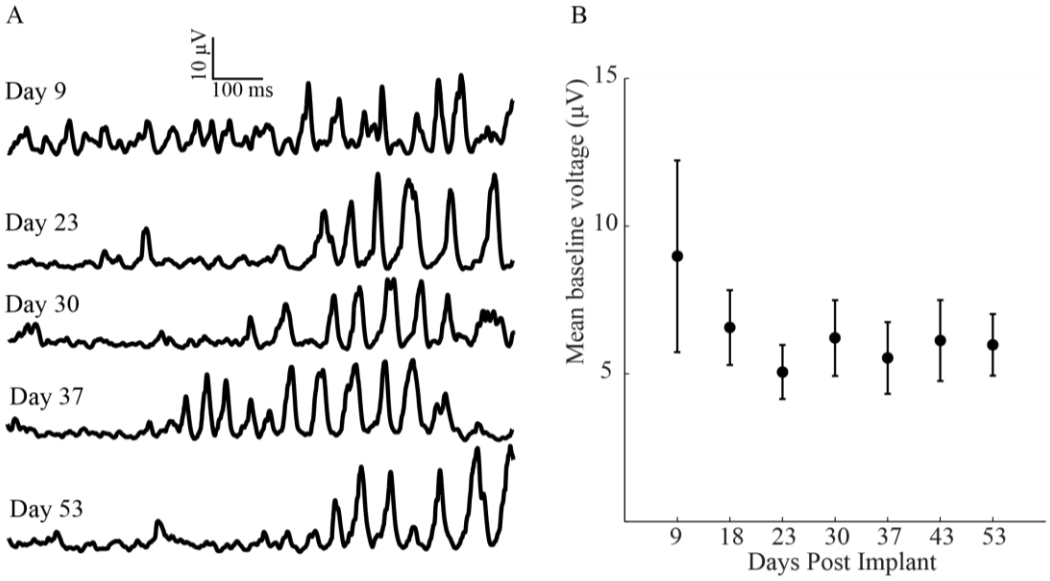

Figure 3.8: EMG provides a stable control signal

A) EMG recordings from example trials from 5 sessions between post-implant days 9 and 53. Whisking typically begins 300–500 ms after trial initiation and consistent amplitudes and waveforms are overserved throughout the recording period. **B)** The mean baseline voltage

(average EMG potential in the first 200 ms of each trial in a session) shows stability after an initial period of high variation (during post-surgical recovery, prior to data collection) (mean +/- std).

We observed EMG recordings through post-implant day 53 (the last day of data collection for this mouse). Example trials from 5 sessions over that span are shown in figure 3.8A. On these trials, the mouse typically begins whisking around 300–500 ms after trial onset. We observed consistent EMG amplitudes and waveform shapes during this period. To quantify the stability of EMG recordings, we evaluated the mean baseline voltage during the first 200 ms of each trial (before significant large amplitude whisking typically begins) within a recording session. Following an initial period of larger variation in baseline voltage corresponding to the post-surgical recovery period, we observed stable baseline voltages for the remainder of the test period (Figure 3.8B).

3.2.5 Discussion

OptoZIF Drive seeks to address a common challenge with rodent recording drives with repositionable electrodes- that they are difficult and time consuming to assemble reliably and consistently, especially by users without specialized training. Small operator errors in conceptually simple operations can result in significant problems later in the construction process and impaired performance in the finished drive. For example, if the holes drilled for the control screws are not parallel to those for the cannula/polyimide/electrode assembly then the ability of the drive to smoothly advance by a repeatable distance with each turn of the screw will be reduced. We mitigated this specific problem by also 3D

printing (in stainless steel) drill guides to ensure accurate and repeatable drilling. In general, we identified steps throughout the construction process that were time consuming and/or vulnerable to operator inconsistencies and developed appropriate assembly tools as needed.

Apart from construction concerns, a major design objective was to limit the height and weight of the implant as much as possible, while still retaining repositionable microdrives. Significant savings in both areas was achieved by incorporating a vertical circuit board to natively support ZIF-clip connections without the use of an adapter. Removing the adapter resulted in a savings of 0.78g and 21 mm. Other design features were targeted specifically towards weight reduction, for example using 3D printed polyimide top pieces to replace metal ones, and cut-outs were incorporated in the design of the drive and protective shell to reduce the weight of large features. The result is a low profile drive weighing less than 3 grams and supporting direct connection to TDT headstages.

Open-loop stimulation experiments that perturb a system and observe the output on neural activity and/or behavior have been a staple of neuroscience labs for decades. It is becoming increasingly apparent, however, that closed-loop stimulation paradigms offer a powerful method to study circuits in which the brain integrates information in real-time while coordinating future outputs. The ability to record a control signal (EMG), process it in real-time, and deliver real-time feedback while simultaneously recording neural

activity from 6 tetrodes (24 wires) demonstrates the power of OptoZIF Drive for closed-loop stimulation experiments. Similarly, many neuroscience experiments have isolated particular aspects of a target system for study (i.e. anesthetized preps, head fixation, and whisker trimming in the rodent whisker system). The importance of experiments that allow for more natural behaviors is also becoming clear [195]. By incorporating the ability to easily perform closed-loop stimulation experiments within a drive that has been engineered to accommodate more natural behaviors (i.e. weight reduction and lower profile), OptoZIF Drive provides an excellent platform to study a range of relevant neuroscience question in mice.

OptoZIF Drive is the first optical stimulation capable drive design that supports adapter-free interfacing with the ZIF-clip system. The innovative drive design, along with the associated fixtures and guides to aid in repeatable assembly represent an important step forward. Validation of OptoZIF Drive in a real-time feedback experiment delivering stimulation timed to whisker motions demonstrates the drive's utility for closed-loop experiments in freely moving animals.

3.3 Real-time feedback timed to active sensing motions

3.3.1 Executive Summary

We developed methods to deliver optogenetic feedback to mouse primary somatosensory cortex (SI), time-locked to active sensing motions (whisking) estimated through facial

electromyography (EMG). To explore the impact of SI activity on individual whisker motions, we delivered stimulation controlled by self-motion, as estimated from EMG. In a preliminary experiment testing the impact of sensory cortex stimulation on whisking behavior, we found that stimulation regularized whisking (increasing overall periodicity), and shifted whisking frequency. These behavioral changes emulate changes observed when rodents actively contact objects, suggesting a role for SI in the coordination of motor outputs during active sensing.

3.3.2 Introduction

Active sensing, in which behavioral choices modulate or maximize information acquisition, is important in exploration and object manipulation [37,58]. The neural basis of active sensing is likely to be central to efforts to restore sensation through stimulating neuroprosthetics. The rodent whisker system provides an ideal model for active sensing: rats and mice modulate the frequency, rate, and average position of whisker motions during object contact and exploration [51,58,88,91,92,98], much of the anatomy and physiology of whisker sensory and motor pathways are well characterized [52,78,121,139], and mice are a genetically tractable mammal [111].

A central question is how sensing strategies (e.g. rhythmic whisking) are related to activity in primary somatosensory cortex (SI), when incorporating already acquired sensory information into future sensing behavior. Figure 3.9 schematizes the tactile loop in rodents. Some SI neurons show tuning to preferred phases of whisking, with a

population bias towards firing near retraction onset (when the whisker is near maximal protraction) [51,62–64,68]. Tuning persists during object contact [76], indicating that relative timing in SI could be critical for sensory processing. Rats are able to direct whisker motions toward targets identified only by the timing of SI electrical microstimulation [28]. Moreover, in one study, stimulation of SI induced whisker retractions with short latency, possibly via a direct projection to pre-motor brainstem, consistent with the population bias in preferred phase [60]. However, that study delivered stimulus trains unrelated to prior behavior, and was conducted in quiescent, head-fixed animals. We have developed a real-time system that delivers stimulation to SI triggered by individual whisker motions, and enables us to observe the impact of this stimulation on future motions (Figure 3.9, artificial loop). We find that locking stimulation to self-motion results in increased regularity of whisking, possibly analogous to changes following true object contacts [58,98].

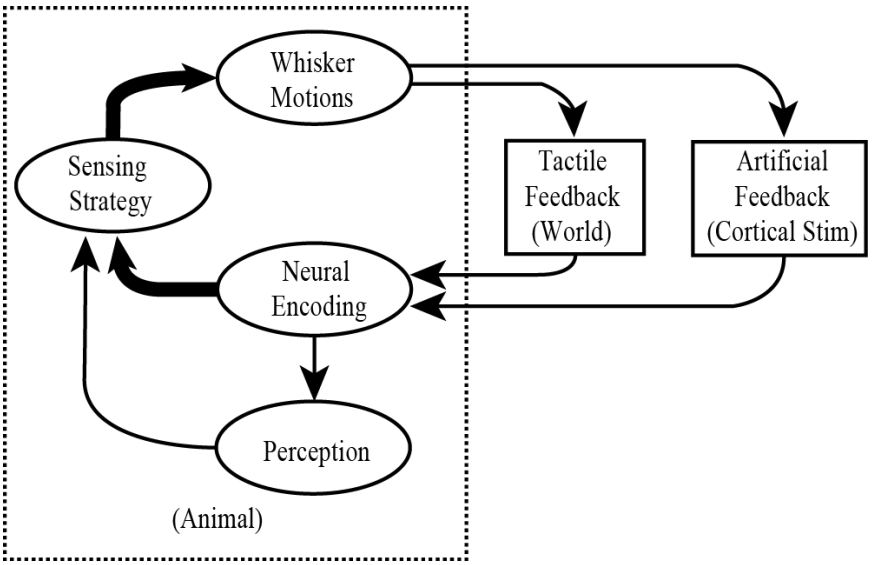

Figure 3.9 Schematic of sensorimotor feedback loops

Whisker touch produces tactile inputs and neural encoding in SI. This neural activity drives perception, but also changes subsequent active sensing, including timing and amplitude of whisking. Direct SI stimulation allows artificial feedback to change the relation between sensing and neural activity.

3.3.3 Methods

Animals and behavioral paradigm

Water restricted animals were trained prior to implantation to alternately traverse a linear polycarbonate track (30cm x 9cm) to receive water rewards. The behavior is easily learned and encourages active tactile exploration. Sessions were conducted in a sound and light isolated cabinet under IR illumination. For this preliminary study, data is presented from a single Thy1-ChR2 mouse (B6.Cg-Tg$^{Thy1\text{-}COP4/EYFP)18Gfng)/J}$), Jackson Laboratories), collected over 7 experimental sessions. This mouse line expresses the light sensitive ion channel Channelrhodopsin-2 (ChR2) strongly in layer 5 cortical neurons [111,114].

Signal acquisition and processing

We have previously described our custom hyperdrives for optogenetic stimulation and recording of SI [168] (see chapter 3.2), and adaptation of EMG from rats [86,88] to mice [89] (see chapter 3.1) for real-time identification of whisk timing.

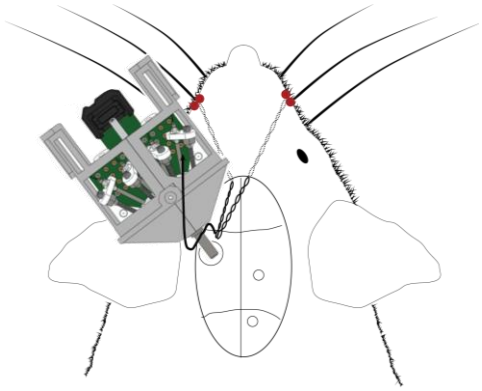

Figure 3.10 Schematic of hyperdrive implant and facial EMG placement

Briefly, in a single surgery, hyperdrives were implanted over left SI (3.75 mm lateral, 1.5 mm posterior from Bregma), and bilateral, bipolar EMG electrodes inserted under the facial pad to measure aggregate muscular activity. Figure 3.10 shows the placement of OptoZIF Drive implant and facial EMG electrodes. The differential EMG input was bandpassed (0.4–3 kHz), rectified, and lowpassed (40 Hz) to extract the EMG envelope. EMGs and neural recordings from six tetrodes in SI were acquired at 24.4 kHz and processed in real-time on a DSP-based system (RZ2, Tucker Davis Technologies). A motorized optoelectronic commutator minimized restriction of animal motion by the tether. Additional signals recorded camera synchronization and mouse position at infrared beambreaks, drove reward delivery, and commanded optical stimulation delivered by a 473 nm laser (MLL-III, Opto Engine) coupled to a 200 μm diameter fiber fixed above the SI cortical surface (Figure 3.11). Implant location was confirmed in post-mortem histology.

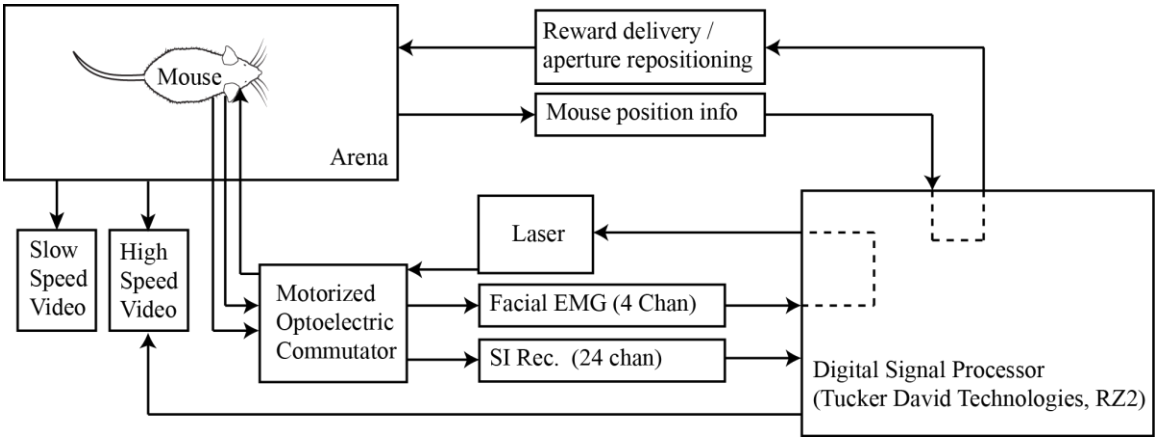

Figure 3.11 Schematic of signal acquisition and feedback

Signal for facial EMG (4 channels) and SI neural recordings (24 channels) pass through an optoelectric commutator and are recorded at 24.4 kHz. EMG signals are processed in real-time to drive closed-loop optogenetic feedback. The system also receives input on mouse position within the arena, which is used to drive reward delivery and reward port repositioning. Both slow speed (30 fps) and high speed (500 fps) videos are recorded, with the saving of high speed clips under automated control by the DSP.

High-speed videography

To confirm offline the EMG relation to whisker motion, we collected high speed video (HSV) at 500 frames per second (pco.1200hs, Cooke Corporation) on a subset of trials (5–10 per session) [81,92]. Each video clip comprised a single traversal of the linear track. We identified clips containing one or more whisking bouts in each stimulation condition (see below) and manually tracked two points on a single, large posterior whisker on the right side of the face using a custom matlab GUI. We determined the angle of the whisker relative to the snout (180° = protracted (fully forward), 0° = retracted (fully backward)). In addition, body motion was tracked in all trials via a camcorder (DCR-SR42, Sony).

3.3.4 Results

Tracking of exploratory whisking for stimulation control

We sought to perturb neural processing during active sensing, to probe how activity in SI drives ongoing sensing behaviors. As such, we required real-time determination of when the animal was engaged in exploratory whisking. Individual whisks were identified from right side EMG envelopes by a double threshold crossing method as follows: whisks were defined by positive crossings of the larger of two thresholds; however, additional whisks would not be identified until the envelope dropped below a second, lower threshold. This procedure minimized spurious detections. Identified whisks were classified into bouts, defined to begin when two whisks occurred within 150 ms, and continuing as long as the elapsed time between subsequent whisks did not exceed 500 ms. We manually selected these parameters in preliminary sessions with other animals, such that the majority of bouts were identified correctly.

We developed automated offline tracking techniques in slow speed video (30 fps) to identify the horizontal position of the nose within the arena (Figure 3.12). Using the results of positional tracking, we computed the average head velocity for each bout and excluded from further analysis bouts where the animal had a mean velocity ≤ 10 mm/s. We also excluded bouts with ≤ 4 total whisks. These criteria helped ensure that only exploratory whisking periods were considered.

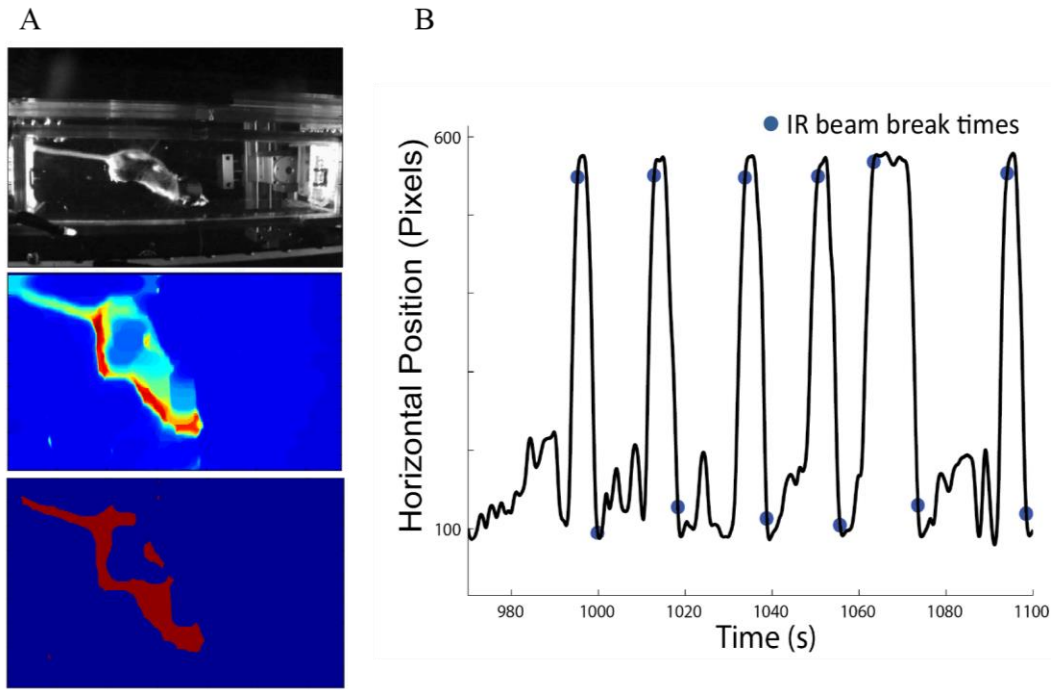

Figure 3.12 Tracking of mouse horizontal position in slow speed video

A, Raw slow speed video recordings (*top*) were processed to identify the horizontal position by smoothing pixel intensities to identify mouse contours (*middle*), then closing contours, thresholding intensities, and identifying nose positions (*bottom*). **B**, The output of slow speed video tracking is the horizontal position of the nose, shown here for six example trials occurring over ~ 30 seconds. Blue dots indicate the time of reward delivery when the mouse reached reward ports on either end of the arena.

With equal probability, bouts were stimulated (laser pulses delivered to SI), or received mock stimulation, with identical processing except that the laser was not enabled. Mock trials serve as controls for naturally highly variable whisking. Since SI activity has been found to be phasically tuned during whisking [51,62,64,68,76], we asked if SI stimulation might impact behavior depending on relative timing.

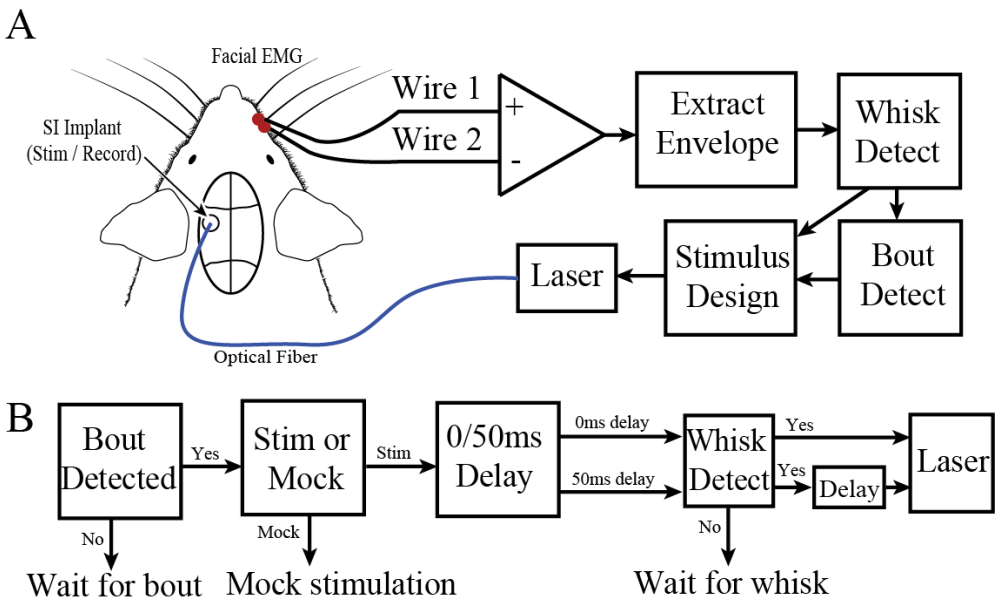

Figure 3.13 Schematic of preliminary closed-loop feedback system

A, The envelope was extracted from bipolar EMGs, and used to detect individual whisks and classify them into bouts. Bout and whisk timing determined stimulus design, driving laser pulses to left SI. **B,** Each bout was selected as stimulated or mock (control) with equal probability. Stimulated bouts were further subdivided, with equal probability, into 0 or 50 ms delay from threshold crossing to laser pulse.

Thus with equal probability, each bout was stimulated with either a 0 ms or 50 ms delay from the threshold crossings of each whisk, consisting of a single 1 ms pulse at 85 mW/mm^2 at the optical fiber tip (Figure 3.13). From the real-time bout definitions, the second whisk in a bout is the first stimulated whisk. Figure 3.14 shows an example of each stimulation condition. Whisker angles relative to the face, estimated from HSV, are included with the EMG for comparison. Vertical blue lines indicate the timing of optical stimulation, or where stimulation would have occurred for mock trials. Importantly, stimulation is driven by each whisk throughout a bout based on the animal's own motions, and not necessarily in a constant frequency train.

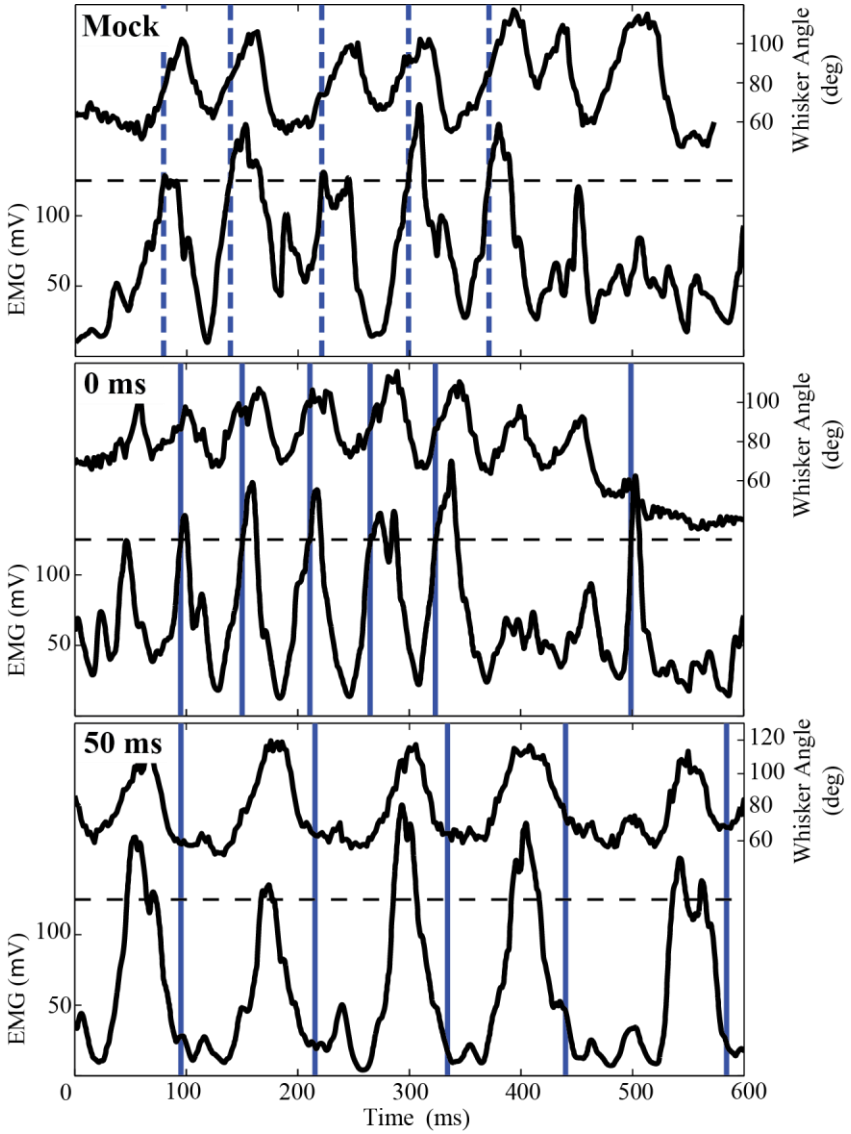

Figure 3.14 Examples show excitatory cortical feedback driven by whisker motions estimated from facial EMG

Traces in each panel show the right side EMG envelope (*bottom*) and the whisker angle (*top*). The dashed horizontal line indicates the upper EMG threshold used for whisk identification. Blue vertical lines indicate laser pulse times (dashed blue lines indicate mock pulses). The example stimulation conditions are mock *(top panel)*, 0 ms delay (*middle panel)*, and 50 ms delay (*bottom panel*). Time zero is arbitrary.

While EMG whisk detection is imperfect, the comparison to angles illustrates that the majority of whisks are detected and stimulated appropriately. Overall for this mouse,

after selecting for bouts of putative exploratory whisking across 7 behavioral sessions, we analyzed 1644 bouts; 828 were mock controls, 394 were stimulated at zero delay, and 422 were stimulated with a 50 ms delay. An average of 2534 1 ms pulses were delivered per 30–60 minute session. While bout lengths were highly variable, the mean bout duration was 1.4 s, and the mean number of whisks per bout was 12.6.

Behavioral changes following SI stimulation

For the Thy1-ChR2 mouse line used here, pulses predominately activated excitatory pyramidal neurons, with strong expression in layer 5 [114]. To confirm that stimulation activated a subpopulation of SI neurons, we looked at single unit activity aligned around laser pulse times. An example raster (*top*) and PSTH (*middle*) for a single session are shown in Figure 3.15A, demonstrating an increase in this unit's spiking probability shortly after laser onset, consistent with excitatory ChR2 stimulation. All pulses within the session are shown; since these were locked to whisks, the timing of subsequent pulses varied with the animal's behavior, with peaks in the pulse-time autocorrelation around characteristic whisk durations ~ 50 and ~100 ms (Figure 3.15A, *bottom*).

We then explored effects of stimulation on whisking and found effects at multiple timescales. The EMG envelope in the 50 ms stimulation condition (Figure 3.14, *bottom*) shows a small increase approximately 10–20 ms following each pulse, which we observed qualitatively throughout our data.

These were usually accompanied by small (≤ 5 deg) protractions seen in HSV reconstructed whisker angles. Moreover, a similar effect is observable in the 0 ms delay

condition, although it is largely obscured by the ongoing whisk, while not present during mock stimulation. Such short latency motions following SI stimulation are similar to an earlier report [60], but here protractions and not retractions are produced (see discussion below).

To reveal changes across whisks, we computed EMG averages aligned around threshold crossings (Figure 3.15B). Aligned averages of rectified but not smoothed EMG (*grey traces*) preserve high frequency features, including the short latency response (*inset*). Smoothing with a 10 ms wide Gaussian kernel highlights the interwhisk structure (*black traces*). The alignment procedure produces a large center peak, but pronounced additional peaks near latencies of 75 ms and 125 ms appear only in the two stimulated conditions, suggesting that subsequent whisks occur with greater regularity during stimulation. However, increased oscillations in the aligned averages could be due either to changes in amplitude or changes in phase precision. We further quantified this apparent whisking regularization through interwhisk intervals (IWI), defined as times between subsequent EMG threshold crossings. In order to suppress any effects of altered bout length, for example if the animal became generally more active during stimulation, we considered only the first 4 stimulated whisks in each bout.

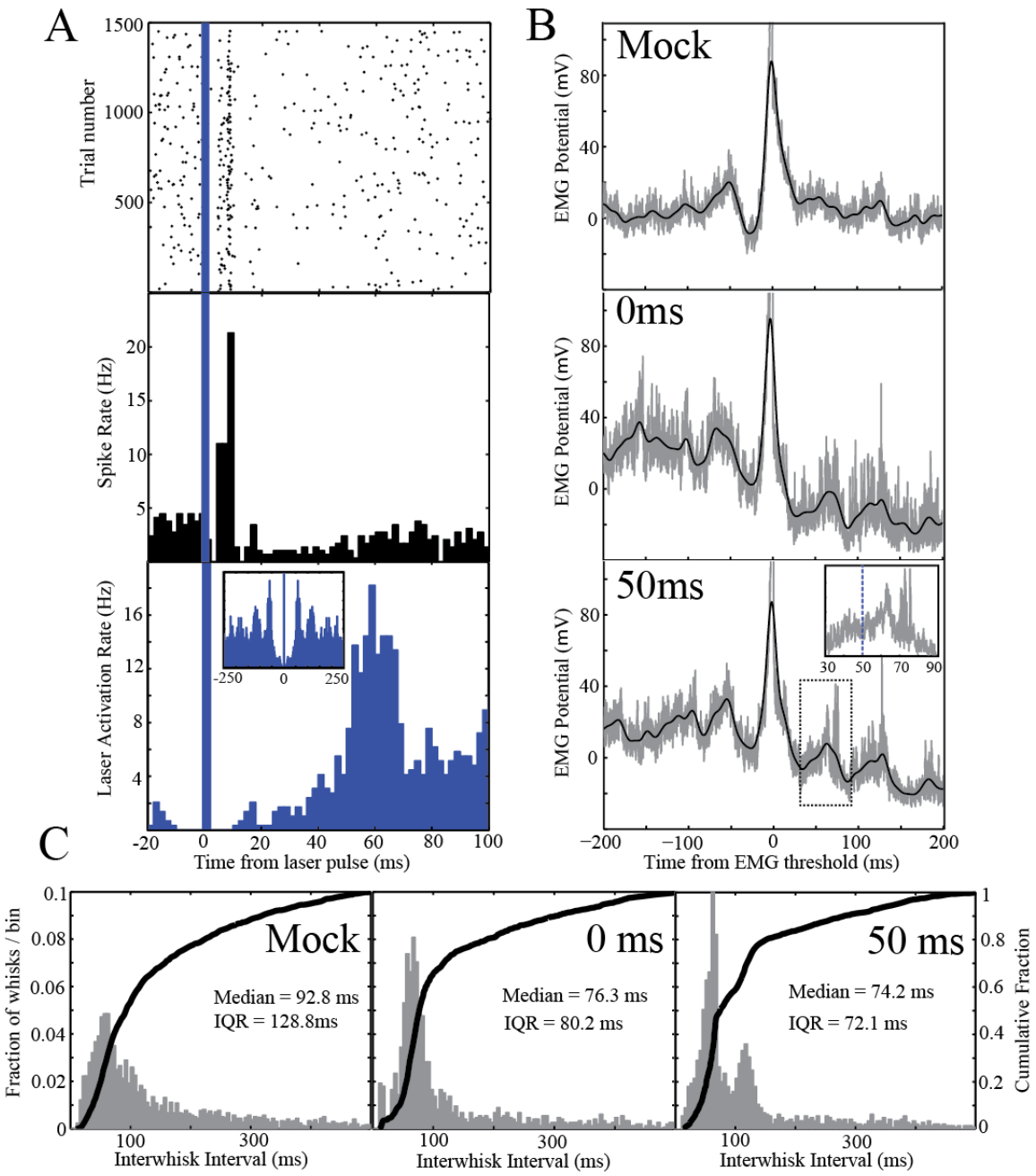

Figure 3.15 Behavioral responses to cortical feedback

A, The laser pulse aligned raster (*top*) and PSTH (*middle*) show an example SI single unit that rapidly responds to stimulation. The relative timing of other pulses (*bottom*) depends on whisking patterns. Inset: pulse timing over ± 250 ms. **B,** Average EMG aligned around EMG threshold crossings for mock, 0 ms delay, and 50 ms delay conditions (*gray traces*), and temporally smoothed (*black traces*). Stimulated cases show prominent side peaks following alignment (n=3900 whisks in each condition). Zoomed (*inset*) shows EMG deflection ~ 15 ms following

pulses. **C,** Interwhisk interval distributions for each condition (*gray histograms*), and cumulative density function (*black traces*), indicate increased regularity of interwhisk intervals with stimulation: peaks become higher and more narrow, and interquartile ranges decrease.

The distribution of IWIs across all bouts for all seven sessions are shown in Figure 3.15C. Comparison of the interquartile ranges (IQR) for each of these distributions shows a decrease across conditions from 129 ms (mock) to 80 ms (no delay) and 72 ms (50 ms delay). This decrease in IQR is consistent with regularization of whisking, and whisking at a more consistent rate. We also observed a decrease in the median IWI from 93 ms (mock) to 76.3 ms (no delay) and 74.2 ms (50~ms delay). The medians in each stimulated condition were significantly different from mock stimulation (Wilcoxon rank sum test, $p < 0.01$). This difference suggests a slight acceleration of whisking, corresponding to a ~3 Hz increase in whisking frequency for stimulated bouts.

3.3.5 Discussion

We have shown that optogenetic stimulation of SI pyramidal neurons, when locked to whisker motions, regularizes the timing of whisking. These results support that SI is not simply a recipient of sensory information, but during active sensing also plays a role in guiding motor patterns for subsequent sensing motions. Several caveats should be made. Although animals were not trained on a specific whisker-dependent task, object contacts with the floor and walls of the arena were common. Behavioral context is likely relevant to how animals respond to neurostimulation. The stimulation delivered was likely not "natural"; both the firing rate and synchrony of the evoked activity were likely atypically

high, and we did not preserve the laminar flow of activation following thalamic input [52]. Although placement over SI was confirmed by observing neural activity responsive to whisker deflection on tetrodes located in a fixed geometry to the stimulating fiber, it is also possible that stimulation over SI directly recruited activity in other areas. The detailed mechanism of SI modulation of whisking is the subject of ongoing work with cortical recording and varying ChR2 expression.

We used EMG threshold crossings for whisk detection, and delivered laser pulses with a fixed duration and amplitude. Future studies will include EMG frequency and amplitude information to vary stimulation parameters and may deliver stimulation timed to specific whisker events (*e.g.* protractions or retractions) rather than stimulation at various fixed delays from EMG threshold crossings. A central question is the perceptual impact of stimulation, which we do not address here. Ongoing work with real and virtual object search tasks could provide a dissociation of sensory and motor processing in SI.

A previous study found SI activation drove short latency retractions [60], in the same optogenetic mouse line used here. Our results suggest the effects may be more complicated, as we found protractions could be produced. Here animals were freely moving, and stimulation was locked to self-motion. In contrast, the previous study delivered fixed pulse trains during periods of quiescence in head-fixed animals. Further work is needed to clarify these differences (see chapter 4).

More generally, we hypothesize that timing of stimulation relative to sensing behavior, and not simply induction of stereotyped “codes” for sensory events, will be a critical element in sensory neuroprosthetic design. The presented paradigm for optogenetic feedback controlled through whisker motions could powerfully address the relation of cortical activity to perception during active sensing.

CHAPTER FOUR- Closed-loop feedback stimulation reveals somatosensory cortex participation in short-latency control of whisk timing

4.1 Executive Summary

In this chapter, we capitalize on the methods developed in previous chapters to investigate the involvement cortical sensory areas in coordinating active sensing motor outputs on short timescales. Actively exploring mice are able to select from a diverse range of available sensing strategies, and the observed sensing motions are unlikely to be purely reflexive. In order to investigate a possible role for primary somatosensory cortex (SI) in coordinating active sensing motions, we delivered closed-loop optogenetic feedback timed to whisker motions in mice, estimated using facial electromyography. We find that stimulation locked to whisking (timed to either protractions or retractions) increases the regularity of whisking (overall periodicity), but that an acceleration in the timing of the next motion occurs only for stimulation locked to whisker protractions. Additionally, we observe these changes to timing even when considering only the first pulse delivered on each trial, suggesting that the effect arises from an SI output, rather than from the animal acting over a longer timescale based on sensory perception and involving multiple cortical areas. Simultaneous neural recordings from SI show cyclic changes to excitability, specifically that responsiveness to retraction-locked stimulation is suppressed, which may suggest an active mechanism to limit responses in SI during times when a natural whisker contact is unlikely and incoming information is therefore more likely to be noise. Parallel experiments that delivered inhibitory optogenetic stimulation

showed a similar cyclic change in SI responses, with protraction-locked stimulation having a more pronounced effect. The short timescale changes to active sensing motions and the observed cyclic nature of cortical excitability in SI suggests spikes must be interpreted within the context of self-motion. This may have important implications for the design of sensory neuroprostheses that exploit active sensing context in delivering feedback stimulation.

4.2 Introduction

A variety of active sensing behaviors have previously been reported in the whisker system, including repositioning whiskers to "look ahead" into the region the head is turning into [58,90], and the manipulation of whisking parameters to maximize contacts and promote minimal impingement of whiskers on subsequent whisks [91]. In general, mice are able to select from among a diverse body of available sensing strategies based on their behavioral goal and on previously acquired sensory information. We previously examined the timing of whisker repositioning relative to head rotations and found that mice reposition whisker set-points prior to initiating a turn, suggesting that the observed repositioning is not simply a reflexive response to the turn itself [195] (chapter 2). These findings suggest the possibility of higher-level control in coordinating active sensing motions.

Primary somatosensory cortex (SI) is a region likely to be involved in the coordination of active sensing. Recent work has shown that electrical or optogenetic activation of SI can

produce whisker retractions with short latency to stimulus onset, even when primary motor cortex (MI) has been chemically inactivated [60]. This study raises additional interesting questions; for example, mice were head-fixed and received stimulation only when in a quiescent state, leading to a speculation regarding what other (head or body) motions would have been observed in a freely moving animal, and whether the state of the animal (whisking or quiescent) at the time of stimulation would impact the observed results. Their conclusion that SI induces whisker retractions via projections from SI to the facial nucleus without MI involvement [60] suggests a role for SI beyond simply being a recipient of sensory information. We seek to better understand this role within the framework of an active sensing task.

Neural recordings from SI have shown evidence of phase tuning, with a population preference towards increased firing near retraction onsets (while the whisker is near maximal protraction) [62,76]. This phase tuning has been observed to vary with cell type and cortical layer [64], and appears to be enhanced during goal directed exploration (as opposed to whisking in air without contacts) [63]. Similar modulation with whisking phase was also observed for intracellular potentials in SI [68]. The observed phase tuning generally shows a small modulation depth and appears only in a subset of SI units. The origin of phase tuning in SI is uncertain and could be explained in several ways. For example, a distribution of cells with different phase preferences could have developed as an evolved system to detect whisker phase at object contact in order to aid in localizing a target relative to the head. Alternatively, the observed phase tuning could arise as a result

of a mechanism that suppressed SI responsiveness at non-preferred phases. Since natural contacts are most likely to occur during forward whisker motions (protractions), such a system could explain the observed phase tuning distributions. By delivering stimulation timed to different parts of the whisk cycle (protraction vs. retraction), we may gain insight towards distinguishing between these possibilities.

Our previous findings regarding sensing strategy selection and the timing of observed changes [195], along with evidence for motor control by sensory cortex stimulation [60], and reports of efference copy signals in SI [51,76,139], have led us to further evaluate the role played by SI in coordinating the whisk-by-whisk timing of motor outputs. We developed a method to deliver optogenetic stimulation locked to whisker motions in real-time using facial electromyography (EMG) to provide an estimate of whisk timing [89] (see chapter 3). We then evaluated the effects of SI stimulation locked to whisking in mice conducting a tactile search task, during the portion of each trial prior to the mouse making contact with the rewarded aperture. Specifically, we asked whether the timing of stimulation relative to the whisk cycle (protraction vs. retraction vs. random) influenced the observed changes in whisk timing and impacts within SI neural populations.

4.3 Methods

Animals and Task Design

We trained three mice (B6.Cg-Th$^{(Thy1\text{-}COP4/EYFP)18Gfng)/J}$, Jackson Laboratories) in a tactile search task describe previously [195] (chapter 2). Briefly, mice repeatedly traverse a

linear, polycarbonate track (31 cm x 9 cm) in the dark in search of a water reward. The reward is placed at the center of a 1.4 cm aperture, which is automatically repositioned to one of four possible locations prior to trial initiation. In this case, all four possible positions lay along the center line of the arena at different distances, meaning the mouse did not know on a particular trial how far along the track he would first make whisker contact (Figure 4.1A). Sessions were conducted in the dark under illumination by custom IR-LED panels placed along the long axis of the arena. Mice were trained in daily sessions with the apertures immobile until the mice routinely exceeded 80 trials per day, at which point the automated reward repositioning was initiated. The mice were implanted with chronic hyperdrives for neural recording and stimulation once they reliably reached a threshold of 100 trials per day.

Hyperdrive and EMG Implants

We implanted custom hyperdrives for optogenetic stimulation and recording which are a modification of our previously described drive design [168]. These drives were modified for ease of manufacturability using 3D printed parts and for improved, low profile connection to the recording apparatus (chapter 3.2). The drives consist of 6 moveable tetrodes plus reference, in a ring surrounding a 200 μm fiber coupled to a laser for 473 nm light delivery. Drives were implanted over left SI (3.75 mm lateral, 1.5 mm posterior from Bregma) following craniotomy and durotomy. In the same surgery, we implanted bilateral EMG electrodes (twisted pairs of 50 μm stainless steel wire, 1 mm contact spacing) into the facial pad, targeting the large posterior whiskers. We have previously

described adaptations to EMG electrode design and implant procedures developed for rats [86,88] to accommodate the much smaller facial pad in mice [89] (chapter 3.1). The implant procedure consists of tunneling a 23 g needle loaded with an EMG electrode subdermally from the anterior edge of the scalp incision and exiting from the posterior region of the whisker pad. The electrode is passed through the skin until it slightly protrudes from the whisker pad, the needle is removed, and the wire is retracted until it is just inside the skin. The wires are secured to the skull using dental acrylic and correct placement is confirmed by passing current through the EMG electrodes and observing small rhythmic whisker motions (10 Hz, biphasic, 50% duty cycle, ~ 100 μA). Mice were allowed to recover for approximately 10 days before the resumption of the water restriction protocol and the initiation of data collection. During this time, tetrodes were advanced while evaluating the quality of neural recordings.

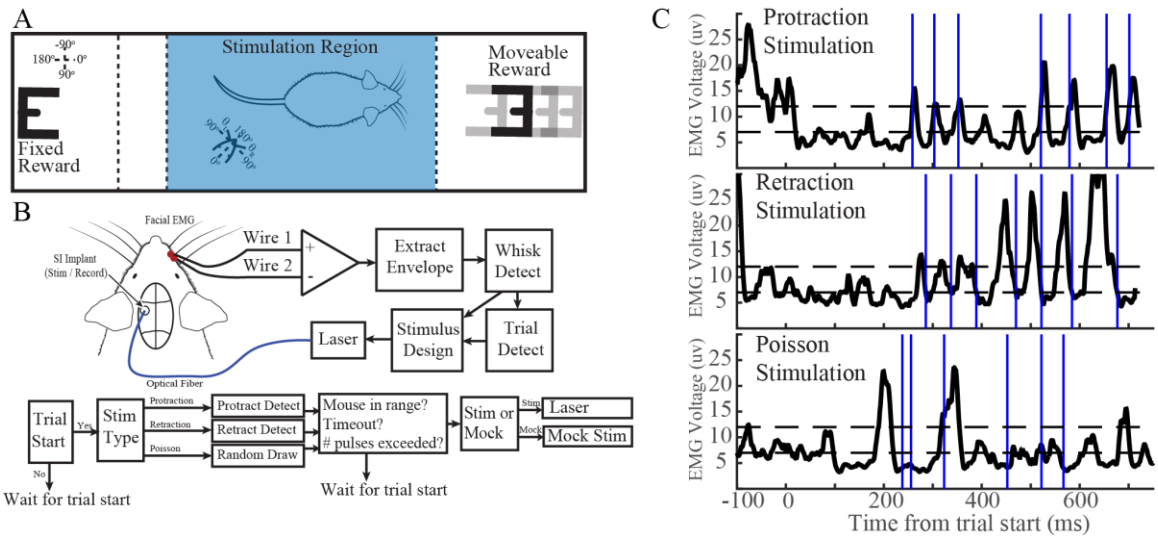

Figure 4.1 Closed-loop feedback timed to whisker motions in an active sensing task

A, Mice repeatedly traversed a linear track in search of a water reward located at the center of a moveable aperture. Closed-loop stimulation was delivered to SI in the stimulation region marked in blue with location in the arena being determined by IR beambreaks (*dashed lines*). Insets:

angle conventions relative to the arena and head. **B,** Block diagram showing the signal processing chain for real-time feedback stimulation (*top*) and the determination of stimulation conditions (*bottom*). **C,** Example trials from each stimulation condition showing the EMG (*black traces*), EMG thresholds (*dashed lines*), and stimulation times (*blue bars*).

Recording, Stimulation and EMG Whisk Extraction

Mice were placed in the behavioral arena and connected to a DSP-based acquisition system (RZ2, Tucker Davis Technologies) via a 32-channel headstage and lightweight tether connected to a motorized commutator, which also accommodated an optical fiber. Signals from 6 tetrodes (24 channels) and 2 EMGs (4 channels) were recorded at 24.4 kHz, along with signals for camera synchronization, reward delivery, and mouse position (via IR-beambreaks placed along the track). The same system drove reward delivery, repositioning of the rewarded aperture, video acquisition times, and output commands for optogenetic stimulation (Figure 3.11). Optogenetic stimulation was delivered by a blue (473 nm) laser coupled to the implant. Light intensity was adjusted to be ~ 38 mW/mm^2 (abs. intensity 1.2 mW) at the tip of the implant. Stimulation intensity was chosen with reference to published levels [114,168] and was shown in pilot studies to produce modulation of SI firing and whisking behavior (chapter 3.3, Figure 1.4). The optical fiber itself does not penetrate the brain, but is resting near the cortical surface once the implant is secured in place. Stimulation was in the form of 1 ms square wave pulses.

EMG signals were processed in real-time by bandpassing the differential input (0.4 – 3 kHz), rectifying the signal, and then lowpass filtering (40 Hz). A protraction was defined as a positive crossing through the greater of two manually identified thresholds. To

prevent multiple identifications of the same whisk, an additional whisk would not be identified until the system had been reset by a negative crossing through the lower threshold. This point was also defined as a retraction, thus EMG provides a real-time method to deliver stimulation that is timed either early in the whisk (protraction) or later in the whisk (retraction). These EMG derived sensing motions provide the basis for real-time optogenetic feedback to SI. We demonstrated previously that EMG whisk identification is relatively insensitive to small errors in manually defined threshold values [89] (chapter 3.1).

In addition to neural recording and stimulation, we also recorded high-speed video (500 fps) for a subset of trials, typically 20–30 per session. The high-speed collection system was automated to save the next trial once the previous had finished saving in order to prevent a user selection bias. Videos were recorded through the bottom of the clear arena and captured approximately ¾ of the track length, including the entire stimulation region. On a subset of videos, a single large whisker on each side of the face was manually tracked to provide a ground truth measure of whisker position. The entire session was also recorded using a standard camcorder (30 fps) to provide an overall record of behavior.

Design of stimulation algorithm

Trials were defined as a track crossing in the direction of the moveable aperture and were initiated by the mouse. Mouse position along the track was monitored with a series of

infrared photodiodes. The output voltage from these photodiode beambreaks decreased when the animal passed in front of the photodiode, providing an estimate of mouse position. A trial begins with the successive crossing of two IR beambreaks (to ensure motion in the correct direction) within one second, and ends with the crossing of a third beambreak that is reached prior to arriving at the rewarded aperture (Figure 4.1A, *dashed lines*). The stimulated region covered approximately the middle third of the track, and no stimulation was delivered while the mouse was making whisker contact with the aperture. A trial can also end by timing out (trial length greater than three seconds, which prevents repeated stimulation on trials if the mouse stops in the middle of the track) or by exceeding a maximum number of pulses (15 pulses/ trial). Additionally, there must be at least one instance of two positive EMG threshold crossings within 150 ms of each other since the last reward was dispensed in order for stimulation to be engaged, this condition was imposed to ensure the mouse is whisking during stimulation (Figure 4.1B).

Once a trial was initiated, it was randomly chosen for protraction-locked stimulation, retraction-locked stimulation, or Poisson stimulation (stimulation unlocked from whisking), and further selected as a stimulated or a mock trial. Mock trials have identical processing at all steps except no output is sent to the optical fiber. Protraction trials deliver a 1 ms pulse on positive crossings of the upper EMG threshold while the conditions described above are met, retraction trials deliver the pulse on negative crossings of the lower threshold, and Poisson trials deliver 6 pulses at intervals determined by a previously computed Poisson distribution (Figure 4.1B,C).

Data analysis

For offline analysis of EMG recordings, we processed raw EMG signals using non-causal filtering methods to ensure accurate relative timing and computed the envelope as the RMS of the bandpassed signal using a 10 ms wide Gaussian kernel [89]. Behavioral changes following SI stimulation were evaluated by computing aligned averages of EMG signals separately for only the first pulses delivered on each trial, or for all pulses in all trials, in each case broken apart by stimulation condition. To compare protraction and retraction stimulation, we aligned retraction trials by the protraction that preceded the stimulated retraction. This alignment facilitated comparisons of relative timing of the whisk following stimulation by ensuring that all trials were aligned to a common phase in the whisk cycle for unbiased comparison.

To evaluate neural responses in SI, we bandpassed (0.6–6 k Hz) and conservatively thresholded (5 std above mean) one channel from each tetrode to determine multiunit activity. Peristimulus time histograms (PSTHs) of this multiunit neural activity were then computed for each stimulation condition, and plotted along with histograms of protraction times to provide a reference for the timing of sensing motions relative to SI neural activity.

4.4 Results

Closed-loop SI feedback locked to whisker motions

We used facial electromyography in mice to estimate the timing of whisker motions during reward approach in a tactile search task (see chapter 3.1). Based on real-time EMG estimates of whisk timing, we delivered optogenetic feedback to SI either timed to protractions, retractions, or at random times during reward approach. Figure 4.1C shows example trials for each type of stimulation, along with the upper and lower EMG thresholds, indicated by dashed lines. For each of the three conditions, half of the trials were stimulated and half were mock stimulation (identical signal processing but no laser output), to provide a baseline for comparison.

In order to evaluate the impact of this real-time feedback stimulation on behavior, we computed aligned averages of EMG signals processed offline with non-causal filters (see Methods above). EMG data was normalized by dividing each trial by its own maximum in order to account for differences in absolute EMG signal amplitude between mice and across sessions. EMGs were aligned around the positive threshold crossing that triggered the start of a stimulated whisk (for protractions this is synonymous with the pulse time, for retractions the pulse times are indicated by inset histograms); for the Poisson stimulation condition, averages were aligned to stimulation times.

SI stimulation timed to protractions alters the next whisk

Aligned average EMGs for evaluating changes to whisking behavior following the first pulse delivered on a trial are shown in Figure 4.2A for real stimulation (*blue*) and mock stimulation (*black*). In order to evaluate changes to whisk timing on the timescale of the next whisk following stimulation, we compared the secondary peaks following stimulation in the aligned average EMGs. We find that stimulation timed to protractions shifts the position of the first post-stimulus whisk forward by approximately 20 ms compared to the timing observed in the mock stimulation condition (Figure 4.2A, *left*). However, stimulation timed to retractions did not produce this temporal shift, as the first post-stimulus whisks remain aligned for the stimulated and mock conditions (Figure 4.2A, *center*). The observation that changes to whisk timing occurred even when comparing only the responses to the first stimulus pulse delivered in each trial indicates that these changes can be induced with short latency by sensory cortex stimulation, and are not simply the result of a long timescale change in motor patterns. For example, if the timing changes were observed only when considering stimulation given on every whisk throughout each trial, it may have been possible that the observed acceleration was the result of a more generalized increase in arousal or attention, rather than a specific motor effect from sensory stimulation.

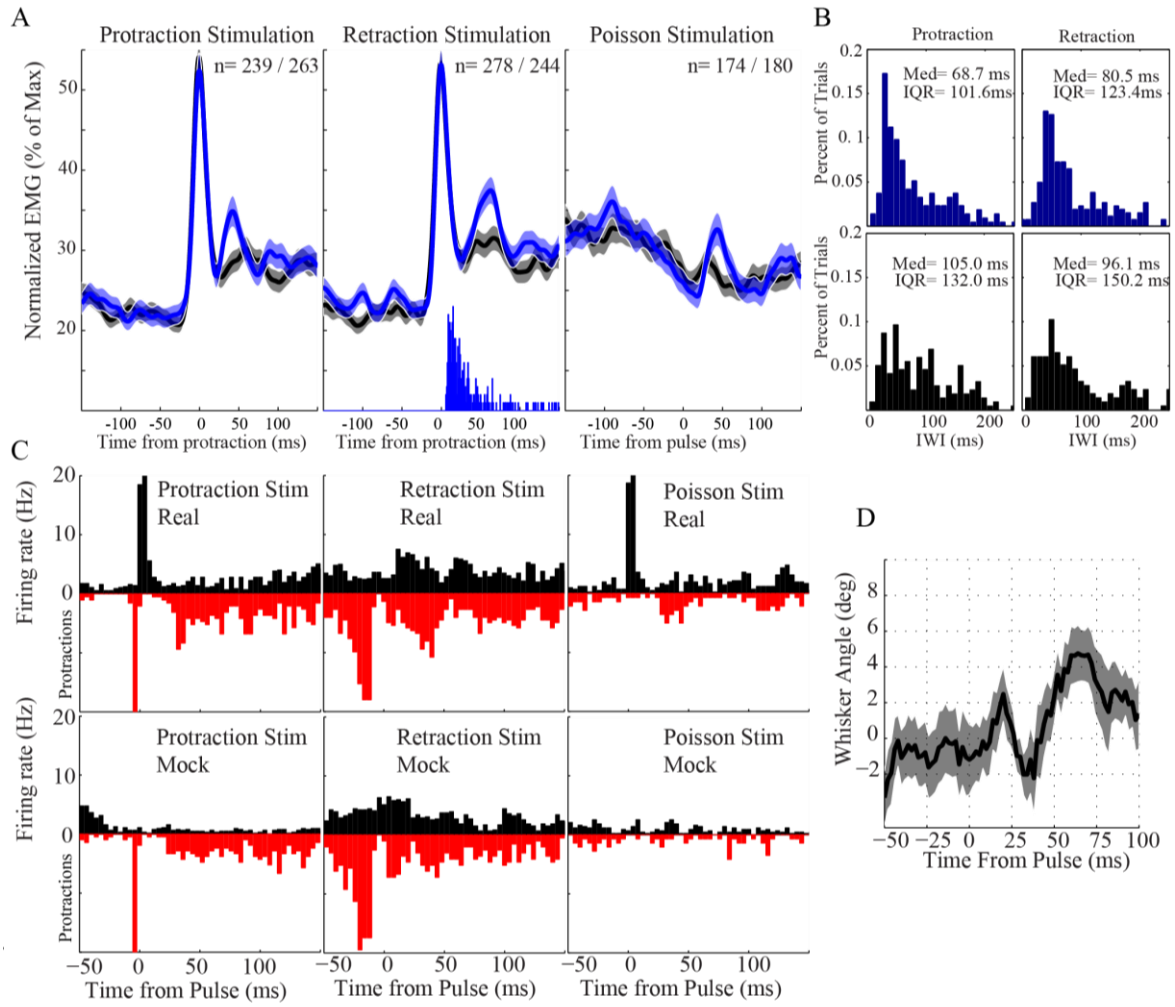

Figure 4.2 Protraction-locked stimulation drives short latency changes in whisk timing

A, Aligned average EMG for each stimulation condition for real stimulation (*blue*) and mock stimulation (*black*) (mean ± SE) considering only the first pulse delivered on each trial. Stimulation locked to protractions accelerates the timing of the next whisk following stimulation and short latency EMG peaks are evident following Poisson stimulation. **B,** Histograms of interwhisk intervals following the first pulse in each trial show a significant acceleration in whisking from protraction-locked stim. Interquartile range decreases with whisk locked stimulation indicate increased regularity of whisk timing across trials. **C,** PSTHs of multiunit recordings from SI aligned to the first pulse in each trial for each stimulation condition (*black)*. Stimulation locked to protractions and random stimulation both increased SI firing, while stimulation locked to retractions did not. EMG derived whisker protraction events (*red*) provide a reference for ongoing whisking behaviors. **D,** Whisker angles from manually coded high speed video aligned to randomly timed pulses show a small increase in whisker angle ~ 20 ms post-stimulus (mean ± SE, n=12)

Changes in inter-whisk interval (IWI) also reflect this change as a comparatively larger decrease in median IWI for protraction as compared to retraction timed stimulation (Figure 4.2B). The IWI change from mock to real retraction stimulation was not significant (t-test, $p = 0.78$), while the change from mock to real for protraction stimulation was significant (t-test, $p = 0.0036$). Finally, the distributions of IWIs for real protraction stimulation and real retraction stimulation were significantly different from each other (t-test, $p = 0.016$).

To assess the neural correlates of this short-timescale alteration in whisk timing, data from tetrode recordings in SI was bandpassed and conservatively thresholded (5 std above mean) in order to determine multiunit spike times during stimulated and unstimulated trials for each condition. PSTHs for multiunit SI responses to the first pulse delivered on each trial (Figure 4.2C, *black bars*) show a robust increase in multiunit firing rate for stimulation timed to protractions and for stimulation delivered at random times. Stimulation timed to retractions, however, failed to result in increased multiunit firing. The correlation between a decreased responsiveness in SI and a lack of observable change to whisk timing following retraction stimulation suggests that SI responsiveness is likely reduced during certain phases of the whisk cycle. EMG derived protraction events (*red bars*) provide a reference for the ongoing whisking behavior relative to the timing of SI multiunit activity.

Interestingly, we also observed the emergence of a strong post-stimulus peak in the aligned average EMGs for Poisson stimulation, whereas the mock stimulation showed no defined structure (Figure 4.2A, *right*). We have previously noted small protractions both in EMG and in high speed video reconstructed whiskers angles for the same type of stimulation in Thy1-ChR1 mice [27] (Figure 3.14, *bottom*). To assess the behavioral impact of the EMG peaks observed following Poisson stimulation, we manually coded whisker and head position for a small subset of video trials during Poisson stimulation. Video reconstructed angles are shown aligned to pulse times (mean +/- SE) with the pre-stimulus mean angle subtracted in order to compare changes across trials (Figure 4.2D). The whisker angle showed a small (2–3 degree) protraction approximately 20 ms after stimulation. We also observed a larger whisker motion occurring on a longer timescale, possibly the result of the mouse responding to a perceived (and likely strange / unexpected) perception with a whisker motion.

Stimulation locked to whisking throughout a trial regularizes whisk timing

We observed that any stimulation timed to whisking (either protractions or retractions) had the effect of regularizing whisking, meaning that subsequent whisker motions occurred with a more consistent temporal structure across trials. This effect is reflected in the emergence of a stronger post stimulus peak in the aligned averages for real stimulation as compared to mock, especially when comparing the results from all pulses delivered in a trial (Figure 4.3A). This effect is not due to entrainment to a user selected stimulation frequency, as the stimulation is timed to the motions selected by the animal.

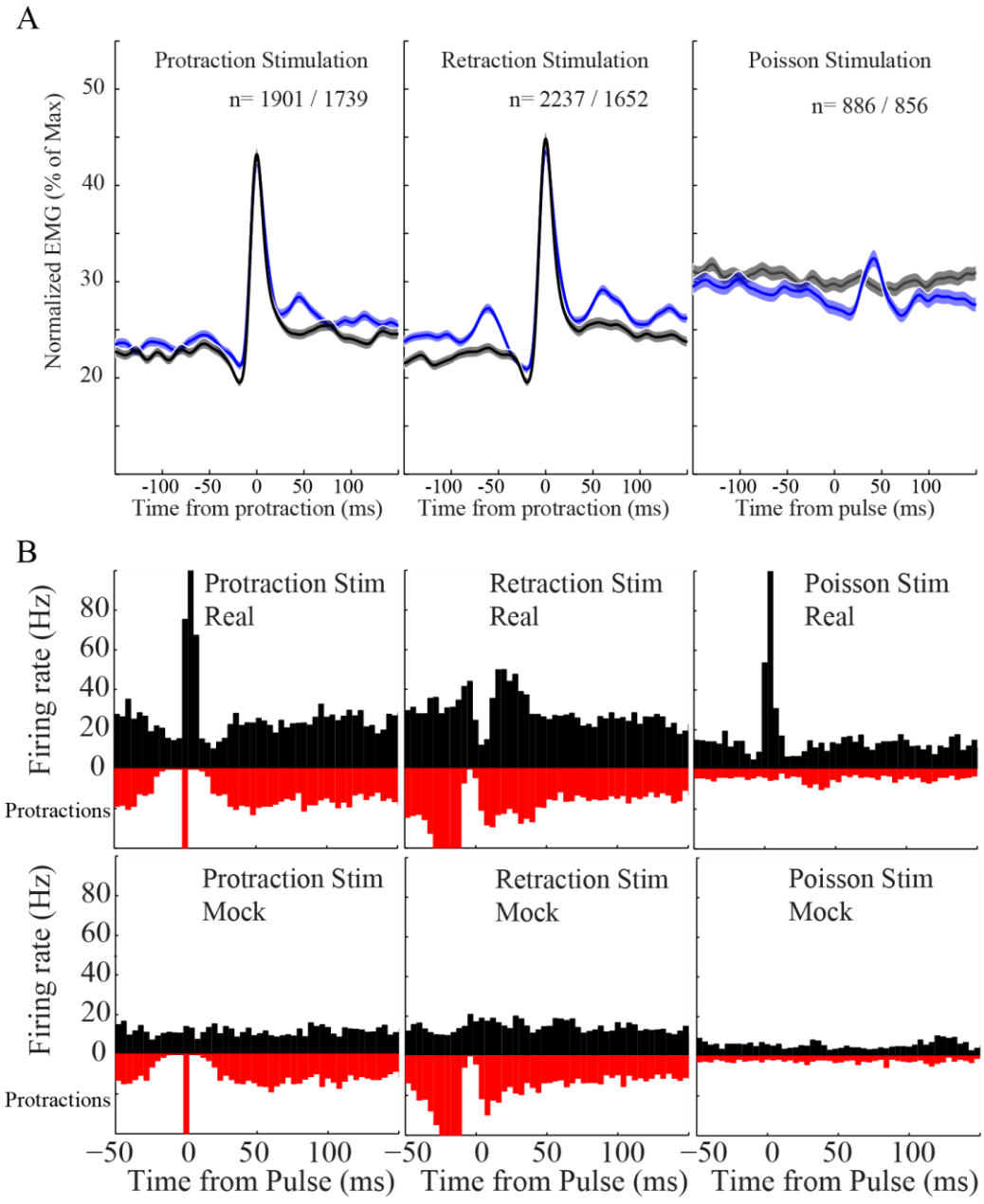

Figure 4.3 Stimulation locked to whisking throughout a trial increases regularity

A, Aligned average EMGs for all pulses in a trial for each stimulation condition with stimulated trials in blue and mock trials in black. The prominence of post-stimulus peaks with whisking locked stimulation indicates increased regularity across trials. Acceleration of whisking is also evident in the protraction- locked case. **B,** PSTHs of multiunit activity in SI aligned to all stimulation times (*black*). Robust increase in firing is observed following protraction timed and Poisson stimulation. Retraction stimulation, however, appears to suppress firing below baseline, possibly indicating cyclic changes in the level of SI excitability. Protraction events derived from EMG are show below for reference (*red*).

It is perhaps more appropriately thought of as reinforcing a pattern of whisking activity initiated independently by the mouse. This regularization is observed both when viewing all stimulated pulses and when including only the first pulse delivered on a given trial (Figure 4.2B), reinforcing that rapid modulation of sensing motions from sensory cortex stimulation is possible. Additionally, the regularization is reflected in a decrease in the interquartile range of IWI distributions following both protraction and retraction timed stimulation (Figure 4.2B). This aligned EMG analysis using all stimulus pulses in all trials also shows the same shift in whisk timing selectively for protraction stimulation that was previously shown for single pulses (Figure 4.2A).

PSTHs encompassing responses from all pulses on a trial showed a robust increase in firing rate for the protraction timed and Poisson stimulation conditions (Figure 4.3B) similar to that observed following only the first pulses in each trial (Figure 4.2C). Stimulation timed to retractions, however, not only failed to increase firing rate, but may in fact reduce firing below the pre-stimulus baseline. A qualification to this conclusion is that MUA will also track changes in whisking, which is aligned differently on retraction stimulation (Figure 4.3B, *red protraction time histograms*), meaning that there may be fewer spikes near retractions even without stimulation. Despite this caveat, however, excitatory stimulation is failing to produce the expected increase in firing rate when delivered during whisker retractions. The suppression of SI responsiveness during retractions provides further evidence for a system that actively modulates cortical excitability, possibly in order to facilitate “windows of opportunity” for sensory

acquisition and suppress responses outside those windows. The timing of multiunit spikes relative to whisker motions (EMG protractions indicated by red histogram bars), also shows that tuning to whisk phase is weakly evident in the unstimulated case and more strongly visible during stimulation.

Parallel experiments with inhibitory stimulation reinforce cyclic changes in SI excitability

In order to better understand the observed differences in SI responsiveness to stimulation during whisker protractions and retractions, we conducted an identical experiment (same implants, training, task, and stimulation conditions) but with optogenetic targeting of inhibitory rather than excitatory cell populations. ChR2 was locally expressed in PV+ inhibitory interneurons of two PV-CRE mice (B6;129P2-Pvalbtm1(cre)Arbr/J, Jackson laboratories) [119] through an initial surgery (~3 weeks prior to implant) to deliver a cortical microinjection of an adenoassociated virus with a “double inverted open” sequence for ChR2 (DIO-ChR2-H134; U. North Carolina Viral Core). When co-localized with CRE, this ChR2 sequence is flipped to allow transcription, facilitating expression that is both localized and cell type specific.

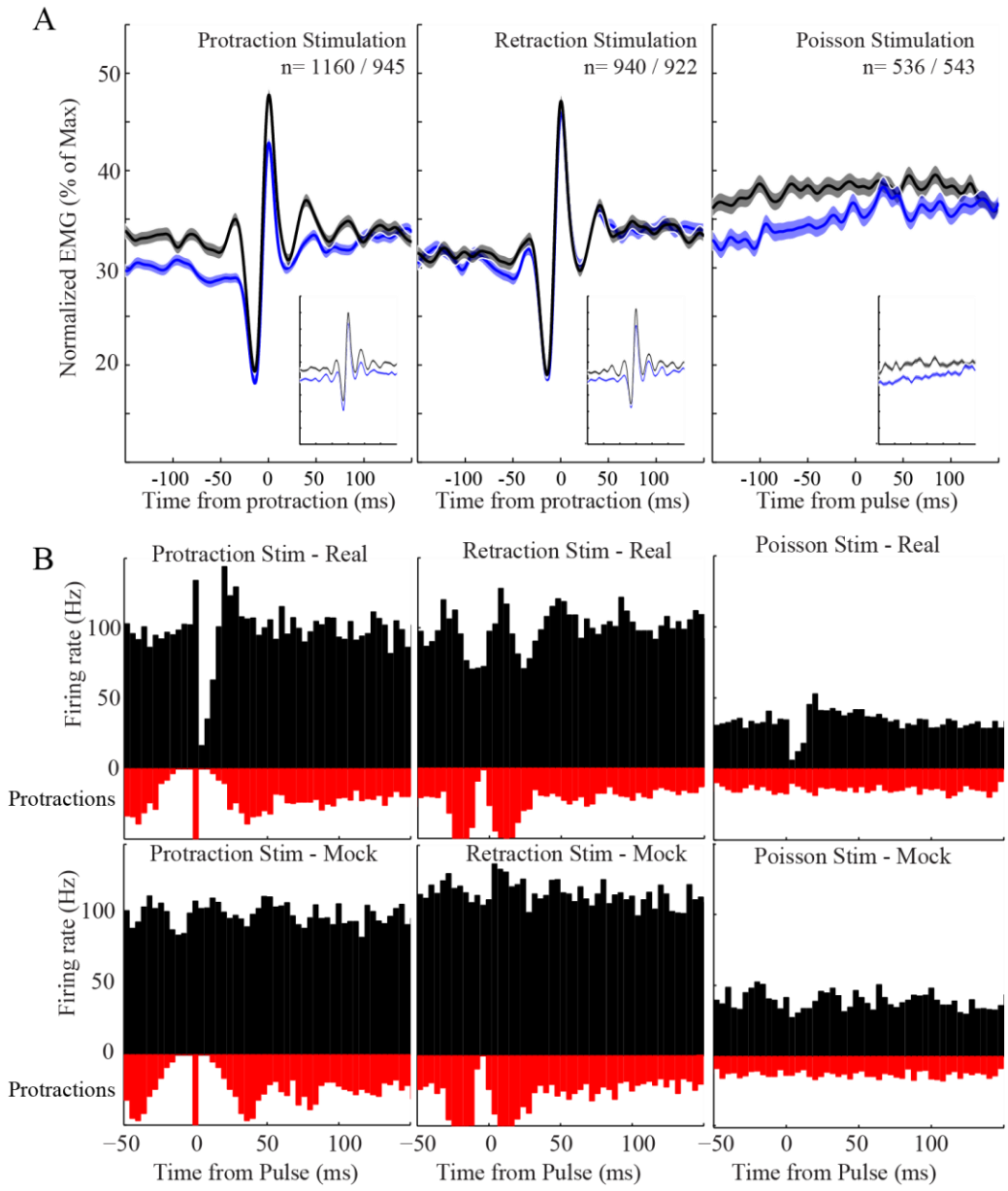

Figure 4.4 Stimulation of SI inhibitory cells shows selective slowing of whisk timing and cyclic changes in excitability

Same analysis as Figure 4.3, for experiments conducted on animals expressing ChR2 in SI PV cells. **A,** Aligned average EMGs for all pulses in a trial for each stimulation condition with stimulated trials in blue and mock trials in black. Stimulation timed to protractions delayed the timing of the next whisk by 10– 15 ms. *Insets*: Aligned average EMGs using the same stimulus intensity as Figures 4.2/4.3 show no clear change to whisk timing. **B,** PSTHs of multiunit activity in SI aligned to all stimulation times for inhibitory stimulation (*black*). Robust post-synaptic inhibition of firing is observed following protraction timed and Poisson stimulation. Retraction

timed stimulation, however, does not appear to have a similar effect. Protraction events derived from EMG are show below for reference (*red*).

We replicated the behavioral (aligned EMG) and neural response analysis from Figure 4.3 using these mice. When stimulating inhibitory cells in PV-Chr2 mice with the same light intensity used for excitatory stimulation in Thy1-Chr2 mice (~38 mW/mm^2) we did not observe the same short time scale changes in whisk timing, and we did not see small protractions resulting from stimulation at random times as we did with excitatory stimulation (Figure 4.4A, *insets*). A modest increase in light intensity (~57 mW/mm^2) however, resulted in a weak delay of the next post-stimulus whisk when stimulation was locked to protractions, with no change in timing evident for retraction stimulation. The neural responses to inhibitory stimulation displayed a similar pattern of cyclic responsiveness to that observed for excitatory stimulation. The expected post-stimulus inhibition is clearly seen for protraction timed and random stimulation, but no inhibition is evident following retraction timed stimulation (Figure 4.4B). A small increase in firing is evident, although this may be a result of reinforcing whisk / spike correlations that are evident without stimulation, as a similar (but smaller) increase is apparent following mock stimulation. Again, we see that the responsiveness of sensory cortex appears sensitive to the timing of stimulation, providing further evidence for an active mechanism for generating windows of opportunity in cortical sensory areas and interpreting spikes within the context of self-motion.

Stimulation during quiescence drives whisker and head repositioning

Finally, we sought to recreate the stimulation conditions previously employed in head-fixed mice [60] using our freely behaving mice in order to evaluate the effects of stimulating sensory areas on both whisker and head repositioning. In that study, head-fixed Thy1-Chr2 mice were stimulated with 500 ms pulse trains of 50 Hz blue light during periods of quiescence (awake, but not actively whisking). It was found that SI stimulation produced contralateral side whisker retractions, even when MI was chemically inactivated. We sought to reproduce this effect in a freely moving (i.e. non-head-fixed) animal of the same type with the same stimulation parameters. On a subset of recording days after collection of active exploration data, the reward mechanism was disabled, leading to periods of quiescence as the mouse became disinterested in the task. We manually triggered stimulation with fixed pulse trains (50 Hz, 1 ms pulses, 500 ms duration) during these periods, and acquired high-speed video, which was then analyzed by manually coding head and whisker angles. We found that stimulation generally caused an initiation of whisking, accompanied by head turns towards the side contralateral from stimulation and induced bilateral whisker set-point retractions. Viewing an example trial (Figure 4.4A) highlights the animal beginning to whisk following stimulation, and averages over all quiescent stimulation trials shows a robust adjustment to head angle and whisker set-points following stimulation onset (Figure 4.4B). This result helped to clarify an important interpretation of the previous study, namely that stimulation to sensory areas may produce more complex motor outputs (as opposed to SI solely acting as a retraction center), and that observing the animal in a head-fixed configuration may obscure

important coordination that occurs between head and whisker motions in rodent active sensing [195].

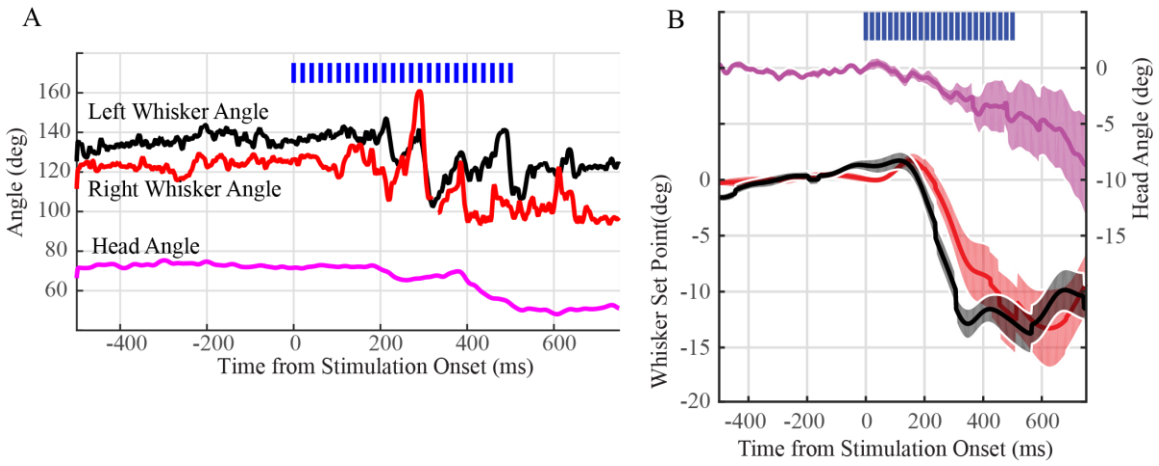

Figure 4.5 Sensory stimulation may drive both whisker and head positioning

A, Example trial aligned to stimulation onset, where stimulation was delivered (in Thy1 mice) using 50 Hz pulse trains for 500 ms during periods of quiescence. Stimulation results in an onset of whisking (*red*- right whisker, *black*- left whisker*)*, bilateral whisker retractions, and head turning (*magenta trace)* to the side contralateral from stimulation. **B,** Averages of bilateral set-points (*red*- right whisker, *black*- left whisker*)* and head angles (*magenta*) show set-point retractions and head turns following stimulus onset. Head turns generally began before whisker repositioning (mean ± SE, n=17 trials).

4.5 Discussion

Distinction between sensory and motor areas

Beginning with the earliest stimulation mapping experiments of human cortical organization in epileptic patients, the loose distinction between sensory and motor areas has been apparent. Penfield and Boldrey state that, “It is not infrequent that stimulation produces sensation and movement both in the same part… therefore it seems appropriate to refer in a broad sense to sensori-motor Rolandic cortex.” [196]. Further studies

determined that motion could be elicited in primates through stimulation in both "sensory" and "motor" areas, albeit with elevated thresholds for sensory stimulation [197–199].

The overlap of sensory and motor function makes sense when considered within the larger framework of cortical evolution, the specifics of which are very clearly illustrated in the whisker tactile system. All extant therian mammals have (or have evidence of vestigial structures for) tactile hairs [200]. The prevalence of similar anatomical structures along with evidence of whisking behavior among diverse groups of both placentals and marsupials suggests that active whisking was an important sensory modality to an early common ancestor of therian mammals (rather than a convergently evolved feature) [58]. This observation is particularly relevant here because marsupials exhibit several key differences in neuroanatomy, including the lack of a distinct primary motor cortex and the lack of a corpus callosum. The finding that marsupials not only whisk but engage in similar active sensing strategies (HTA, etc.) to rodents [58], suggests that the ability to actively modulate whisker motions in response to sensory inputs and behavioral goals is not dependent on the existence of a distinct primary motor area. Significantly, the observed behaviors in marsupials included those that required bilateral whisker control. It appears that sensory and motor functions in placental mammals have become increasingly segregated over the last ~100 million years, although even in primates (including humans, as observed by Penfield etc.) the segregation is incomplete. Primary motor cortex appears to have arrived late and gradually supplanted many aspects

of motor control, but by no means should we expect the segregation of function to be complete. These historical and evolutionary insights suggest that perhaps, rather than focus on the existence of motor responses driven by activity in sensory areas, we should ask how, specifically, sensory cortex plays a role in coordinating sensing motions and in what circumstances is that role most important.

The role of sensory cortex in coordinating active sensing motions

Our results support the hypothesis that primary sensory cortex participates in coordinating whisk timing during active sensing on the timescale of single whisks. This time scale suggests that the observed behavioral changes from stimulating in sensory areas arise from a direct motor output from SI (for example hypothesized projections to brainstem), rather than arising as a consequence of the animal acting in response to perception, involving multiple brain regions. Modulation of motion based on incoming perceptions is certainly relevant on a longer timescale. We propose, however, that SI may play a role in coordinating whisk timing on the timescale of the next whisk, independent of whatever perceptual input may arise from the whisker contact (or stimulation). Both changes to whisker motion (from facial EMG) and SI multiunit spike timing suggest that there may be sensory "windows of opportunity" around the time of whisker protractions in which SI may have the most impact on whisk timing.

The differences we observed between stimulating excitatory and inhibitory cell populations are particularly suggestive. We observed short timescale alteration in

behavior in both cases, especially when stimulation was locked to protractions, however, excitatory stimulation accelerated whisking while inhibitory stimulation slowed whisking. Our excitatory stimulation in these mice targeted layer 5 pyramidal cells implicated as output projections. Indeed, this stimulation may be conceptually similar to "hijacking" the output of SI, which may explain why our excitatory stimulation induced short latency motor changes and accelerated whisking. Stimulation of PV cells in SI may be thought of as delaying spiking in circuits implicated in local processing within SI. To the extent that those signals eventually drive SI outputs, and if the output from SI contributes to the onset of retractions, delaying firing within SI interneurons could lead to the observed deceleration for inhibitory stimulation timed to protractions. Since a higher stimulus intensity was needed to observe timing changes with inhibitory stimulation, more work is needed to determine if this difference reflects different population activation thresholds, a need to recruit inhibition in more cells (possibly over a broader area), or if it is related to changes in the dynamics of inhibitory post-synaptic currents with increased stimulus intensity.

Additionally, the observation that both excitatory and inhibitory stimulation in SI produced strong neural responses (excitation or inhibition respectively) only for protraction-locked stimulation supports that the observed effects could arise within the sensory area itself, rather than from inadvertent activation of other areas, for example MI projections. Since expression in the inhibitory animals was driven by local injection of a viral vector, the stimulated cells were most likely local to SI, and therefore observing

cyclic alterations in neural responsiveness in both types of animals supports that sensory cortex is implicated in the observed effects. The short timescale of changes to whisk timing from excitatory stimulation also supports this conclusion.

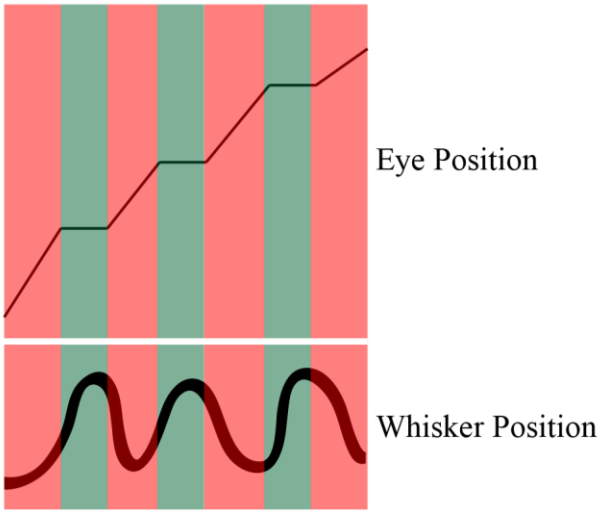

Figure 4.6 Windows of opportunity in active sensing

Schematic depiction of proposed "windows of opportunity" in active sensing. Green bars indicate time of importance to sensory acquisition for vision (fixations) and whisking (protractions). Red bars indicate periods of suppressed responsiveness in active sensing for vision (saccadic motions) and whisking (retractions).

Implications for retraction suppression on sensory coding

The observation of decreased responsiveness to stimulation in sensory cortex during the retraction phase of whisking suggests the possibility of "windows of opportunity" where sensory information may be favorably integrated into the ongoing active sensing motor output (Figure 4.6). Mice and rats typically make object contacts on whisker protractions (as opposed to retractions) and therefore sensory information during whisker retractions is more likely to be noise, suggesting the hypothesis of an evolutionary pressure to reduce responsiveness during times with a low probability of providing useful information. This

dynamic suggests a comparison to saccadic suppression, which has been reported extensively in the visual system (reviewed in [201]). Visual responses in multiple thalamic and cortical areas are less responsive during rapid saccadic eye movements. Significantly, there is evidence that the suppression arises separately in each area (as opposed to being solely driven by thalamus, for instance) and that the suppression begins prior to the onset of eye motion, suggesting an active mechanism driving neural responsiveness rather than a passive response to the ensuing motion [202]. The specific mechanisms underlying saccadic suppression are incompletely understood, and we do not mean to suggest that they are necessarily identical within the whisker tactile system. Instead, the comparison may offer insight into the types of neural mechanisms that may developed in various sensory systems to reduce sensitivity at "noisy" times. It is important to highlight that suppressing visual responses during saccadic motion does not mean that motion is unimportant. Indeed, vision is a deeply active process, and especially in primates relies on near constant foveal repositioning. The *motion* is intrinsically important, even if the act of *moving* produces responses that must be suppressed to maintain stable perception. The result is a "window of opportunity" for sensing that corresponds to the fixations between saccadic motions. The analog in the whisker system may not be substantially different, despite the process riding on a 10–20 Hz carrier signal corresponding to whisking. Even though the whiskers may be moving, we propose that the dynamics of SI responsiveness create a similar "window of opportunity" for sensing which corresponds to the protraction phase of whisking. Under such a proposed framework, the observed "phase tuning" of neurons in the whisker sensory pathway

would emerge as a result of the suppression at non-preferred times. This suggests that perhaps the causal arrow needs to be reversed: rather than phasically tuned neurons providing information about whisker contacts, we may have a system of active suppression that results in the observation of phasically tuned neurons.

Implications

Delivering closed-loop feedback locked to whisker motions has helped deepen our understanding of both how sensory areas contribute to coordinating the timing of active sensing motions on short timescales and how cyclic changes in cortical excitability may create "windows of opportunity" for sensory acquisition. Thinking about active sensing in the whisker system in this framework may invite new avenues of inquiry that would not have been apparent without considering suppression of cortical excitability as a potentially active mechanism for enhancing the quality of incoming sensory information. The potential correlates to human touch, and even other sensory systems, suggest that understanding the motor role played by sensory areas and cyclic alterations in cortical excitability may have important implications in the design of improved prosthetics that incorporate somatosensory feedback through neural stimulation. Specifically, considering both the potential for unintended motor impacts from sensory feedback stimulation and how the timing of feedback stimulation may influence how it is incorporated into the ongoing sensorimotor strategy may be key design criteria in delivering artificial tactile feedback.

APPENDIX 1- OptoZIF Drive Materials and Assembly Instructions

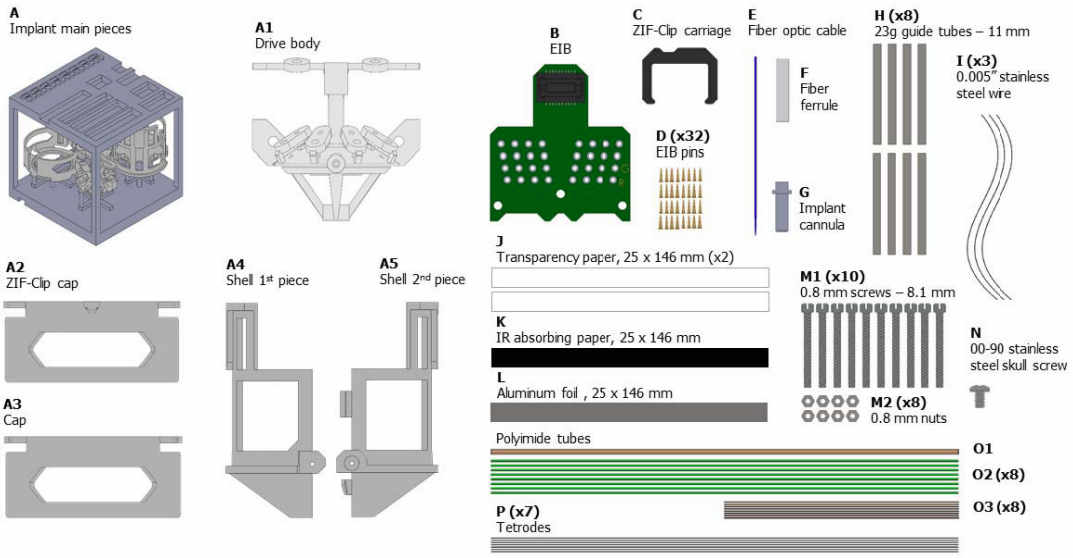

Materials

	Name	Description	Material	Units	Vendor	Cost (USD)	Weight (grams)	Notes
A	Implant main pieces	contains drive body, two caps, and protective shell pieces	3D printed polyamide	1	I-materialize	25	22.77	
A1	Drive body		3D printed polyamide	1	I-materialize	-	0.73	Part of (A)
A2	Cap for use with ZIF-Clip	Protects drive when ZIF-clip or fiber is attached	3D printed polyamide	1	I-materialize	-	0.46	Part of (A)
A3	Cap	Protects drive when drive is not connected with ZIF-clip or fiber	3D printed polyamide	1	I-materialize	-	0.61	Part of (A)
A4	Shell 1st piece	Protects drive body	3D printed polyamide	1	I-materialize	-	0.39	Part of (A)
A5	Shell 2nd piece	Protects drive body	3D printed polyamide	1	I-materialize	-	0.40	Part of (A)
B	EIB	Custom PCB	1/32" FR-4	1	PCB Vendor, e.g. Sunstone Circuits	6.50 (in orders of 100)	0.56	
C	ZIF-Clip carriage	Mechanical brace for ZIF-Clip on EIB	Plastic	1	Tucker Davis Technologies (TDT)	3.00	0.05	Needed to prevent damage of ZIF-Clip. PN: ZC32 Shrouds & Caps
D	EIB pins	Large EIB pins	Gold	32	Neuralynx	5.60	0.25	
E	Fiber optic cable	~ 200 micron diameter	Glass	1	ThorLabs	0.01	0.008	
F	Fiber Ferrule	1.25 mm ferrule	stainless steel	1	Percision Fiber Products	6.13	0.05	PN: MM-FER2007-304-265
G	Implant cannula	Provides a consistent implant height and ensures a smooth bevel	3D Printed HD Stainless Steel	1	I-materialize	9.01	0.07	
H	metal guide tubes	23 gauge metal guide tubes, 11 mm in length	Stainless steel	8	SmallParts	0.55	0.12	
I	Stainless steel wire	0.005" Stainless steel wire, 2 inches in length	Stainless steel	3	AM Systems	0.46	0.03	PN: 791400
J	Plastic transparency paper	Forms protective cover, for home cage use.	plastic	2	Various	~0.03	0.46	
K	IR absorbing	Black Flocked Self-	fine fibers on	1	Thor Labs	0.30	0.58	PN: BFP1

	paper	Adhesive Paper	paper					
L	Aluminum foil	For insulating drive caps from EM noise	Aluminum	1	Various	<0.01	0.21	
M1	0.8mm x 0.32" filleted screw	Micro-drive screw	Stainless Steel	10	Antrin Miniature Specialties	10.5	0.28	PN: NAS721CE80-320
M2	0.8mm hex nut	Micro-drive nut	Stainless Steel	8	Antrin Miniature Specialties	8.80	0.15	PN: M0.80
N	00-90 screw	Skull ground connections,	Stainless Steel	1	Antrin Miniature Specialties	0.75	0.025	PN: AMS90/1P-25 00-90x 1/16 SL PAN SST
O1	Plastic fiber optic guide tube	0.0135" ID	Polyimide	1	NeuraLynx	0.65	0.005	
O2	Plastic guide tubes	33g, 0.0071" ID	Polyimide	8	SmallParts	3.36	0.02	PN: TWPT-0071-30
O3	Plastic shuttle tubes	38g, 0.0035" ID	Polyimide	8	NeuraLynx	5.25	0.01	
P	Tetrodes	12.5 µM	Ni-chrome	7	Sandvik	1.03	< .01	PN: U8-DLKL-ONEO
Q	Male connector pin			1	AM Systems	0.72	0.07	PN: 520200
R	Female Connector pin			1	AM Systems	0.72	0.08	PN: 520100

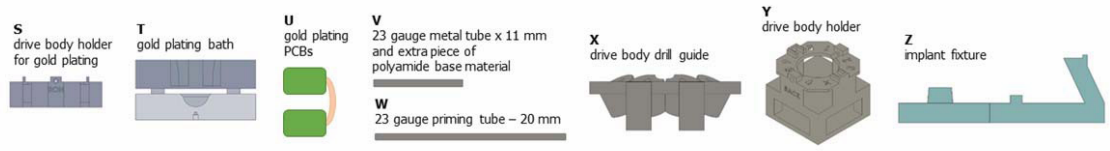

3D Printed Assembly Tools

S – Drive body holder for gold plating – 3D printed polyamide
T – Gold plating bath – 3D printed polyamide
U – Gold plating PCBs – 2x 1/16" FR4 PCB
V – 23g metal guide tube, 11 mm in length – Stainless Steel
W – 23g metal guide tube, 20 mm in length – Stainless Steel
X – Drive body drill guide – 3D High-Definition Stainless Steel
Y – Drive body holder – 3D printed polyamide
Z – Implant fixture – 3D printed polyamide

Recommended Adhesives

Loctite: Cyanoacrylate gel, general purpose adhesive for most assembly gluing operations.
Zap-A-Gap: low viscosity cyanoacrylate, used for gluing guide tubes into implant cannula.
Silverprint: Conductive acrylic paint, used for ground wire connections.

Required Tools for Assembly

1. Ceramic tipped Forceps
2. Serrated Scissors (for final cuts to recording electrodes)
3. Dumont #5 Forceps
4. Measuring Calipers
5. Screwdriver for M0.8 screws
6. Razorblades
7. 27 ½ gauge needles (for precision glue application)
8. Fine sandpaper (200-400 grit)
9. Small sharp scissors
10. Wire cutter for ground wire
11. Heat gun for fusing microelectrodes
12. Small hand drill with bits (#52,#55, #65, #70)
13. Current source and gold cyanide solution for gold plating

Assembly Instructions

Prepare electrodes (2 hours)

Use any suitable protocol (Nguyen et al. 2009; Gray et al. 1995, McNaughton et al. 1983)

Prepare enough electrodes for 7 microdrives, plus extras as desired.

Prepare EIB (up to 4 weeks manufacturer lead time)

- Use custom files and commercial PCB manufacturer to make EIB (B).
    - Circuit board thickness must be 1/32" to be compatible with the ZIF-Clip system. Other sizes may damage the ZIF-Clip head-stage.
- Use PCB assembler to ensure ZIF-Clip connector is soldered correctly.
- Can take 2 to 4 weeks to get EIB boards back from manufacturer.

Prepare Metal Tubes (30 minutes)

- Order custom cannula (G) from 3D Printing service.
    - Ordered using I.Materialize's HD Stainless Steel 3D Printing service.
    - Otherwise a 17g syringe needle, cut to 6.5 mm of length and rounded on the distal end can be used.
    - Can take 2 to 4 weeks to get parts.
- Prepare eight 23g metal guide tubes (H.1-H.8)
    - Tubes should be 11 mm in length.
    - When cut using a dremel cutting wheel, approximately 2 mm of material is used.
    - Deburr ends of tubes with appropriate tool.
    - Clean out ends with a 27 ½ gauge syringe needle.
- Prepare various polyimide tubes (O1, O2.1-O2.8, O3.1-O3.8)
    - One fiber optic cable guide tube, cut 50 mm (2 inch) of a 0.0137" polyimide tube (O1)
    - Eight guide tubes, cut 50 mm (2 inch) of 33 gauge polyimide tube (O2.1-O2.8)
    - Eight shuttle tubes, cut 25 mm (1 inch) of 38 gauge polyimide tube (O3.1-O3.8)

Prepare Drive Body (15 minutes)

- Check quality of 3D printed main pieces. The designed implant was designed for the highest print qualities using SLS polyamide printing. Most development was completed using I.Materialize's selective laser sintering center in Europe (Belgium). Build qualities from different centers and companies must be carefully inspected for high-quality printing, especially of small features.

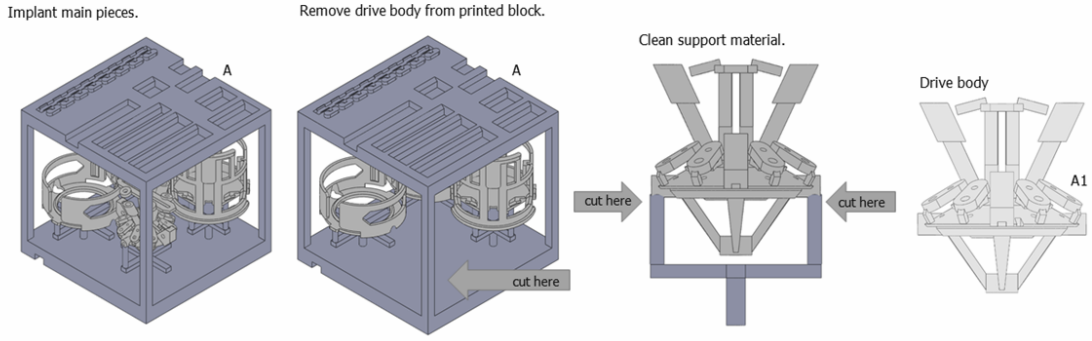

- Remove drive body (A1) from printed piece (A) with wire cutters. The remaining material on the body can be cleared with a razor blade.

- Most holes are purposely undersized and must be cleared with the appropriate drill bits. Process is done with manual tool set.

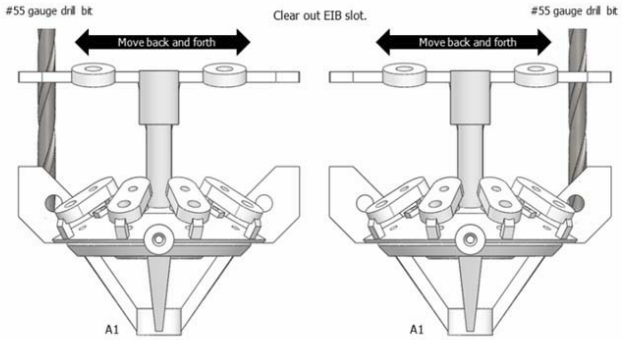

- If necessary, clear out the EIB space with #55 gauge drill bit.
    - Test by placing EIB board in its position and checking if the holes line up on both sides.

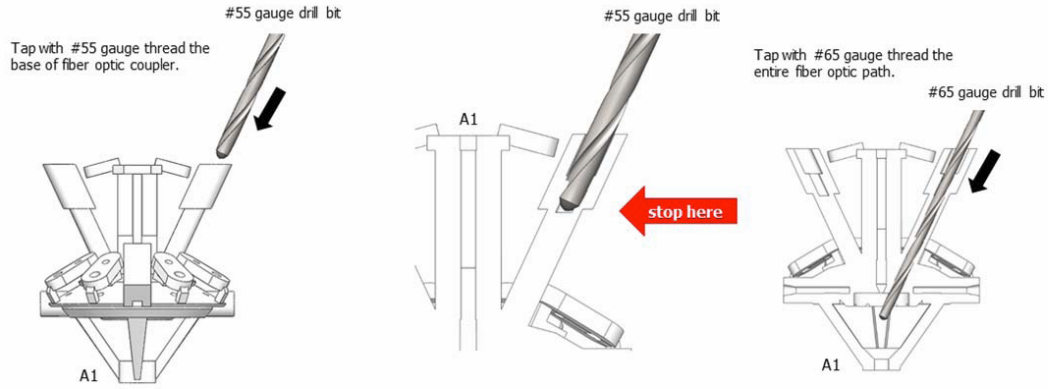

Clean fiber optic receptacle. Use fingers to the support the tube while drilling.

- Use #55 gauge drill bit to clear out the top of the fiber receptacle, i.e. where the fiber ferrule is attached later. This is approximately 2.5 mm deep.
- User smaller #65 gauge drill bit to clear remaining fiber optic path in drive body. This is approximately 14 mm deep from the top of the receptacle.

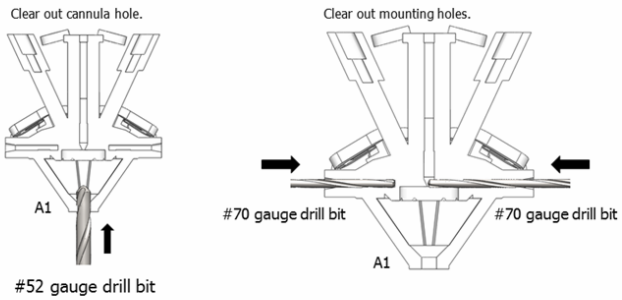

- Clean bottom cannula hole for implant cannula (G) using #52 drill bit.
    - Make sure drill is inserted straight. This step is usually performed with the drive upside down.
- Clean side mounting holes with #70 gauge drill bit. Between 6 mm to 9 mm of material should be cleared out on both sides.

Load Drive Body in Holder (5 minutes)

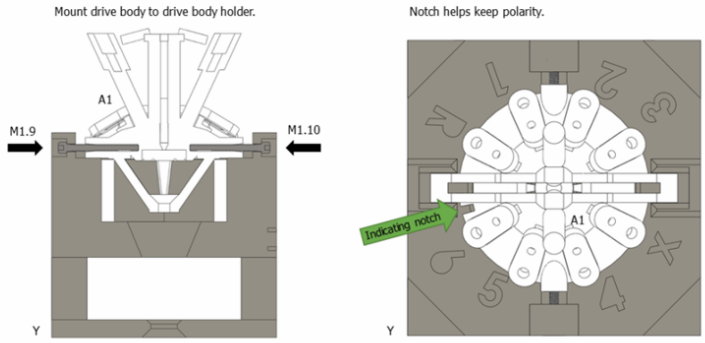

- The drive has two sides, but is completely symmetric, except for a small notch on one side. Thus, it's possible to select front (optical fiber) and back (ground pin) sides to ensure naming consistency. The standard convention employed here is to have the notch on the back side. The EIB front side (with text) and fiber will be on the front side of the drive body.
    - With this convention, R is the reference, 6 tetrodes are listed in clockwise direction (1 through 6), with an unused (labelled X) position interrupting on the back side.
- The drive will be inserted and removed from the holder multiple times during the assembly process.

Prime Microdrive Holes in Drive Body (30 minutes)

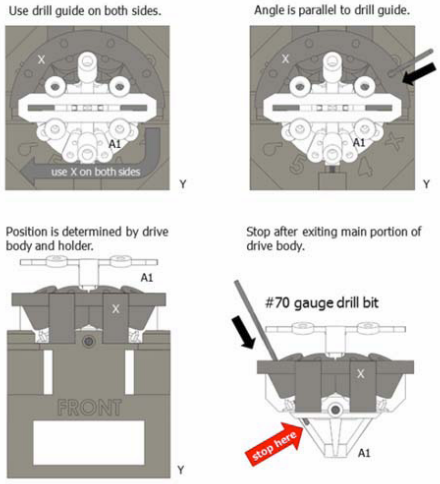

- Using the drive body drill guide (X), create #70 gauge drill bit holes for all eight Microdrive positions. Use the #70 gauge drill bit for all 16 holes, 8 on each side, 2 for each microdrive.
- Entry direction should be parallel with guide holes.
- Complete manual drilling of each hole until the drill bit appears underneath the main drive body. This is approximately 12 mm deep.
- Flush out all the holes using a long 23 gauge stainless steel tube when complete.

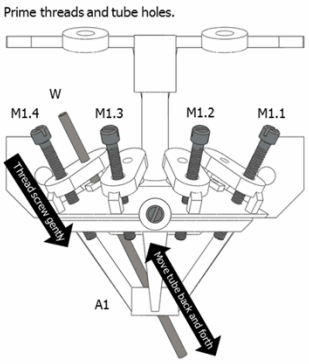

- Do not remove drive body from holder.
- Prime the drive by screwing in all eight 0.8 mm screws (M1.1-M1.8).
- When screwing in each screw, place the long 23 gauge tube (W) as a priming tube to improve drive performance. Note, for clarity of presentation, the screws are shown removed in the illustration below.
- Carefully thread the 0.8 mm screws (M1.1-M1.8), keeping in mind that one should back up a few turns after each advance to ensure smooth threads (Approximately 2 turns back for each ½ -1 full forward turn).
- The screws should remain parallel to the hole while threading with the screw.
- Flush out all the holes using a long 23 gauge steel tube (W), moving the tube back and forth.

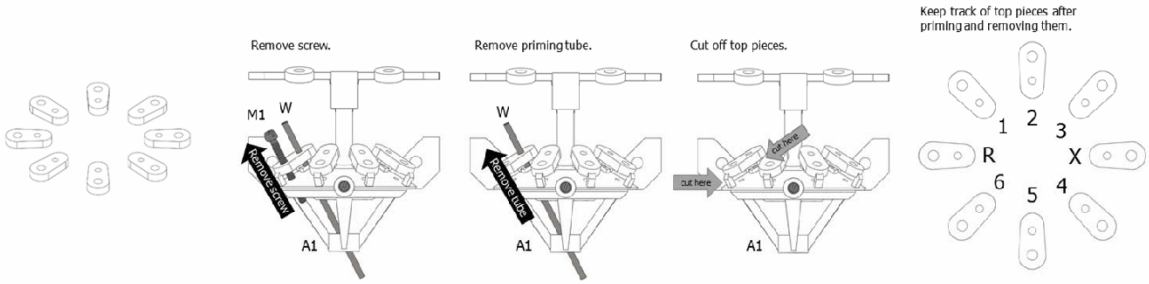

- Remove all eight microdrives from main body.
  - Remove the screw (M1) with the priming tube (W) inserted.
  - Remove the priming tube (W).
  - Cut off individual top piece using wire cutters and trim excess material on top piece with a razor blade.
  - Keep track of each top piece's original location.

Build Microdrive assemblies (30 minutes + 2 hours)

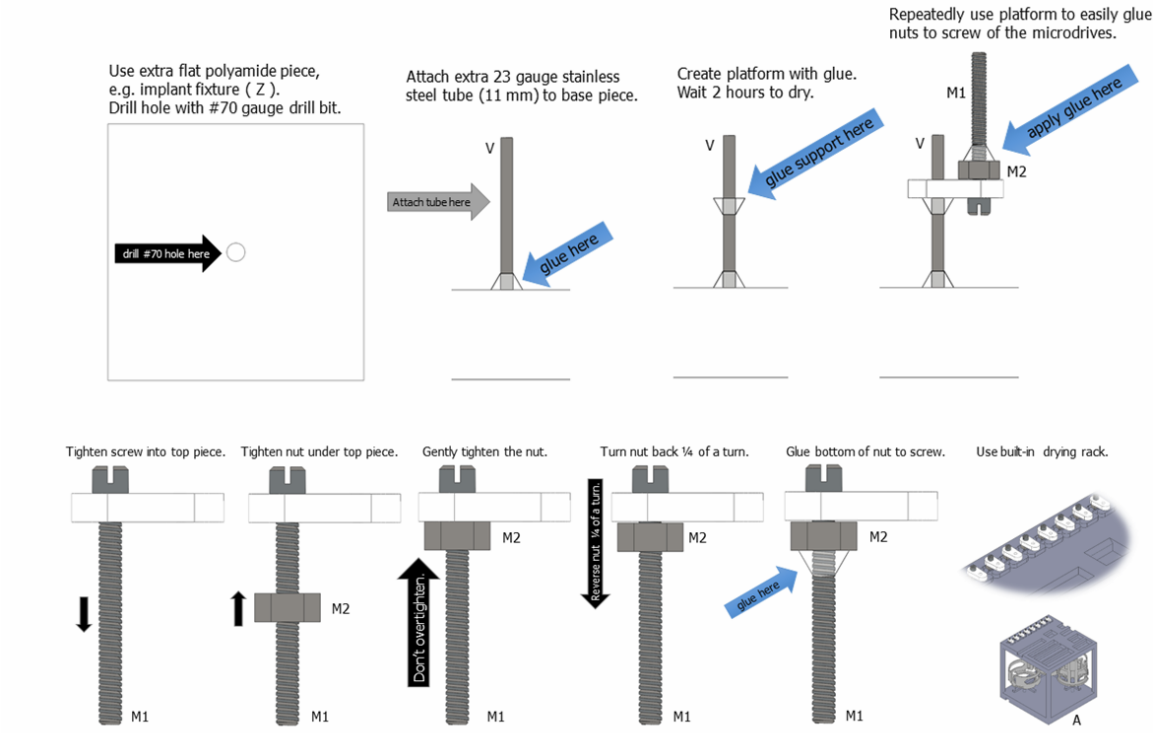

- Prepare all eight microdrives from top pieces.

  - Screw (M1) into top piece.
  - Tighten nut (M2) to the underside of the top piece.
  - Make sure to tighten the nut all the way into top piece, but don't overdo it. It has been found that tightening and then a slight untightening (¼ turn) provides the most appropriate fitting. It can be helpful to hold the nut with a forceps while tightening.
  - Use Loctite on the underside of the nut to lock the top piece into a freely rotating, but tightly controlled mechanical microdrive.
    - A simple apparatus shown above can be used to easily glue drives.
    - It's recommend to apply the Loctite with a 27 ½ gauge syringe needle under a microscope.
  - Wait two hours for glue to dry.
  - Keep track of top pieces and their original location on the drive.
    - Use the built-in drying rack that's part of the main Implant main pieces (A).

Place Guide Tubes and Cannula in Drive Body (30 minutes + 2 hours)

Remove drive body from holder.

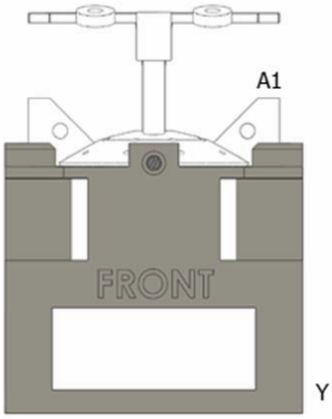

Feed guide tubes through respective holes.

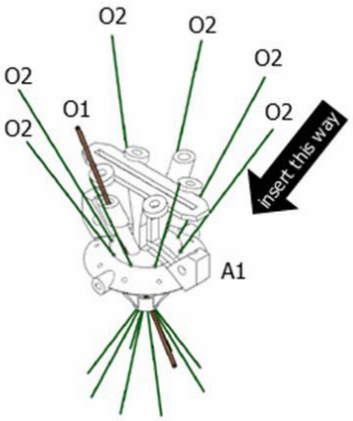

Wedge cannula through polyimide tubes.

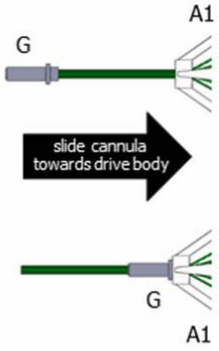

Position microdrive guide tubes to stick out 3 mm from the drive body.

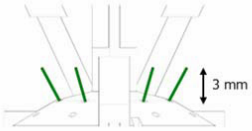

Fiber optic polyimide guide must be properly positioned into fiber tube.

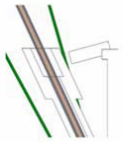

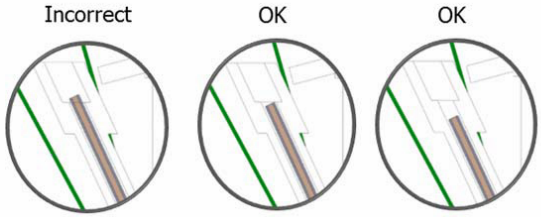

- Remove drive body (A1) from drive body holder (Y).
- Through the top, thread fiber optic guide tube (O1) and eight guide tubes (O2) through their respective holes in the drive body.
- Allow tubes to exit the small bottom hole of the drive body.
    - Most tubes will fit easily, use tweezers to push the other tubes through.
- Wedge implant cannula (G) through tubes into bottom of drive body.
- Before gluing guide tubes into place, position tubes appropriately.
- Microdrive guide tubes (O2) should extend 3 mm from drive body (A1).
- Fiber optic guide tube (O1) must be positioned below the larger hole.

Glue cannula to bottom of the drive body.

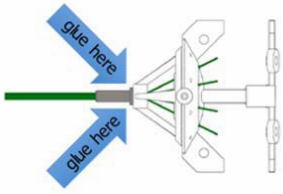

Apply 2 drops in total of zap-a-gap glue to entrance of cannula. Apply with tubes parallel to ground and capillary forces will wick glue into cannula.

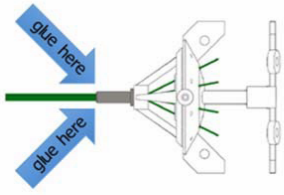

Slice off excess polyimide tubes with razor blade.

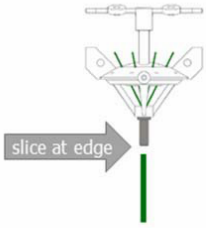

- Using Loctite, glue cannula (G) to drive body.
- Using Zap-a-Gap glue, apply two drops of glue to entrance of cannula. Apply with tubes parallel to ground so that capillary forces wick glue into the cannula.
- Wait 2 hours for glue to dry.
- Slice off excess polyimide tubes with a razor blade at the end of the cannula.

Install Microdrives and Attach Guide Tubes into Drive Body (30 minutes + 2 hours)

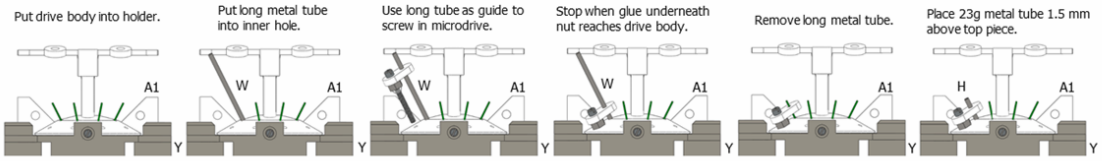

- Put drive body (A1) back in holder (Y).
- For all eight microdrives:
    - Put long metal tube (W) into inner hole.
    - Use long metal tube as guide while screwing in microdrive.
    - Tighten until the glue underneath the nut touches the drive body. Continuing to tighten will strip the guide threads. This distance is about 0.2 mm above the drive body.
    - Take out the long metal tube (W).
    - Insert 23 gauge metal tube (H) into drive body and microdrive.
        - 23 gauge metal tube (H) should be 1.5 mm above the top piece. This is slightly above the top of the screw.

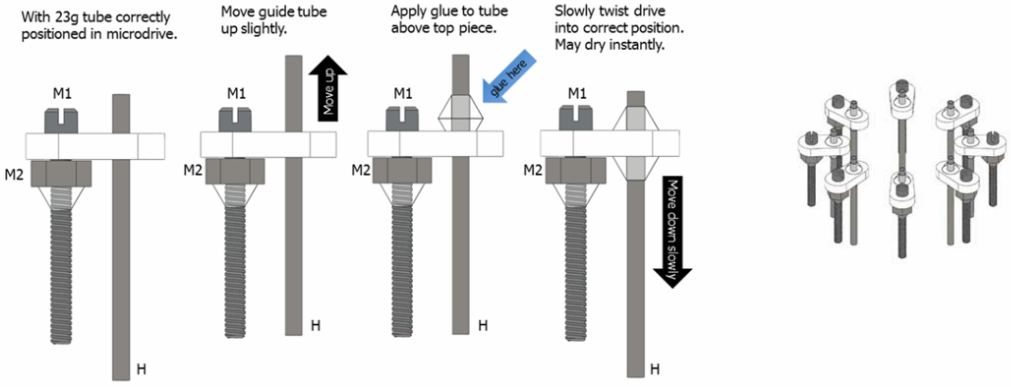

- Glue 23 gauge metal tubes (H) to microdrives:
    - Recommended procedure is to move guide tube up slightly.
    - Apply Loctite glue to bottom of tube using a 27 ½ g needle.
    - Slowly twist metal tube downward to correct position. If done correctly, this will form an instant bond. Be careful not to push too fast.
    - Wait 2 hours for glue to dry.

Install Shuttle Tubes into Microdrives (45 minutes + 2 hours)

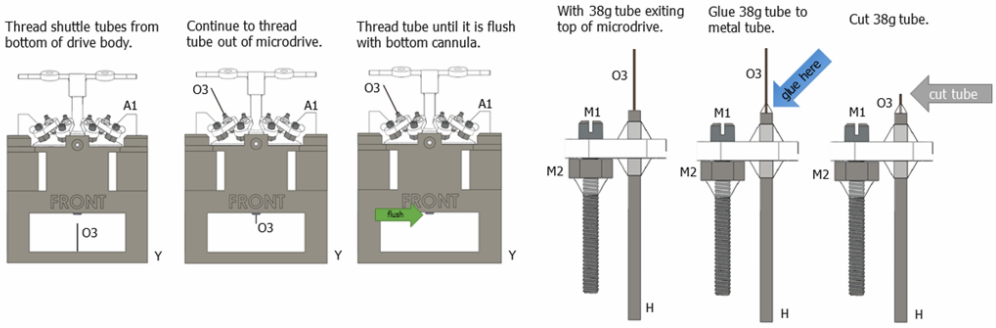

- For all eight microdrives:
  - Via bottom of drive, thread 38 gauge polyimide shuttle tubes (O3) through guide tubes (O2).
    - This is an appropriate time to map position where each Microdrive exists the implant cannula for later reference.
    - If desired, the drive can be removed from the holder and placed upside down under a microscope for this step.

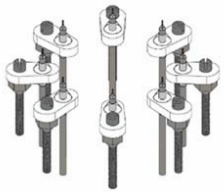

  - Thread tubes until they are flush with the bottom cannula (G).
  - Glue 38 gauge polyimide shuttle tubes (O3) to 23 gauge metal tube (H). Excessive glue may cause damage to the polyimide on run down and fuse the shuttle tube to the guide tube.
  - Wait 2 hours for glue to dry.
  - Cut top of tube, leaving about 1 mm above 23 gauge metal guide tube (H).

Install Fiber Optic Cable (15 minutes + 2 hours)

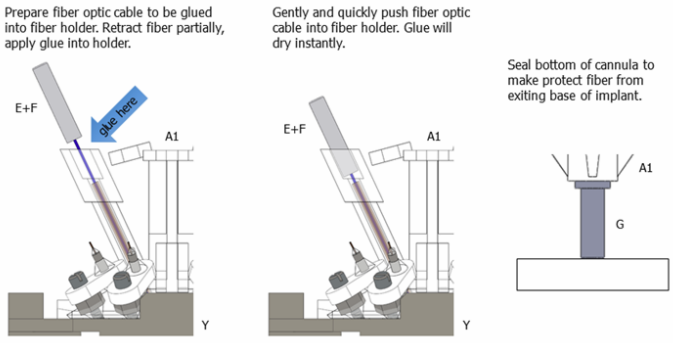

- Make sure that the bottom of the cannula (G) is pressed against a rigid surface to prevent the fiber from protruding from the cannula.
- Thread fiber optic cable (E) through the fiber guide polyimide tube (O1).
- With the fiber cable and ferrule (E+F) slightly retracted, apply Loctite glue to fiber holder.
- Quickly insert fiber cable and fiber cannula (E+F) into fiber holder.
- Glue will dry almost instantly, but be careful not to push too fast or the fiber cable may break.

Integrate EIB into Drive Body (15 minutes + 2 hours)

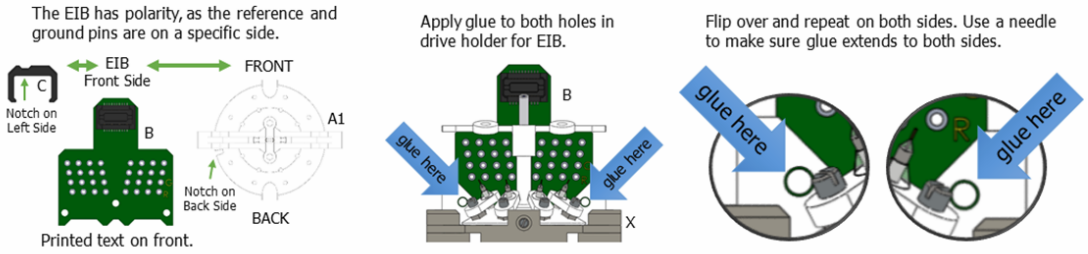

- Insert EIB (B) into drive body (A1).
    - The front size of the EIB contains text. The front side of the drive body doesn't contain a notch.
- Apply Loctite to both holes when EIB is lined up with drive body.
- Repeat on other side of the drive.
- Use a needle to ensure that glue spans the length of the EIB and drive body on both the top and bottom of the EIB.
- Attach ZIF-Clip carriage (C) to EIB. The plastic carriage (C) indicates and determines connector polarity. The notch on the left side indicates the front side. The front side of the EIB contains printed text.

Integrate Gold Pin Ground Connection and Pin to EIB (15 min)

- Solder a 2 inch length of 0.005" stainless steel wire (I) to a female gold pin connector (R). Make sure that the solder on the outside of the connector doesn't substantially change the outer diameter or it won't find in the ground pin receptacle.
- Test find the gold pin connector in the ground pin receptacle.
- Once a good fit has been established, remove the pin, place a drop of Loctite in the hold, and then quickly reinsert the pin.
- Use a small needle to add additional glue at the junction between the gold pin and the receptacle.
- Pin the wire from the ground pin to the one of the ground slots on the EIB.
    - This can be done either before or after installing recording electrodes, depending on preference.
    - The wire can be passed underneath the microdrives in positions 5 and 6 in order to avoid interfering with the fragile microwires.

Integrate Microwires (Tetrodes) into Microdrives (2 hours + 2 hours)

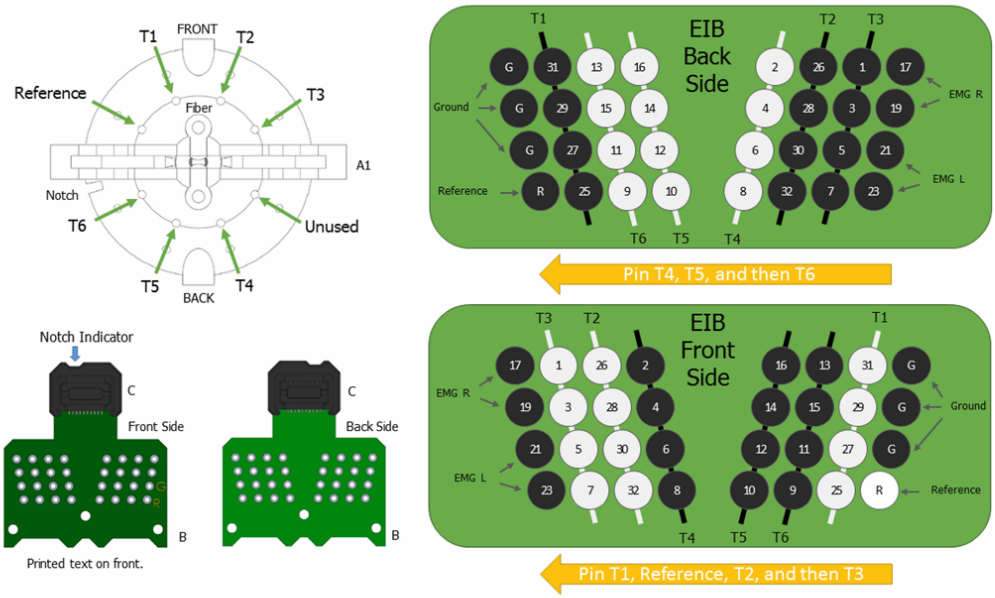

- Wiring Patterns:
  - When connecting the microelectrode wiring, the recommended positions are shown.
  - Wiring is easiest going from center out.
  - Start with the back side, connect T4, T5, and then T6.
  - Flip, and finish with the front side, connect the reference, T1, T2, and then T3.
    - Only connect one electrode when connecting the reference electrode. Additional parallel wires being simultaneously pinned will create an impedance mismatch with other channels. The remaining wires can be placed in the holes without pinning.

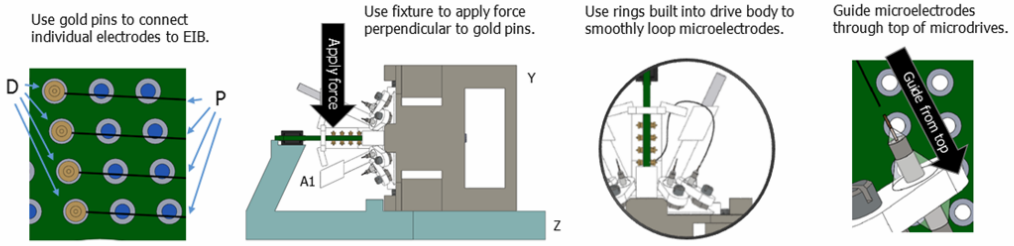

- For all eight microdrives:
  - Working under a microscope, place the wires into the appropriate holes on the EIB.
  - Use gold pins (D) to connect electrodes to EIB (B).
  - Use fixture (Z) and holder (Y) to apply force perpendicular to gold pins. This can be done by pressing the pin with a small screw driver. Excessive force may break the wire.
  - Use built-in rings to loop the microelectrodes (P). The loop should be as small as possible without putting tension on the wire.
  - Guide tetrodes (P) through top of microdrives.

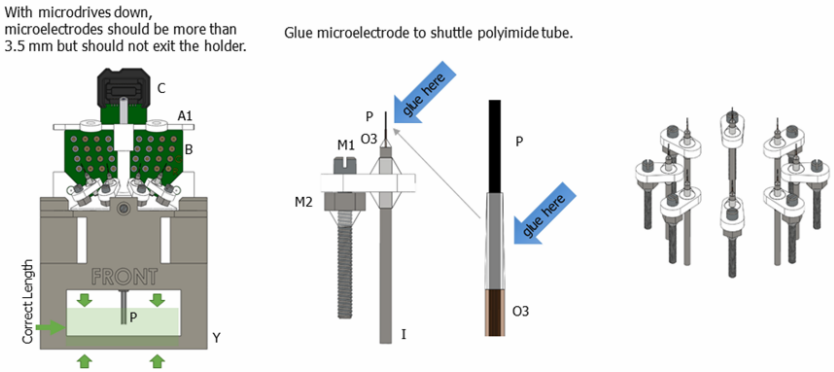

- For all eight microdrives:
  - With the microdrives at their lowest level, cut the microelectrodes (P) so that they are longer than 3.5 mm, but do not exit the holder.
  - Glue microelectrodes (P) to 38 gauge polyimide shuttle tubes (O3). Best done under microscope.
  - Wait two hours for glue to dry.
  -

Final Microelectrode Cuts (2 hours)

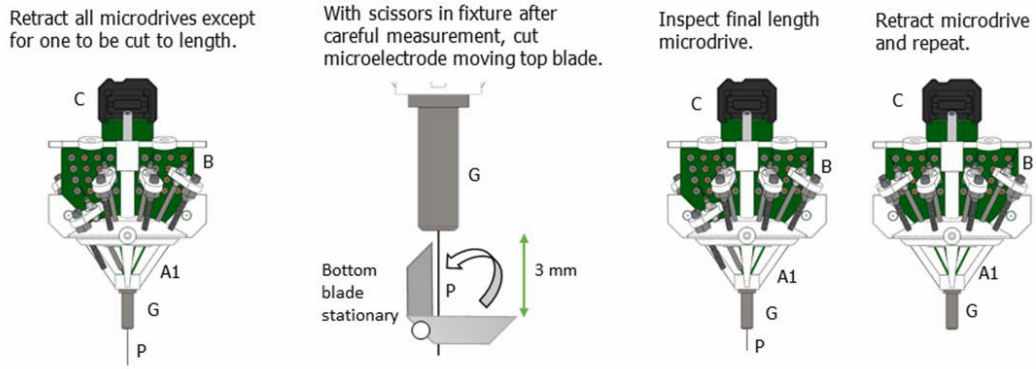

- Remove drive body (A1) from drive holder (Y).
- Retract all microelectrodes (P) into cannula (G).
- Place drive body (A1) in a vice next to serrated microelectrode cutting scissors in second vice.
- Position bottom blade of scissors 3 mm from base of cannula.
- When cutting, move top blade down across the bottom blade.
- Retract finished microelectrode (P) and repeat for all microelectrodes.

Gold Plating of Microelectrodes (1 hour)

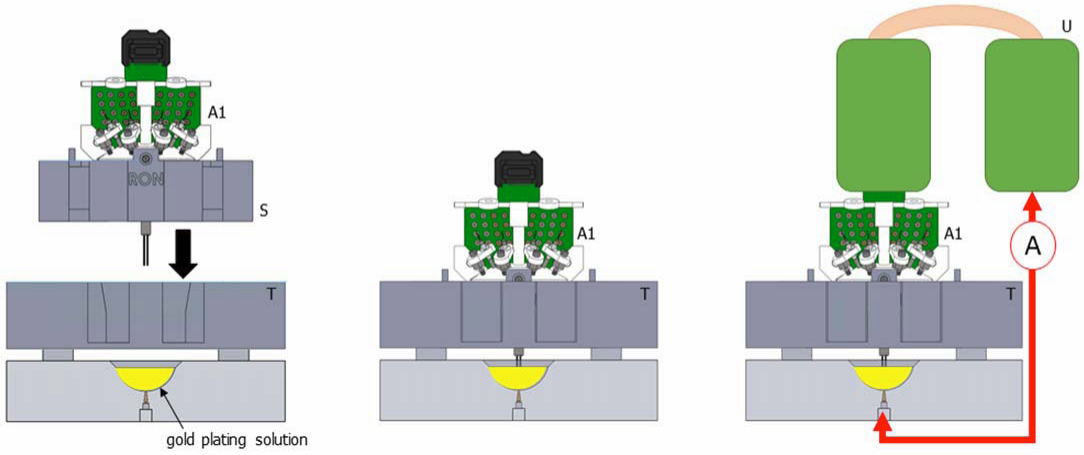

- Place drive in custom gold plating holder (S) with all drives retracted.
- Press the holder into the gold plating base piece (T).
- Turn screws on all microdrives to advance electrode tips into gold solution well.
- Connect ground to the pin in the gold plating fixture.
- Plate each wire to desired impedance by applying direct current (1.0 µA) through the microwire to the ground pin according to desired protocol. Use gold plating PCBs (U) for easy access to each microelectrode.
- Record impedance of each wire before and after plating.
- Carefully remove the drive holder from the base piece with the electrodes still extended
- Clean tip of drive by immersing in ethanol.
- Allow time for the electrodes to dry, then retract each drive until the electrode tip is still 2 full screw turns into the cannula (G) (best done under microscope). This will ensure that there is a consistent and known number of turns before the wires exit the cannula after implantation.

Prepare protective shell and cap (30 minutes)

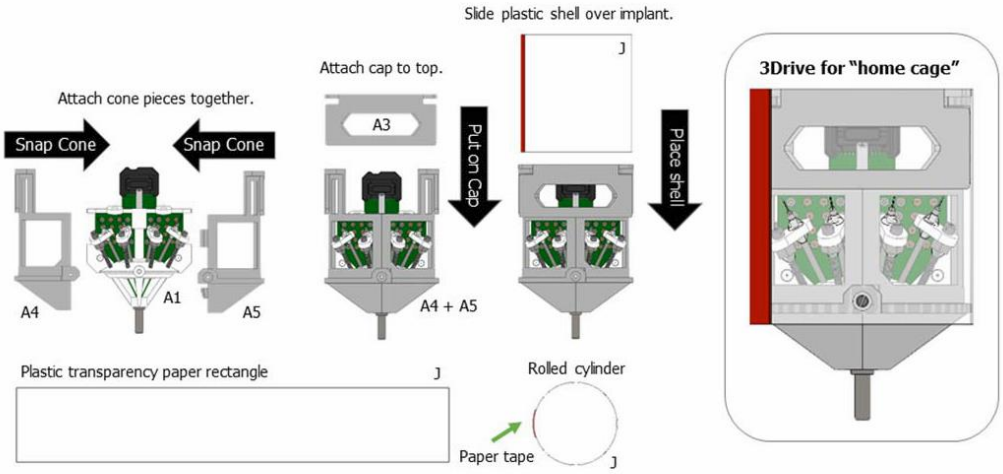

- Cut remaining pieces from the main implant block, i.e. ZIF-Clip cap (A2), cap (A3), and two protective shell pieces (A4+A5) from implant main pieces block (A).
    - Deburr main edges.
- Snap shell pieces (A4+A5) together around drive body (A1).
- Don't screw in. This is only used to make outer shields, the final shell assembly will occur during the implant surgery.
- Snap cap (A3) over top of shell pieces (A4 + A5).
- Make plastic outer shield for "home cage".
    - Cut a rectangle out of transparency paper (J), 25 mm (1 inch) x 146 mm (5 ¾ inches).
    - Roll rectangle into cylinder that fits tightly around cap and shell pieces.
    - Use paper tape to keep cylinder shape.

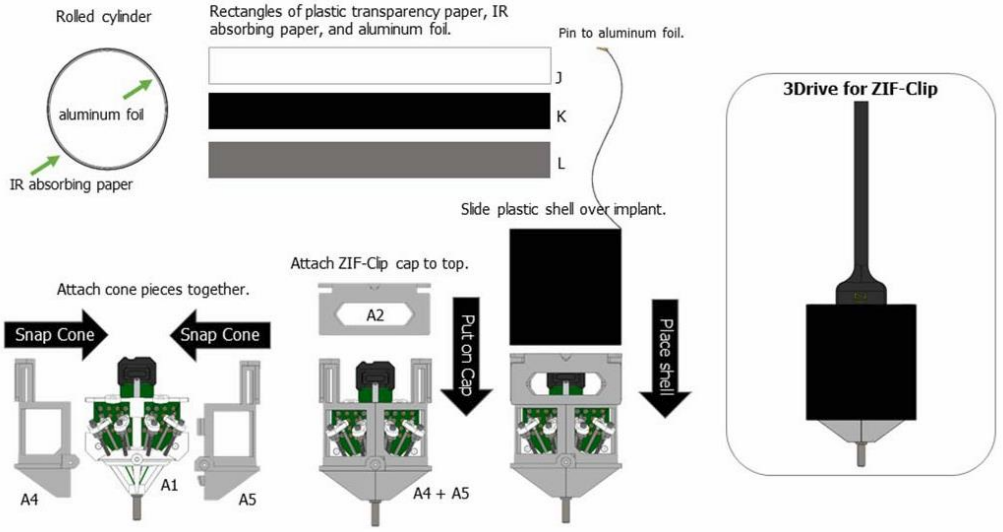

- Make ground shield for electrophysiological recordings.
    - Cut rexctangles out of transparancy paper (J), IR absorbing paper (K), and aluminium foil (L).
        - Approximately 25 mm (1 inch) x 146 mm (5 ¾ inches)
    - The aluminum foil cylinder goes inside the plastic transparency cylinder. The IR absorbing paper goes on the outside of the plastic transparency cylinder.
        - Scotch tape be used in addition to paper tape.
    - A male gold pin (Q) is attached to the aluminum foil by using silver print and a length of 0.005" stainless steel wire (I) about 50 mm (2 inches) long.
    - The ground shield can be reused for multiple mice, although having a backup on hand is recommended.

Record Drive Parameters (15 minutes)

- Record drive weight.
- Record fiber optic transmittance.
- Record cannula output map

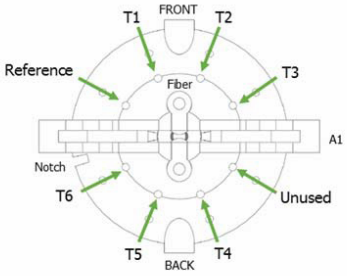

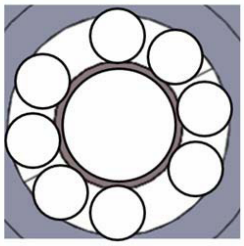

Prepare screw for skull ground (15 minutes)

- Prepare a length of ~3" of stainless steel wire (I) and strep about 1 cm from one end.
- Wrap the stripped end of the wire several times around a 00-90 screw (N) just under the screw head.
- Position the tip of the wire on top of the screw head and secure using silverprint.
    - It is usually necessary to apply multiple coats to ensure a solid bond.
    - Make sure that the slot on the screw head is not obstructed.

Implant Surgery Notes

- Retract all microelectrodes before placing the implant.
- Attach the grounded skull screw to a ground slot on the EIB.
- Attach the wires from EMG (or other auxiliary recordings to the open space on the EIB)
- After snapping together the protective shell, secure to drive body with two screws

BIBLIOGRAPHY

List of Abbreviated Journal Titles

Acta Physiol. Scand. ..... Acta Physiologica Scandinavica

Anat. Rec..... Anatomical Record

Ann. NY Acad. Sci.. .....Annals of the New York Academy of Sciences

Annu. Rev. Biomed. Eng. ..... Annual Review of Biomedical Engineering

Annu. Rev. Neurosci. ..... Annual Review of Neuroscience

Atten. Percept. Psychophys.....Attention, Perception & Psychophysics

Auton. Robots. .....Autonomous Robots

Behav. Brain Res. ..... Behavioural Brain Research

Biol. Cybern. .....Biological Cybernetics

Brain Res. Bull. ..... Brain Research Bulletin

Cereb. Cortex .....Cerebral Cortex

Curr. Biol. ..... Current Biology

Curr. Opin. Neurobiol. .....Current Opinion in Neurobiology

Eur. J. Neurosci. ..... European Journal of Neuroscience

Exp. Brain Res. ..... Experimental Brain Research

Exp. Neurol. .....Experimental Neurology

Exp. Physiol. ..... Experimental Physiology

Front. Behav. Neurosci .....Frontiers in Behavioral Neuroscience

Front. Integr. Neurosci. .....Frontiers in Integrative Neuroscience

Front. Neural Circuits ..... Frontiers in Neural Circuits

Front. Neuroengineering ..... Frontiers in Neuroengineering

Front. Neurorobotics ..... Frontiers in Neurorobotics

Front. Neurosci. ..... Frontiers in Neuroscience

Front. Syst. Neurosci. ..... Frontiers in Systems Neuroscience

IEEE Eng. Med. Biol. ..... IEEE Engineering in Medicine and Biology

IEEE Trans. Biomed. Eng. ..... IEEE Transactions on Biomedical Engineering

IEEE Trans. Neural Syst. Rehabil. Eng. ..... IEEE Transactions on Neural Systems & Rehabilitation Engineering

Int. J. Robot Res. ..... International Journal of Robotics Research

J. Acoust. Soc. Am. ..... Journal of the Acoustical Society of America

J. Am. Stat. Assoc. ..... Journal of the American Statistical Association

J. Anat. ..... Journal of Anatomy

J. Neural. Eng. ..... Journal of Neural Engineering

J. NeuroEngineering Rehabil. ..... Journal of NeuroEngineering and Rehabilitation

J. Neurophysiol ..... Journal of Neurophysiology

J. Neurosci. ..... Journal of Neuroscience

J. Neurosci. Methods ..... Journal of Neuroscience Methods

J. Neurosurg. ..... Journal of Neurosurgery

J. Physiol-Paris ..... Journal of Physiology- Paris

J. Vis. Exp ..... Journal of Visualized Experiments

Nat. Methods. ..... Nature Methods

Nat. Neurosci. ..... Nature Neuroscience

Nat. Protoc. .....Nature Protocols

Nat. Rev. Neurosci..... Nature Reviews. Neuroscience

Neurourol. Urodyn.....Neurourology and Urodynamics

Neurosci. Lett.....Neuroscience Letters

Neurosurg. Focus ..... Neurosurgical Focus

Percept. Psychophys .....Perception & Psychophysics

Philo. Trans. R Soc. Lond. B Biol. Sci. .....

Philosophical Transactions of the Royal Society of London. Series B, Biological Sciences

Physiol Behav. ..... Physiology and Behavior

PLoS Biol.....PLoS Biology

PLoS Comput. Biol.....PLoS Computational Biology

Proc. Biol. Sci ..... Proceedings. Biological Sciences / The Royal Society

Proc. Natl. Acad. Sci. USA.....

.....Proceedings of the National Academy of Sciences of the United States of America

Prog. Neurobiol..... Progress in Neurobiology

Psychol. Rev. .....Psychological Review

Sci. Transl. Med.....Science Translational Medicine

Somatosens. Mot. Res.....Somatosensory and Motor Research

Trends Neurosci. .....Trends in Neuroscience

Vet. Res. Commun..... Veterinary Research Communications

Vision Res..... Vision Research

Wiley Interdiscip Rev. Cogn. Sci. ..... Wiley Interdisciplinary Reviews: Cognitive Science

1. Nicolas-Alonso LF, Gomez-Gil J. Brain Computer Interfaces, a Review. Sensors. 2012;12: 1211–1279. doi:10.3390/s120201211

2. Carmena JM, Lebedev MA, Crist RE, O'Doherty JE, Santucci DM, Dimitrov DF, et al. Learning to control a brain-machine interface for reaching and grasping by primates. PLoS Biol. 2003;1: E42. doi:10.1371/journal.pbio.0000042

3. Chapin JK, Moxon KA, Markowitz RS, Nicolelis MA. Real-time control of a robot arm using simultaneously recorded neurons in the motor cortex. Nat Neurosci. 1999;2: 664–670. doi:10.1038/10223

4. Lebedev MA, Nicolelis MAL. Brain–machine interfaces: past, present and future. Trends Neurosci. 2006;29: 536–546. doi:10.1016/j.tins.2006.07.004

5. Markowitz DA, Wong YT, Gray CM, Pesaran B. Optimizing the Decoding of Movement Goals from Local Field Potentials in Macaque Cortex. J Neurosci. 2011;31: 18412 –18422. doi:10.1523/JNEUROSCI.4165-11.2011

6. Moritz CT, Perlmutter SI, Fetz EE. Direct control of paralysed muscles by cortical neurons. Nature. 2008;456: 639–642. doi:10.1038/nature07418

7. Osborne LC, Bialek W, Lisberger SG. Time Course of Information about Motion Direction in Visual Area MT of Macaque Monkeys. J Neurosci. 2004;24: 3210–3222. doi:10.1523/JNEUROSCI.5305-03.2004

8. Taylor DM, Tillery SIH, Schwartz AB. Direct cortical control of 3D neuroprosthetic devices. Science. 2002;296: 1829–1832. doi:10.1126/science.1070291

9. Velliste M, Perel S, Spalding MC, Whitford AS, Schwartz AB. Cortical control of a prosthetic arm for self-feeding. Nature. 2008;453: 1098–1101. doi:10.1038/nature06996

10. Wessberg J, Stambaugh CR, Kralik JD, Beck PD, Laubach M, Chapin JK, et al. Real-time prediction of hand trajectory by ensembles of cortical neurons in primates. Nature. 2000;408: 361–365. doi:10.1038/35042582

11. Brumberg JS, Wright EJ, Andreasen DS, Guenther FH, Kennedy PR. Classification of intended phoneme production from chronic intracortical microelectrode recordings in speech-motor cortex. Front Neurosci. 2011;5: 65. doi:10.3389/fnins.2011.00065

12. Wodlinger B, Downey JE, Tyler-Kabara EC, Schwartz AB, Boninger ML, Collinger JL. Ten-dimensional anthropomorphic arm control in a human brain−machine interface: difficulties, solutions, and limitations. J Neural Eng. 2015;12: 016011. doi:10.1088/1741-2560/12/1/016011

13. Hochberg LR, Serruya MD, Friehs GM, Mukand JA, Saleh M, Caplan AH, et al. Neuronal ensemble control of prosthetic devices by a human with tetraplegia. Nature. 2006;442: 164–171. doi:10.1038/nature04970

14. Chestek CA, Batista AP, Santhanam G, Yu BM, Afshar A, Cunningham JP, et al. Single-neuron stability during repeated reaching in macaque premotor cortex. J Neurosci. 2007;27: 10742 –10750. doi:10.1523/JNEUROSCI.0959-07.2007

15. Chestek CA, Gilja V, Nuyujukian P, Foster JD, Fan JM, Kaufman MT, et al. Long-term stability of neural prosthetic control signals from silicon cortical arrays in rhesus macaque motor cortex. J Neural Eng. 2011;8: 045005. doi:10.1088/1741-2560/8/4/045005

16. Bensmaia SJ, Miller LE. Restoring sensorimotor function through intracortical interfaces: progress and looming challenges. Nat Rev Neurosci. 2014;15: 313–325. doi:10.1038/nrn3724

17. Gilja V, Chestek CA, Diester I, Henderson JM, Deisseroth K, Shenoy KV. Challenges and Opportunities for Next-Generation Intracortically Based Neural Prostheses. IEEE Trans Biomed Eng. 2011;58: 1891–1899. doi:10.1109/TBME.2011.2107553

18. Peckham PH, Knutson JS. Functional electrical stimulation for neuromuscular applications. Annu Rev Biomed Eng. 2005;7: 327–360. doi:10.1146/annurev.bioeng.6.040803.140103

19. Goldman HB, Amundsen CL, Mangel J, Grill J, Bennett M, Gustafson KJ, et al. Dorsal genital nerve stimulation for the treatment of overactive bladder symptoms. Neurourol Urodyn. 2008;27: 499–503. doi:10.1002/nau.20544

20. Lertmanorat Z, Durand DM. A novel electrode array for diameter-dependent control of axonal excitability: a Simulation study. IEEE Trans Biomed Eng. 2004;51: 1242–1250. doi:10.1109/TBME.2004.827347

21. Grill WM, Mortimer, JT. Stimulus waveforms for selective neural stimulation. IEEE Eng Med Biol. 1995;14(4): 375–385

22. Humayun MS, Weiland JD, Fujii GY, Greenberg R, Williamson R, Little J, et al. Visual perception in a blind subject with a chronic microelectronic retinal prosthesis. Vision Res. 2003;43: 2573–2581. doi:10.1016/S0042-6989(03)00457-7

23. van Hoesel RJM. Sensitivity to binaural timing in bilateral cochlear implant users. J Acoust Soc Am. 2007;121: 2192–2206.

24. Sennaroglu L, Ziyal I. Auditory brainstem implantation. Auris Nasus Larynx. 2012;39: 439–450. doi:10.1016/j.anl.2011.10.013

25. Pezaris JS, Eskandar EN. Getting signals into the brain: visual prosthetics through thalamic microstimulation. Neurosurg Focus. 2009;27: E6. doi:10.3171/2009.4.FOCUS0986

26. O'Doherty JE, Lebedev MA, Ifft PJ, Zhuang KZ, Shokur S, Bleuler H, et al. Active tactile exploration using a brain-machine-brain interface. Nature. 2011;479: 228–231. doi:10.1038/nature10489

27. Schroeder JB, Mariano VJ, Telian GI, Ritt JT. Stimulation of somatosensory cortex locked to whisker motions in a mouse model of active sensing. 2013 6th International IEEE/EMBS Conference on Neural Engineering (NER). 2013. pp. 637–640. doi:10.1109/NER.2013.6696015

28. Venkatraman S, Carmena JM. Active Sensing of Target Location Encoded by Cortical Microstimulation. IEEE Trans Neural Syst Rehabil Eng. 2011;19: 317–324. doi:10.1109/TNSRE.2011.2117441

29. Chatterjee A, Aggarwal V, Ramos A, Acharya S, Thakor NV. A brain-computer interface with vibrotactile biofeedback for haptic information. J NeuroEngineering Rehabil. 2007;4: 40. doi:10.1186/1743-0003-4-40

30. O'Doherty JE, Lebedev MA, Hanson TL, Fitzsimmons NA, Nicolelis MAL. A Brain-Machine Interface Instructed by Direct Intracortical Microstimulation. Front Integr Neurosci. 2009;3. doi:10.3389/neuro.07.020.2009

31. Kim S, Callier T, Tabot GA, Gaunt RA, Tenore FV, Bensmaia SJ. Behavioral assessment of sensitivity to intracortical microstimulation of primate somatosensory cortex. Proc Natl Acad Sci U S A. 2015;112: 15202–15207. doi:10.1073/pnas.1509265112

32. Tabot GA, Dammann JF, Berg JA, Tenore FV, Boback JL, Vogelstein RJ, et al. Restoring the sense of touch with a prosthetic hand through a brain interface. Proc Natl Acad Sci U S A. 2013;110: 18279–18284. doi:10.1073/pnas.1221113110

33. Dadarlat MC, O'Doherty JE, Sabes PN. A learning-based approach to artificial sensory feedback leads to optimal integration. Nat Neurosci. 2015;18: 138–144. doi:10.1038/nn.3883

34. Schiefer M, Tan D, Sidek SM, Tyler DJ. Sensory feedback by peripheral nerve stimulation improves task performance in individuals with upper limb loss using a myoelectric prosthesis. J Neural Eng. 2016;13: 016001. doi:10.1088/1741-2560/13/1/016001

35. Tan DW, Schiefer MA, Keith MW, Anderson JR, Tyler J, Tyler DJ. A neural interface provides long-term stable natural touch perception. Sci Transl Med. 2014;6: 257ra138–257ra138. doi:10.1126/scitranslmed.3008669

36. Ching S, Ritt J. Control strategies for underactuated neural ensembles driven by optogenetic stimulation. Front Neural Circuits. 2013;7: 54. doi:10.3389/fncir.2013.00054

37. Gibson JJ. Observations on active touch. Psychol Rev. 1962;69: 477–491.

38. Reynolds JH, Chelazzi L. Attentional modulation of visual processing. Annu Rev Neurosci. 2004;27: 611–647. doi:10.1146/annurev.neuro.26.041002.131039

39. Yarbus, Alfred. Eye Movements and Vision. Plenum Press; 1965.

40. Verhagen JV, Wesson DW, Netoff TI, White JA, Wachowiak M. Sniffing controls an adaptive filter of sensory input to the olfactory bulb. Nat Neurosci. 2007;10: 631–639. doi:10.1038/nn1892

41. Burstedt, Flanagan, Johansson. Control of grasp stability in humans under various frictional conditions during multi-digit lifting. Acta Physiol Scand. 1999;167: A22–A23.

42. Klatzky RL, Loomis JM, Lederman SJ, Wake H, Fujita N. Haptic identification of objects and their depictions. Percept Psychophys. 1993;54: 170–178.

43. Lederman SJ, Summers C, Klatzky RL. Cognitive salience of haptic object properties: role of modality-encoding bias. Perception. 1996;25: 983–998.

44. Lederman SJ, Klatzky RL. Haptic perception: a tutorial. Atten Percept Psychophys. 2009;71: 1439–1459. doi:10.3758/APP.71.7.1439

45. Godde B, Diamond ME, Braun C. Feeling for space or for time: task-dependent modulation of the cortical representation of identical vibrotactile stimuli. Neurosci Lett. 2010;480: 143–147. doi:10.1016/j.neulet.2010.06.027

46. Goossens HH, Van Opstal AJ. Human eye-head coordination in two dimensions under different sensorimotor conditions. Exp Brain Res. 1997;114: 542–560.

47. Jenks RA, Vaziri A, Boloori A-R, Stanley GB. Self-Motion and the Shaping of Sensory Signals. J Neurophysiol. 2010;103: 2195–2207. doi:10.1152/jn.00106.2009

48. Gamzu E, Ahissar E. Importance of temporal cues for tactile spatial- frequency discrimination. J Neurosci. 2001;21: 7416–7427.

49. Johansson RS, Flanagan JR. Coding and use of tactile signals from the fingertips in object manipulation tasks. Nat Rev Neurosci. 2009;10: 345–359. doi:10.1038/nrn2621

50. McDonnell MN, Ridding MC, Flavel SC, Miles TS. Effect of human grip strategy on force control in precision tasks. Exp Brain Res. 2005;161: 368–373. doi:10.1007/s00221-004-2081-0

51. Kleinfeld D, Deschênes M. Neuronal Basis for Object Location in the Vibrissa Scanning Sensorimotor System. Neuron. 2011;72: 455–468. doi:10.1016/j.neuron.2011.10.009

52. Petersen CCH. The Functional Organization of the Barrel Cortex. Neuron. 2007;56: 339–355. doi:10.1016/j.neuron.2007.09.017

53. Diamond ME, von Heimendahl M, Knutsen PM, Kleinfeld D, Ahissar E. "Where" and "what" in the whisker sensorimotor system. Nat Rev Neurosci. 2008;9: 601–612. doi:10.1038/nrn2411

54. Hartmann MJZ. A night in the life of a rat: vibrissal mechanics and tactile exploration. Ann N Y Acad Sci. 2011;1225: 110–118. doi:10.1111/j.1749-6632.2011.06007.x

55. Carvell G, Simons D. Biometric analyses of vibrissal tactile discrimination in the rat. J Neurosci. 1990;10: 2638–2648.

56. Towal RB, Hartmann MJZ. Variability in Velocity Profiles During Free-Air Whisking Behavior of Unrestrained Rats. J Neurophysiol. 2008;100: 740–752. doi:10.1152/jn.01295.2007

57. Quist BW, Hartmann MJZ. Mechanical Signals at the Base of a Rat Vibrissa: The Effect of Intrinsic Vibrissa Curvature and Implications for Tactile Exploration. J Neurophysiol. 2012;107: 2298–2312. doi:10.1152/jn.00372.2011

58. Mitchinson B, Grant RA, Arkley K, Rankov V, Perkon I, Prescott TJ. Active Vibrissal Sensing in Rodents and Marsupials. Philos Trans R Soc B Biol Sci. 2011;366: 3037–3048. doi:10.1098/rstb.2011.0156

59. Kleinfeld D, Berg RW, O'Connor SM. Anatomical loops and their electrical dynamics in relation to whisking by rat. Somatosens Mot Res. 1999;16: 69–88.

60. Matyas F, Sreenivasan V, Marbach F, Wacongne C, Barsy B, Mateo C, et al. Motor Control by Sensory Cortex. Science. 2010;330: 1240–1243. doi:10.1126/science.1195797

61. Brecht M. Barrel cortex and whisker-mediated behaviors. Curr Opin Neurobiol. 2007;17: 408–416. doi:10.1016/j.conb.2007.07.008

62. Fee MS, Mitra PP, Kleinfeld D. Central versus peripheral determinants of patterned spike activity in rat vibrissa cortex during whisking. J Neurophysiol. 1997;78: 1144–1149.

63. Ganguly K, Kleinfeld D. Goal-directed whisking increases phase-locking between vibrissa movement and electrical activity in primary sensory cortex in rat. Proc Natl Acad Sci U S A. 2004;101: 12348–12353. doi:10.1073/pnas.0308470101

64. de Kock CPJ, Sakmann B. Spiking in primary somatosensory cortex during natural whisking in awake head-restrained rats is cell-type specific. Proc Natl Acad Sci U S A. 2009;106: 16446–16450. doi:10.1073/pnas.0904143106

65. Simons DJ. Response properties of vibrissa units in rat SI somatosensory neocortex. J Neurophysiol. 1978;41: 798–820.

66. Boloori A-R, Jenks RA, Desbordes G, Stanley GB. Encoding and decoding cortical representations of tactile features in the vibrissa system. J Neurosci. 2010;30: 9990–10005. doi:10.1523/JNEUROSCI.0807-10.2010

67. Szwed M, Bagdasarian K, Ahissar E. Encoding of vibrissal active touch. Neuron. 2003;40: 621–630. doi:10.1016/S0896-6273(03)00671-8

68. Crochet S, Petersen CCH. Correlating whisker behavior with membrane potential in barrel cortex of awake mice. Nat Neurosci. 2006;9: 608–610. doi:10.1038/nn1690

69. Shuler MG, Krupa DJ, Nicolelis MAL. Bilateral integration of whisker information in the primary somatosensory cortex of rats. J Neurosci. 2001;21: 5251–5261.

70. Shuler MG, Krupa DJ, Nicolelis MAL. Integration of bilateral whisker stimuli in rats: Role of the whisker barrel cortices. Cereb Cortex. 2002;12: 86–97. doi:10.1093/cercor/12.1.86

71. Krupa DJ, Matell MS, Brisben AJ, Oliveira LM, Nicolelis MAL. Behavioral properties of the trigeminal somatosensory system in rats performing whisker-dependent tactile discriminations. J Neurosci. 2001;21: 5752–5763.

72. Vijayan S, Hale GJ, Moore CI, Brown EN, Wilson M. Activity in the barrel cortex during active behavior and sleep. J Neurophysiol. 2010;103: 2074–2084. doi:10.1152/jn.00474.2009

73. Ahissar E, Sosnik R, Haidarliu S. Transformation from temporal to rate coding in a somatosensory thalamocortical pathway. Nature. 2000;406: 302–306. doi:10.1038/35018568

74. Sosnik R, Haidarliu S, Ahissar E. Temporal frequency of whisker movement. I. Representations in brain stem and thalamus. J Neurophysiol. 2001;86: 339–353.

75. Khatri V, Hartings JA, Simons DJ. Adaptation in thalamic barreloid and cortical barrel neurons to periodic whisker deflections varying in frequency and velocity. J Neurophysiol. 2004;92: 3244–3254. doi:10.1152/jn.00257.2004

76. Curtis JC, Kleinfeld D. Phase-to-rate transformations encode touch in cortical neurons of a scanning sensorimotor system. Nat Neurosci. 2009;12: 492–501. doi:10.1038/nn.2283

77. Katz Y, Heiss JE, Lampl I. Cross-whisker adaptation of neurons in the rat barrel cortex. J Neurosci. 2006;26: 13363–13372. doi:10.1523/JNEUROSCI.4056-06.2006

78. Dörfl J. The musculature of the mystacial vibrissae of the white mouse. J Anat. 1982;135: 147–154.

79. Haidarliu S, Simony E, Golomb D, Ahissar E. Muscle architecture in the mystacial pad of the rat. Anat Rec. 2010;293: 1192–1206. doi:10.1002/ar.21156

80. Hill DN, Bermejo R, Zeigler HP, Kleinfeld D. Biomechanics of the vibrissa motor Plant in rat: Rhythmic whisking consists of triphasic neuromuscular activity. J Neurosci. 2008;28: 3438 –3455. doi:10.1523/JNEUROSCI.5008-07.2008

81. Ritt JT. High speed videography of embodied active sensing in the rodent whisker system. Neuromethods. 2012;67:283–302.

82. Clack NG, O'Connor DH, Huber D, Petreanu L, Hires A, Peron S, et al. Automated Tracking of Whiskers in Videos of Head Fixed Rodents. PLoS Comput Biol. 2012;8: e1002591. doi:10.1371/journal.pcbi.1002591

83. Perkon I, Košir A, Itskov PM, Tasič J, Diamond ME. Unsupervised quantification of whisking and head movement in freely moving rodents. J Neurophysiol. 2011;105: 1950–1962. doi:10.1152/jn.00764.2010

84. Voigts J, Sakmann B, Celikel T. Unsupervised whisker tracking in unrestrained behaving animals. J Neurophysiol. 2008;100: 504–515. doi:10.1152/jn.00012.2008

85. Knutsen PM, Derdikman D, Ahissar E. Tracking Whisker and Head Movements in Unrestrained Behaving Rodents. J Neurophysiol. 2005;93: 2294–2301. doi:10.1152/jn.00718.2004

86. Carvell GE, Simons DJ, Lichtenstein SH, Bryant P. Electromyographic activity of mystacial pad musculature during whisking behavior in the rat. Somatosens Mot Res. 1991;8:159–164.

87. Berg RW, Kleinfeld D. Vibrissa movement elicited by rhythmic electrical microstimulation to motor cortex in the aroused rat mimics exploratory whisking. J Neurophysiol. 2003;90: 2950–2963. doi:10.1152/jn.00511.2003

88. Berg RW, Kleinfeld D. Rhythmic whisking by rat: Retraction as well as protraction of the vibrissae is under active muscular control. J Neurophysiol. 2003;89: 104 –117. doi:10.1152/jn.00600.2002

89. Schroeder JB, Ritt JT. Extraction of intended palpation times from facial EMGs in a mouse model of active sensing. 2013 35th Annual International Conference of the IEEE Engineering in Medicine and Biology Society (EMBC). 2013. pp. 2016–2019. doi:10.1109/EMBC.2013.6609926

90. Towal RB, Hartmann MJ. Right–left asymmetries in the whisking behavior of rats anticipate head movements. J Neurosci. 2006;26: 8838–8846. doi:10.1523/JNEUROSCI.0581-06.2006

91. Mitchinson B, Martin CJ, Grant RA, Prescott TJ. Feedback control in active sensing: rat exploratory whisking is modulated by environmental contact. Proc Biol Sci. 2007;274: 1035–1041. doi:10.1098/rspb.2006.0347

92. Ritt JT, Andermann ML, Moore CI. Embodied information processing: Vibrissa mechanics and texture features shape micromotions in actively sensing rats. Neuron. 2008;57: 599–613. doi:10.1016/j.neuron.2007.12.024

93. Prigg T, Goldreich D, Carvell GE, Simons DJ. Texture discrimination and unit recordings in the rat whisker/barrel system. Physiol Behav. 2002;77: 671–675. doi:10.1016/S0031-9384(02)00917-4

94. von Heimendahl M, Itskov PM, Arabzadeh E, Diamond ME. Neuronal activity in rat barrel cortex underlying texture discrimination. PLoS Biol. 2007;5: e305. doi:10.1371/journal.pbio.0050305

95. Zuo Y, Perkon I, Diamond ME. Whisking and whisker kinematics during a texture classification task. Philos Trans R Soc Lond B Biol Sci. 2011;366: 3058–3069. doi:10.1098/rstb.2011.0161

96. Knutsen PM, Pietr M, Ahissar E. Haptic object localization in the vibrissal system: Behavior and performance. J Neurosci. 2006;26: 8451 –8464. doi:10.1523/JNEUROSCI.1516-06.2006

97. O'Connor DH, Clack NG, Huber D, Komiyama T, Myers EW, Svoboda K. Vibrissa-based object localization in head-fixed mice. J Neurosci. 2010;30: 1947–1967. doi:10.1523/JNEUROSCI.3762-09.2010

98. O'Connor DH, Peron SP, Huber D, Svoboda K. Neural activity in barrel cortex underlying vibrissa-based object localization in mice. Neuron. 2010;67: 1048–1061. doi:10.1016/j.neuron.2010.08.026

99. Ahissar E, Knutsen PM. Object localization with whiskers. Biol Cybern. 2008;98: 449–458. doi:10.1007/s00422-008-0214-4

100. Gordon G, Dorfman N, Ahissar E. Reinforcement active learning in the vibrissae system: Optimal object localization. J Physiol-Paris. 2013;107: 107–115. doi:10.1016/j.jphysparis.2012.06.004

101. Pammer L, O'Connor DH, Hires SA, Clack NG, Huber D, Myers EW, et al. The mechanical variables underlying object localization along the axis of the whisker. J Neurosci. 2013;33: 6726–6741. doi:10.1523/JNEUROSCI.4316-12.2013

102. Horev G, Saig A, Knutsen PM, Pietr M, Yu C, Ahissar E. Motor–sensory convergence in object localization: a comparative study in rats and humans. Philos Trans R Soc Lond B Biol Sci. 2011;366: 3070–3076. doi:10.1098/rstb.2011.0157

103. Voigts J, Herman DH, Celikel T. Tactile object localization by anticipatory whisker motion. J Neurophysiol. 2015;113: 620–632. doi:10.1152/jn.00241.2014

104. Grant RA, Mitchinson B, Fox CW, Prescott TJ. Active touch sensing in the rat: Anticipatory and regulatory control of whisker movements during surface exploration. J Neurophysiol. 2009;101: 862–874. doi:10.1152/jn.90783.2008

105. Sellien H, Eshenroder DS, Ebner FF. Comparison of bilateral whisker movement in freely exploring and head-fixed adult rats. Somatosens Mot Res. 2005;22: 97–114. doi:10.1080/08990220400015375

106. Grant RA, Prescott TJ. The role of orienting in vibrissal touch sensing. Front Behav Neurosci. 2012;6: 39. doi:10.3389/fnbeh.2012.00039

107. Arkley K, Grant RA, Mitchinson B, Prescott TJ. Strategy change in vibrissal active sensing during rat locomotion. Curr Biol. 2014;24: 1507–1512. doi:10.1016/j.cub.2014.05.036

108. Saraf-Sinik I, Assa E, Ahissar E. Motion makes sense: An adaptive motor-sensory strategy underlies the perception of object location in rats. J Neurosci. 2015;35: 8777–8789. doi:10.1523/JNEUROSCI.4149-14.2015

109. Erlich JC, Bialek M, Brody CD. A cortical substrate for memory-guided orienting in the rat. Neuron. 2011;72: 330–343. doi:10.1016/j.neuron.2011.07.010

110. Brecht M. Movement, confusion, and orienting in frontal cortices. Neuron. 2011;72: 193–196. doi:10.1016/j.neuron.2011.10.002

111. Fenno L, Yizhar O, Deisseroth K. The development and application of optogenetics. Annu Rev Neurosci. 2011;34: 389–412. doi:10.1146/annurev-neuro-061010-113817

112. Gorski JA, Talley T, Qiu M, Puelles L, Rubenstein JLR, Jones KR. Cortical excitatory neurons and glia, but not GABAergic neurons, are produced in the Emx1-expressing lineage. J Neurosci. 2002;22: 6309–6314. doi:20026564

113. Madisen L, Mao T, Koch H, Zhuo J, Berenyi A, Fujisawa S, et al. A toolbox of Cre-dependent optogenetic transgenic mice for light-induced activation and silencing. Nat Neurosci. 2012;15: 793–802. doi:10.1038/nn.3078

114. Arenkiel BR, Peca J, Davison IG, Feliciano C, Deisseroth K, Augustine GJ, et al. In vivo light-induced activation of neural circuitry in transgenic mice expressing channelrhodopsin-2. Neuron. 2007;54: 205–218. doi:10.1016/j.neuron.2007.03.005

115. Zhao S, Ting JT, Atallah HE, Qiu L, Tan J, Gloss B, et al. Cell-type specific optogenetic mice for dissecting neural circuitry function. Nat Methods. 2011;8: 745–752.

116. Lin JY. A user's guide to channelrhodopsin variants: features, limitations and future developments. Exp Physiol. 2011;96: 19–25. doi:10.1113/expphysiol.2009.051961

117. Zhang F, Gradinaru V, Adamantidis AR, Durand R, Airan RD, de Lecea L, et al. Optogenetic interrogation of neural circuits: technology for probing mammalian brain structures. Nat Protoc. 2010;5: 439–456. doi:10.1038/nprot.2009.226

118. Huber D, Petreanu L, Ghitani N, Ranade S, Hromadka T, Mainen Z, et al. Sparse optical microstimulation in barrel cortex drives learned behaviour in freely moving mice. Nature. 2008;451: 61–64. doi:10.1038/nature06445

119. Hippenmeyer S, Vrieseling E, Sigrist M, Portmann T, Laengle C, Ladle DR, et al. A developmental switch in the response of DRG neurons to ETS transcription factor signaling. PLoS Biol. 2005;3: e159. doi:10.1371/journal.pbio.0030159

120. Diamond ME. Texture sensation through the fingertips and the whiskers. Curr Opin Neurobiol. 2010;20: 319–327. doi:10.1016/j.conb.2010.03.004

121. Feldmeyer D, Brecht M, Helmchen F, Petersen CCH, Poulet JFA, Staiger JF, et al. Barrel cortex function. Prog Neurobiol. 2013;103: 3–27. doi:10.1016/j.pneurobio.2012.11.002

122. Bermejo R, Friedman W, Zeigler HP. Topography of whisking II: Interaction of whisker and pad. Somatosens Mot Res. 2005;22: 213–220. doi:10.1080/08990220500262505

123. Carvell GE, Simons DJ. Task- and subject-related differences in sensorimotor behavior during active touch. Somatosens Mot Res. 1995;12: 1–9.

124. Gao P, Hattox AM, Jones LM, Keller A, Zeigler HP. Whisker motor cortex ablation and whisker movement patterns. Somatosens Mot Res. 2003;20: 191–198. doi:10.1080/08990220310001622924

125. Deutsch D, Pietr M, Knutsen PM, Ahissar E, Schneidman E. Fast feedback in active sensing: Touch-induced changes to whisker-object interaction. PLoS One. 2012;7: e44272. doi:10.1371/journal.pone.0044272

126. Smith JB, Alloway KD. Rat whisker motor cortex is subdivided into sensory-input and motor-output areas. Front Neural Circuits. 2013;7. doi:10.3389/fncir.2013.00004

127. Harvey MA, Bermejo R, Zeigler HP. Discriminative whisking in the head-fixed rat: Optoelectronic monitoring during tactile detection and discrimination tasks. Somatosens Mot Res. 2001;18: 211–222.

128. O'Connor DH, Hires SA, Guo ZV, Li N, Yu J, Sun Q-Q, et al. Neural coding during active somatosensation revealed using illusory touch. Nat Neurosci. 2013;16: 958–965. doi:10.1038/nn.3419

129. Stüttgen MC, Schwarz C. Integration of vibrotactile signals for whisker-related perception in rats is governed by short time constants: Comparison of neurometric and psychometric detection performance. J Neurosci. 2010;30: 2060–2069. doi:10.1523/JNEUROSCI.3943-09.2010

130. Mehta SB, Whitmer D, Figueroa R, Williams BA, Kleinfeld D. Active spatial perception in the vibrissa scanning sensorimotor system. PLoS Biol. 2007;5. doi:10.1371/journal.pbio.0050015

131. Wolfe J, Hill DN, Pahlavan S, Drew PJ, Kleinfeld D, Feldman DE. Texture coding in the rat whisker system: Slip-stick versus differential resonance. PLoS Biol. 2008;6. doi:10.1371/journal.pbio.0060215

132. Prescott TJ, Diamond ME, Wing AM. Active touch sensing. Philos Trans R Soc Lond B Biol Sci. 2011;366: 2989–2995. doi:10.1098/rstb.2011.0167

133. Jenks RA, Vaziri A, Boloori A-R, Stanley GB. Self-motion and the shaping of sensory signals. J Neurophysiol. 2010;103: 2195–2207. doi:10.1152/jn.00106.2009

134. Hutson KA, Masterton RB. The sensory contribution of a single vibrissa's cortical barrel. J Neurophysiol. 1986;56: 1196–1223.

135. Brecht M, Preilowski B, Merzenich MM. Functional architecture of the mystacial vibrissae. Behav Brain Res. 1997;84: 81–97.

136. Cleveland WS. Robust locally weighted regression and smoothing scatterplots. J Am Stat Assoc. 1979;74: 829–836. doi:10.2307/2286407

137. Sachdev RNSB. Unilateral vibrissa contact: Changes in amplitude but not timing of rhythmic whisking. Somatosens Mot Res. 2003;20: 163.

138. Nguyen Q-T, Kleinfeld D. Positive feedback in a brainstem tactile sensorimotor loop. Neuron. 2005;45: 447–457. doi:10.1016/j.neuron.2004.12.042

139. Hill DN, Curtis JC, Moore JD, Kleinfeld D. Primary motor cortex reports efferent control of vibrissa motion on multiple timescales. Neuron. 2011;72: 344–356. doi:10.1016/j.neuron.2011.09.020

140. Petreanu L, Gutnisky DA, Huber D, Xu N, O'Connor DH, Tian L, et al. Activity in motor-sensory projections reveals distributed coding in somatosensation. Nature. 2012;489: 299–303. doi:10.1038/nature11321

141. Chen JL, Carta S, Soldado-Magraner J, Schneider BL, Helmchen F. Behaviour-dependent recruitment of long-range projection neurons in somatosensory cortex. Nature. 2013;499: 336–340. doi:10.1038/nature12236

142. Guić-Robles E, Valdivieso C, Guajardo G. Rats can learn a roughness discrimination using only their vibrissal system. Behav Brain Res. 1989;31: 285–289.

143. Celikel T, Sakmann B. Sensory integration across space and in time for decision making in the somatosensory system of rodents. Proc Natl Acad Sci U S A. 2007;104: 1395–1400. doi:10.1073/pnas.0610267104

144. Somers DC, Dale AM, Seiffert AE, Tootell RBH. Functional MRI reveals spatially specific attentional modulation in human primary visual cortex. Proc Natl Acad Sci U S A. 1999;96: 1663–1668.

145. Somers DC, Sheremata SL. Attention maps in the brain. Wiley Interdiscip Rev Cogn Sci. 2013;4: 327–340. doi:10.1002/wcs.1230

146. Shadlen MN, Kiani R. Decision making as a window on cognition. Neuron. 2013;80. doi:10.1016/j.neuron.2013.10.047

147. Carrasco M. Visual attention: The past 25 years. Vision Res. 2011;51: 1484–1525. doi:10.1016/j.visres.2011.04.012

148. Solomon JH, Hartmann MJZ. Extracting object contours with the sweep of a robotic whisker using torque information. Int J Robot Res. 2009; doi:10.1177/0278364908104468

149. Schroeder CL, Hartmann MJZ. Sensory prediction on a whiskered robot: A tactile analogy to "optical flow." Front Neurorobotics. 2012;6. doi:10.3389/fnbot.2012.00009

150. Seth AK, McKinstry JL, Edelman GM, Krichmar JL. Texture discrimination by an autonomous mobile brain-based device with whiskers. 2004 IEEE International Conference on Robotics and Automation, 2004 Proceedings ICRA '04. 2004. pp. 4925–4930 Vol. 5. doi:10.1109/ROBOT.2004.1302498

151. Mihaylova L, Lefebvre T, Bruyninckx H, Gadeyne K, Schutter JD. A comparison of decision making criteria and optimization methods for active robotic sensing. In I. Dimov et al. (eds.) Numerical Methods and Applications: 5th International Conference, NMA 2002. Lecture Notes in Computer Science, Vol. 2542. Berlin, New York: Springer, 2003. pp. 316–324.

152. Fox CW, Evans MH, Lepora NF, Pearson M, Ham A, Prescott TJ. CrunchBot: A mobile whiskered robot platform. In: Groß R, Alboul L, Melhuish C, Witkowski M, Prescott TJ, Penders J, editors. Towards Autonomous Robotic Systems. Springer Berlin Heidelberg; 2011. pp. 102–113. Available: http://link.springer.com/chapter/10.1007/978-3-642-23232-9_10

153. Fend M. Whisker-based texture discrimination on a mobile robot. In: Capcarrère MS, Freitas AA, Bentley PJ, Johnson CG, Timmis J, editors. Advances in Artificial Life. Springer Berlin Heidelberg; 2005. pp. 302–311. Available: http://link.springer.com/chapter/10.1007/11553090_31

154. Sharp PE, Blair HT, Cho J. The anatomical and computational basis of the rat head-direction cell signal. Trends Neurosci. 2001;24: 289–294.

155. Taube JS. Head direction cells and the neurophysiological basis for a sense of direction. Prog Neurobiol. 1998;55: 225–256.

156. Taube JS, Goodridge JP, Golob EJ, Dudchenko PA, Stackman RW. Processing the head direction cell signal: a review and commentary. Brain Res Bull. 1996;40: 477–484; discussion 484–486.

157. Sofroniew NJ, Cohen JD, Lee AK, Svoboda K. Natural whisker-guided behavior by head-fixed mice in tactile virtual reality. J Neurosci. 2014;34: 9537–9550. doi:10.1523/JNEUROSCI.0712-14.2014

158. Harvey CD, Collman F, Dombeck DA, Tank DW. Intracellular dynamics of hippocampal place cells during virtual navigation. Nature. 2009;461: 941–946. doi:10.1038/nature08499

159. Leinweber M, Zmarz P, Buchmann P, Argast P, Hübener M, Bonhoeffer T, et al. Two-photon calcium imaging in mice navigating a virtual reality environment. J Vis Exp. 2014; e50885. doi:10.3791/50885

160. Dombeck DA, Harvey CD, Tian L, Looger LL, Tank DW. Functional imaging of hippocampal place cells at cellular resolution during virtual navigation. Nat Neurosci. 2010;13: 1433–1440. doi:10.1038/nn.2648

161. Diamond ME, Armstrong-James M, Ebner FF. Experience-dependent plasticity in adult rat barrel cortex. Proc Natl Acad Sci U S A. 1993;90: 2082–2086.

162. Maier DL, Grieb GM, Stelzner DJ, McCasland JS. Large-scale plasticity in barrel cortex following repeated whisker trimming in young adult hamsters. Exp Neurol. 2003;184: 737–745. doi:10.1016/S0014-4886(03)00335-2

163. Polley DB, Kvasnák E, Frostig RD. Naturalistic experience transforms sensory maps in the adult cortex of caged animals. Nature. 2004;429: 67–71. doi:10.1038/nature02469

164. Margolis DJ, Lütcke H, Schulz K, Haiss F, Weber B, Kügler S, et al. Reorganization of cortical population activity imaged throughout long-term sensory deprivation. Nat Neurosci. 2012;15: 1539–1546. doi:10.1038/nn.3240

165. Kätzel D, Miesenböck G. Experience-dependent rewiring of specific inhibitory connections in adult neocortex. PLoS Biol. 2014;12: e1001798. doi:10.1371/journal.pbio.1001798

166. Hartmann MJ. Active sensing capabilities of the rat whisker system. Auton Robots. 2001;11: 249–254. doi:10.1023/A:1012439023425

167. Mitchinson B, Prescott TJ. Whisker movements reveal spatial attention: A unified computational model of active sensing control in the rat. PLoS Comput Biol. 2013;9: e1003236. doi:10.1371/journal.pcbi.1003236

168. Siegle JH, Carlen M, Meletis K, Tsai L-H, Moore CI, Ritt J. Chronically implanted hyperdrive for cortical recording and optogenetic control in behaving mice. Engineering in Medicine and Biology Society, EMBC, 2011 Annual International Conference of the IEEE. 2011. pp. 7529–7532. doi:10.1109/IEMBS.2011.6091856

169. Halassa MM, Siegle JH, Ritt JT, Ting JT, Feng G, Moore CI. Selective optical drive of thalamic reticular nucleus generates thalamic bursts & cortical spindles. Nat

Neurosci. 2011;14: 1118–1120. doi:10.1038/nn.2880

170. Ahmadian Y, Packer AM, Yuste R, Paninski L. Designing optimal stimuli to control neuronal spike timing. J Neurophysiol. 2011;106: 1038–1053. doi:10.1152/jn.00427.2010

171. Pinto DJ, Brumberg JC, Simons DJ. Circuit dynamics and coding strategies in rodent somatosensory cortex. J Neurophysiol. 2000;83: 1158 –1166.

172. Aravanis AM, Wang L-P, Zhang F, Meltzer LA, Mogri MZ, Schneider MB, et al. An optical neural interface: In vivo control of rodent motor cortex with integrated fiberoptic and optogenetic technology. J Neural Eng. 2007;4: S143–S156. doi:10.1088/1741-2560/4/3/S02

173. Boyden ES, Zhang F, Bamberg E, Nagel G, Deisseroth K. Millisecond-timescale, genetically targeted optical control of neural activity. Nat Neurosci. 2005;8: 1263–1268. doi:10.1038/nn1525

174. Zhang F, Wang L-P, Brauner M, Liewald JF, Kay K, Watzke N, et al. Multimodal fast optical interrogation of neural circuitry. Nature. 2007;446: 633–639. doi:10.1038/nature05744

175. McNaughton BL, O'Keefe J, Barnes CA. The stereotrode: A new technique for simultaneous isolation of several single units in the central nervous system from multiple unit records. J Neurosci Methods. 1983;8: 391–397.

176. Gray CM, Maldonado PE, Wilson M, McNaughton B. Tetrodes markedly improve the reliability and yield of multiple single-unit isolation from multi-unit recordings in cat striate cortex. J Neurosci Methods. 1995;63: 43–54.

177. Kloosterman F, Davidson TJ, Gomperts SN, Layton SP, Hale G, Nguyen DP, et al. Micro-drive array for chronic in vivo recording: Drive fabrication. J Vis Exp. 2009; doi:10.3791/1094

178. Nguyen DP, Layton SP, Hale G, Gomperts SN, Davidson TJ, Kloosterman F, et al. Micro-drive array for chronic in vivo recording: Tetrode assembly. J Vis Exp. 2009; doi:10.3791/1098

179. Voigts J, Siegle JH, Pritchett DL, Moore CI. The flexDrive: An ultra-light implant for optical control and highly parallel chronic recording of neuronal ensembles in freely moving mice. Front Syst Neurosci. 2013;7. doi:10.3389/fnsys.2013.00008

180. Brunetti PM, Wimmer RD, Liang L, Siegle JH, Voigts J, Wilson M, et al. Design and fabrication of ultralight weight, adjustable multi-electrode probes for electrophysiological recordings in mice. J Vis Exp. 2014; doi:10.3791/51675

181. Chang EH, Frattini SA, Robbiati S, Huerta PT. Construction of microdrive arrays for chronic neural recordings in awake behaving mice. J Vis Exp. 2013; doi:10.3791/50470

182. Fee MS, Leonardo A. Miniature motorized microdrive and commutator system for chronic neural recording in small animals. J Neurosci Methods. 2001;112: 83–94. doi:10.1016/S0165-0270(01)00426-5

183. Jackson N, Sridharan A, Anand S, Baker M, Okandan M, Muthuswamy J. Long-term neural recordings using MEMS based movable microelectrodes in the brain. Front Neuroengineering. 2010;3. doi:10.3389/fneng.2010.00010

184. Yamamoto J, Wilson MA. Large-scale chronically implantable precision motorized microdrive array for freely behaving animals. J Neurophysiol. 2008;100: 2430–2440. doi:10.1152/jn.90687.2008

185. Yang S, Cho J, Lee S, Park K, Kim J, Huh Y, et al. Feedback controlled piezo-motor microdrive for accurate electrode positioning in chronic single unit recording in behaving mice. J Neurosci Methods. 2011;195: 117–127. doi:10.1016/j.jneumeth.2010.09.006

186. Anikeeva P, Andalman AS, Witten I, Warden M, Goshen I, Grosenick L, et al. Optetrode: A multichannel readout for optogenetic control in freely moving mice. Nat Neurosci. 2011;15: 163–170. doi:10.1038/nn.2992

187. Ozden I, Wang J, Lu Y, May T, Lee J, Goo W, et al. A coaxial optrode as multifunction write-read probe for optogenetic studies in non-human primates. J Neurosci Methods. 2013;219: 142–154. doi:10.1016/j.jneumeth.2013.06.011

188. Royer S, Zemelman BV, Barbic M, Losonczy A, Buzsáki G, Magee JC. Multi-array silicon probes with integrated optical fibers: light-assisted perturbation and recording of local neural circuits in the behaving animal. Eur J Neurosci. 2010;31: 2279–2291. doi:10.1111/j.1460-9568.2010.07250.x

189. Lee J, Ozden I, Song Y-K, Nurmikko AV. Transparent intracortical microprobe array for simultaneous spatiotemporal optical stimulation and multichannel electrical recording. Nat Methods. 2015;12: 1157–1162. doi:10.1038/nmeth.3620

190. Wang J, Wagner F, Borton DA, Zhang J, Ozden I, Burwell RD, et al. Integrated device for combined optical neuromodulation and electrical recording for chronic in vivo applications. J Neural Eng. 2011;9: 016001. doi:10.1088/1741-2560/9/1/016001

191. McAlinden N, Gu E, Dawson MD, Sakata S, Mathieson K. Optogenetic activation of neocortical neurons in vivo with a sapphire-based micro-scale LED probe. Front Neural Circuits. 2015;9. doi:10.3389/fncir.2015.00025

192. Lin L, Chen G, Xie K, Zaia KA, Zhang S, Tsien JZ. Large-scale neural ensemble recording in the brains of freely behaving mice. J Neurosci Methods. 2006;155: 28–38. doi:10.1016/j.jneumeth.2005.12.032

193. Fan D, Rich D, Holtzman T, Ruther P, Dalley JW, Lopez A, et al. A Wireless Multi-Channel Recording System for Freely Behaving Mice and Rats. PLoS One. 2011;6. doi:10.1371/journal.pone.0022033

194. Wentz CT, Bernstein JG, Monahan P, Guerra A, Rodriguez A, Boyden ES. A wirelessly powered and controlled device for optical neural control of freely-behaving animals. J Neural Eng. 2011;8: 046021. doi:10.1088/1741-2560/8/4/046021

195. Schroeder JB, Ritt JT. Selection of Head and Whisker Coordination Strategies During Goal Oriented Active Touch. J Neurophysiol. 2016; jn.00465.2015. doi:10.1152/jn.00465.2015

196. Penfield W, Boldrey E. Somatic Motor and Sensory Representation in the Cerebral Cortex of Man as Studied by Electrical Stimulation. Brain. 1937;60: 389–443. doi:10.1093/brain/60.4.389

197. Welker WI, Benjamin RM, Miles RC, Woolsey CN. Motor Effects of Stimulation of Cerebral Cortex of Squirrel Monkey (saimiri Sciureus). J Neurophysiol. 1957;20: 347–364.

198. Woolsey, CN. Organization of Somatic Sensory and Motor Areas of the Cerebral Cortex. Biological and Biochemical Bases of Behavior. Madison: University of Wisconsin Press; 1958.

199. Woolsey CN, Erickson TC, Gilson WE. Localization in somatic sensory and motor areas of human cerebral cortex as determined by direct recording of evoked potentials and electrical stimulation. J Neurosurg. 1979;51: 476–506. doi:10.3171/jns.1979.51.4.0476

200. Ahl AS. The role of vibrissae in behavior: a status review. Vet Res Commun. 1986;10: 245–268.

201. Ibbotson M, Krekelberg B. Visual Perception and Saccadic Eye Movements. Curr Opin Neurobiol. 2011;21: 553–558. doi:10.1016/j.conb.2011.05.012

202. Bremmer F, Kubischik M, Hoffmann K-P, Krekelberg B. Neural Dynamics of Saccadic Suppression. J Neurosci. 2009;29: 12374–12383. doi:10.1523/JNEUROSCI.2908-09.2009

Curriculum Vitae

Joseph B. Schroeder
Department of Biomedical Engineering,
44 Cummington Mall
Boston, MA 02215
jbs7@bu.edu 612-710-3674

Education

Boston University, Boston MA, May, 2016
PhD, Ritt Lab, Department of Biomedical Engineering

Boston University, Boston MA
M.S., Biomedical Engineering, Fall 2012

Case Western Reserve University, Cleveland OH
B.S., Biomedical Engineering, May 2010
Senior Capstone "Measurement of Perineurium Resistivity"

Experience

Ritt Lab: Boston University, Boston, Massachusetts
Graduate Research Assistant, Department of Biomedical Engineering
September 2010 – Present

- Performs studies of sensory neuroscience in awake, behaving rodents to better understand the role of sensory cortex in coordinating exploratory behaviors to inform the design of prosthetics that incorporate sensory feedback.
- Development of real-time feedback control systems for sensory manipulation.
- Key techniques: electrophysiology, optogenetics, digital signal processing, real time control systems, 3D modeling, rapid prototyping, DSP programming, optics and lasers, high speed videography, rodent surgery, Matlab.
- Responsible for training and mentoring undergraduate research students and high school summer students.
- Assists with preparation of NSF and NIH grant applications.

Department of Biomedical Engineering: Boston University, Boston, Massachusetts
Teaching Fellow
September 2011 – December 2013

- Assisted with an undergraduate course in signal processing and a lab course in biomedical instrumentation.
- Contributed to restructuring the prior version of this course to integrate real world engineering design problems.

- Taught weekly small group recitation sections and led reviews for exams.
- Ran weekly lab sections, including assisting with new curriculum development and grading.

Boston Scientific Cardiac Rhythm Management: St. Paul, Minnesota
Internship, Leads Design
Summer 2009, Summer 2010

- Research focused on electrode design optimization for left ventricular pacing leads. Work resulted in numerous design recommendations for directing electrical stimulation towards target areas and away from unintended targets.
- Developed a test method for evaluating the fixation of leads placed in the coronary veins. This test method enables the evaluation of new lead design concepts for stability over time.
- Established a collaboration with University of Minnesota to take measurements from their heart library in order to better inform the design of pacemaker leads.
- Key techniques: finite element modeling (COMSOL and Ansoft Maxwell), test method development and validation, statistical analysis.
- Worked on cross-functional teams that included design engineering, test engineering, process development, and clinical affairs.
- Worked with outside legal counsel on invention disclosures, prior art searches, and patent applications.

NDI Medical: Cleveland, Ohio
Internship, Operations and Quality Control
Summer 2008 full time and August 2008– May 2009 part time

- Developed new procedures for the in-house manufacturing of the CheckPoint surgical nerve stimulator that shortened assembly operations and reduced costs.
- Created a new connection method for the stimulator tip that increased reliability and improved manufacturability.
- Worked with Quality Control, Regulatory Affairs, and Design Engineering to develop and implement improvements to the Quality Control database to streamline the approvals of engineering design changes.
- Completed invention disclosures on concepts related to the new stimulator tip connection method.

Durand Lab: Case Western Reserve University, Cleveland, Ohio
Undergraduate Research Assistant
August 2008– May 2010

- Developed a novel round nerve cuff electrode for recording nerve impulses in laboratory animals in an acute animal model for blocking pain responses.
- Developed a method to measure the resistivity of nerve membranes in order to improve the accuracy of finite element modeling for peripheral nerve stimulation.

Tuberculosis Research Unit- CWRU School of Medicine, Cleveland, Ohio
Student Research Assistant
January 2007– May 2010

- Synthesizing, interpreting, and entering data from studies in Brazil, Uganda, and Philippines
- Familiarity with IRB protocols, human subjects research ethics, and medical terminology.

Publications

J. B. Schroeder and J. T. Ritt (2016). "Selection of Head and Whisker Coordination Strategies During Goal Oriented Active Touch." Journal of Neurophysiology. In Press.

David Freedman*, **Joseph B. Schroeder***, Gregory I. Telian, Zhengyang Zhang, and Jason T. Ritt (2016). "OptoZIF Drive: a 3D printed implant and assembly tool package for neural recording and optical stimulation in freely moving mice." Journal of Engineering. Submitted.
*Authors contributed equally

J. B. Schroeder and J. T. Ritt (2013). "Extraction of Intended palpation times from facial EMGs in a mouse model of active sensing". Conf. Proc. IEEE Eng. Med. Biol. Soc. 2013: 2016–2019

J. B. Schroeder, V. J. Mariano, G. I. Telian, and J. T. Ritt (2013). "Stimulation of Somatosensory Cortex Locked to Whisker Motions in a Mouse Model of Active Sensing". Conf. Proc. IEEE Eng. Med. Biol. Soc. 2013: 637–640.

Patents

US8463398. Timothy R. Jackson and **Joseph Schroeder**. Electrode Surface Modification for Imparting Current Density Directionality in Lead Electrodes. Publication Date: June 11, 2013. Filing Date: Nov 15, 2010. Priority Date: Dec 30, 2009.

US20110160822 (Patent Pending). Timothy R. Jackson and **Joseph Schroeder**. Implantable Lead Electrode With Asymmetrically Distributed Current Density and Methods for Imparting Current Density Directionality in Lead Electrodes. Publication Date: June 30, 2011. Filing Date: Nov 15, 2010. Priority Date: Dec 30, 2009.

Teaching

- Biomedical Measurements Lab (BE491), Graduate Teaching Fellow- Fall 2012
- Signals and Systems (BE401), Graduate Teaching Fellow- Fall 2011
- Biomedical Measurements Lab (BE491), Graduate Teaching Fellow- Fall 2011

Professional Memberships

- Society for Neuroscience
- American Physiological Society
- Institute of Electrical and Electronics Engineers

Qualifications

- **Rodent Handling and Surgery training, Boston University- Fall 2010**
- **Responsible Research Conduct Seminar, Boston University- 2010–2011**
  Four part seminar series, fulfills NIH research ethics training requirement
- **Human Subjects Research Training, Case Western Reserve University- Fall 2007**

Award/ Honors / Leadership

- Boston University Graduate Student Committee- faculty committee representative
- Best Oral Presentation- NIH Quantitative Biology and Physiology Training Grant Annual Symposium- April 2014
- Boston University PhD Qualification Exam- Pass with Honors- June 2011
- NIH Quantitative Biology and Physiology Training Grant recipient- 2010–2011
- Outstanding BME Senior, Case Western Reserve University – May 2010
- Deans High Honors, Case Western Reserve University- Various
- Alpha Eta Mu Beta, Biomedical Engineering Honor Society, Case Western Reserve University
- Gamma Sigma Alpha, Greek Academic Honor Society, Case Western Reserve University
- Eagle Scout Award, Boy Scouts of America, 2001

Presentations

- **Futures of Light Symposium (Neurophotonics), Boston University- Dec 1, 2011**
  Poster Presentation: "Closed Loop Optogenetic Control of Active Touch"
- **QBP Graduate Research Symposium, Boston University- February 17, 2012**
  Poster Presentation: "Closed Loop Optogenetic Control of Active Touch"
- **Boston University Graduate Program in Neuroscience Recruitment- March 5, 2012**
  Poster Presentation: "Closed Loop Optogenetic Control of Active Touch"
- **Boston University Science and Engineering Graduate Research Symposium, March 21, 2012**
  Poster Presentation: "Closed Loop Optogenetic Control of Active Touch"
- **International Conference on Cognitive and Neural Systems, Boston, May, 2012**
  Poster Presentation: "Closed Loop Optogenetic Control of Active Touch"
- **Society of Neuroscience Annual Meeting, New Orleans, October 13–17, 2012**
  Poster Presentation: "Effects of Closed Loop Feedback During Active Tactile Exploration"

- **IEEE Engineering in Medicine and Biology Conference, Osaka Japan, July 3–7 2013**
  Poster Presentation: “Extraction of Intended Palpation Times from Facial EMGs in a Mouse Model of Active Sensing
- **IEEE Neural Engineering Conference, San Diego, November 6–8 2013**
  Poster Presentation: “Stimulation of Somatosensory Cortex Locked to Whisker Motions in a Mouse Model of Active Sensing"
- **QBP Graduate Research Symposium, Boston University- April 4, 2014**
  Oral Presentation: “Stimulation of Somatosensory Cortex Locked to Whisker Motions in a Mouse Model of Active Sensing”
- **Society of Neuroscience Annual Meeting, Washington D.C, November 15–19, 2014**
  Poster Presentation: "Selection of active sensing strategies by mice during tactile search"
- **Neural Processing in Humans, Animals, and Machines, Boston, June 10–12, 2015**
  Poster Presentation: "“Stimulation of Somatosensory Cortex Locked to Whisker Motions in a Mouse Model of Active Sensing”
- **Society of Neuroscience Annual Meeting, Chicago, October 17–21, 2015**
  Poster Presentation: "Closed-loop optogenetic stimulation reveals primary somatosensory cortex participation in whisk timing"

Community Outreach

- **U-Design, Boston University College of Engineering- July 25th, 2014**
  Prepared and conducted demonstrations of simple engineering technology for groups of middle and high schools students to encourage student interest in science and engineering.
- **Massachusetts State Science and Engineering Fair- May 2, 2014**
  Volunteer judge for high school level science projects
- **Massachusetts State Science and Engineering Fair- May, 3 2013**
  Volunteer judge for high school level science projects
- **U-Design, Boston University College of Engineering- July 21st, 2011**
  Prepared and conducted demonstrations of simple engineering technology for groups of middle and high schools students to encourage student interest in science and engineering.
- **U-Design, Boston University College of Engineering- July, 2012**
  Prepared and conducted demonstrations of simple engineering technology for groups of middle and high schools students to encourage student interest in science and engineering.
- **Medical Initiative for Nations under Development (MIND) - 2006–2010**
  Repaired and tested donated medical equipment prior to shipment to developing nations
- **Replay for Kids, Cleveland OH- 2006– 2010**
  Adapted donated toys for use by physical and mentally handicapped children

- **Rainbow Babies and Children's Hospital, Cleveland OH - 2006–2008**
  Volunteer duties included staffing play room, assisting parents, and aiding medical staff
- **Tutoring, Arc of the Covenant Church, Cleveland, OH - 2006–2010**
  Tutored K-12 students from impoverished neighborhoods, with particular emphasis on passing the Ohio graduate requirement exam

Skills and Techniques

- **Electrophysiology**: neural recordings in awake behaving rodents, optogenetics, stereotactic surgery to implant chronic recording drives, custom instrumentation for automated behavioral testing.
- **Data Analysis**: MATLAB, statistics, high-speed video analysis, spike sorting.
- **Device Design**: 3D modeling (ProEngineer and Solidworks), printed circuit board layout, rapid prototyping, manufacturing protocol development, test development and validation, finite element modeling of design concepts (COMSOL and Ansoft Maxwell).
- **Real Time Control**: DSP programming, signal processing, algorithm design, control theory.
- **Intellectual property**: prior art searches, invention disclosures, patent applications.